LIBRARY COPY

FINAL REPORT

for

A STUDY OF LASER WAVE SCATTERING DUE TO REFRACTIVE INDEX PERTURBATIONS IN THE PROPAGATING MEDIUM

Period Covered

5 October 1965 to 15 August 1966

Contract NAS9-5315

Melpar Job No. 5591.00100

Prepared for:

National Aeronautics and Space Administration
Manned Spacecraft Center
Houston, Texas

Prepared by:

S. B. Sample, Ph.D.
S. J. Campanella, D.E.E.

Electronics Research Laboratory
Melpar, Inc.
7700 Arlington Blvd.
Falls Church, Virginia 22046

August 1966

ABSTRACT

The purpose of this contract was to expand the GT-7 Laser Communicator Experiment into a scientific study of laser wave scattering due to refractive index perturbations in the atmosphere.

This report contains a complete description of the two data recording and processing systems that were constructed on the contract. It also describes the activities of the Melpar personnel who were stationed at the White Sands and Ascension Island Laser Communicator Sites during the flight of GT-7. An analysis of the data obtained during static laser wave propagation experiments at the WSMR site is included. Finally, the report presents recommendations for future space-to-earth and ground-based laser wave propagation experiments that seem necessary in order to further clarify the nature of optical propagation over great distances in the atmosphere.

TABLE OF CONTENTS

TABLE OF CONTENTS (Continued)

LIST OF ILLUSTRATIONS

LIST OF ILLUSTRATIONS (Continued)

LIST OF ILLUSTRATIONS (Continued)

LIST OF ILLUSTRATIONS (Continued)

1. INTRODUCTION

The purpose of this contract was to provide the personnel, equipment, and data reduction capabilities for expanding the GT-7 Laser Communicator Experiment into a scientific study of laser wave scattering due to refractive index perturbations in the atmosphere. Specifically, the contract called for:

   a. Constructing two separate data recording and processing systems.

   b. Installing one of these systems at the White Sands Missile Range Laser Communicator Site, and the other at the Ascension Island Laser Communicator Site.

   c. Operating the two systems during the flight of GT-7.

   d. Analyzing the data obtained during the flight with respect to the variance and autocorrelation of the received signal.

   e. Recommending what additional experiments might be necessary in order to clarify further the nature of optical propagation over great distances in the atmosphere.

Figure 1-1 is a sketch of the overall operation of the Laser Communicator Experiment at the WSMR receiving facility. The FPS-16 radar was to have first acquired the spacecraft as it began its pass over the receiving facility. The optical pedestal, which was slaved to the radar, was then to have aimed automatically both the optical receiver and the beacon laser directly at the capsule. The astronaut was to have visually acquired the powerful beacon laser, and was then to have aimed his hand-held spacecraft laser transmitter directly at the ground beacon. The hand-held transmitter contained four GaAs laser diodes, and could be operated in either a low pulse rate mode (~100 pps), or a high pulse rate mode (~8,000 pps) capable of carrying the astronaut's voice by pulse position modulation. The laser energy emitted by the hand-held transmitter was to have been collected by the optical receiver on the ground, and focused onto a MPT. The output of the MPT was then to have been fed to the Melpar Field Laboratory, where the signals were to have been processed and recorded.

The primary scientific significance of the GT-7 Laser Communicator Experiment lay in the fact that it presented, for the first time, a long-distance optical propagation experiment wherein the relationship between range and the statistics of the received signal might have been determined. A significant and singular advantage is obtained through the use of a spaceborne transmitter as the energy is propagated through the entire vertical profile of the atmosphere. The results are, therefore, directly applicable to long-range deep-space communications. In the low pulse rate mode of operation, the experiment might have yielded data on the variance in received signal as a function of range. In the high pulse rate mode of
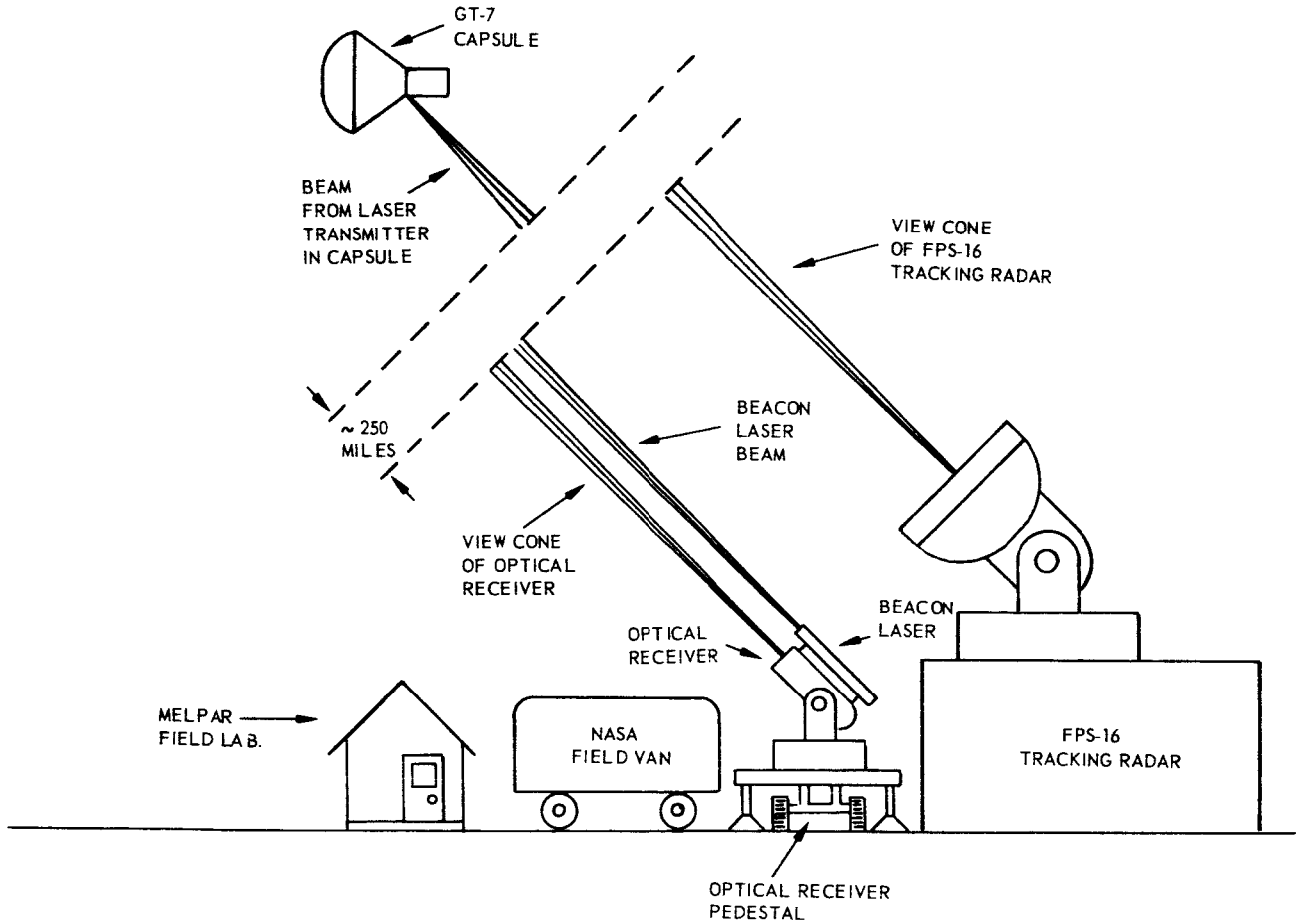
Figure 1-1. Overall Operation of Laser Communication Experiment at WSMR
Receiving Facility

operation, data might have been acquired on the spectral distribution of energy in the received signal as a function of range. In addition, the high pulse rate mode might have given considerable information on the relationship between range and the time autocorrelation function of the refractive index perturbations along nearly vertical atmospheric paths.

Another important possible contribution of the experiment lay in the fact that the emitted pulses were only about 100 nanoseconds in duration. This presented an opportunity for measuring the delay time between multiple arrivals, provided this delay time were equal to or greater than 20 nanoseconds. With a spacecraft transmitter beam divergence of 4 milliradians, a ground receiver angle of view of 1 milliradian, and at a range of 600 kilometers, the maximum delay time between the direct arrival and a singly scattered arrival would be 7 nanoseconds. Therefore, in the event the experiment had indicated multiple arrivals, the later arrivals would almost certainly have been due to multiple scattering.

Unfortunately, for various reasons (see section 4), no data was received or recorded during this experiment. However, the availability of a hand-held laser communicator at the WSMR site permitted short-range static propagation measurements at this location. The data from this experiment is presented and analyzed in section 5.

2. REVIEW OF PREVIOUS WORK ON OPTICAL SCATTERING BY ATMOSPHERIC TURBULENCE

2.1 General Discussion of Scattering Mechanisms

The turbulent character of the atmosphere gives rise to a random distribution of regions of air whose densities are either greater than or less than the average atmospheric density. Since the refractive index of a gas depends on its density, these small regions of dense or rarefied air may be thought of as refractive index perturbation patches. An electromagnetic wave or beam propagating through the atmosphere is randomly refracted or scattered by these patches, particularly if the wavelength is small compared to the patch dimensions. This random scattering phenomenon gives rise to random spatial variations in the amplitude and phase across the wave front. The fact that both the spatial distribution and magnitudes of the patches are random functions of time implies that the spatial distributions of amplitude and phase across the beam front are also random functions of time.

There are generally two distinct types of interactions between a laser beam and a perturbation patch. The first of these, called beam bending or steering, is illustrated in figure 2-1. It is characterized by a refractive bending of the entire beam by the perturbation patch, and occurs when the beam diameter is much less than the patch dimensions. The second mechanism, which might be called beam focusing and defocusing, is illustrated in figure 2-2. This phenomenon is characterized by a convergence or divergence of all or part of the beam front, and occurs when the beam diameter is on the same order as, or larger than, the patch dimensions.

If an optical receiver were set up to receive a laser beam propagating through the atmosphere, the scattering of the beam by refractive index perturbation patches would cause random fluctuations in the received signal level. The statistical character of these fluctuations would be a function not only of the spatial and temporal characteristics of the perturbation patches, but of the properties of the transmitter and receiver as well. Some of the more important effects of the transmitter and receiver are as follows:

a. Transmitter beam diameter and beam divergence - if the diameter of the beam at the transmitter is smaller than the perturbation patch dimensions, then beam bending can occur. Depending on the amount of beam divergence, the beam might be deflected off the receiver entirely. Furthermore, the beam might be bent several times, thereby changing the angle of arrival of the beam at the receiver. Of course, if the diameter of the beam at the transmitter is larger than the patch dimensions, then no significant bending can occur.
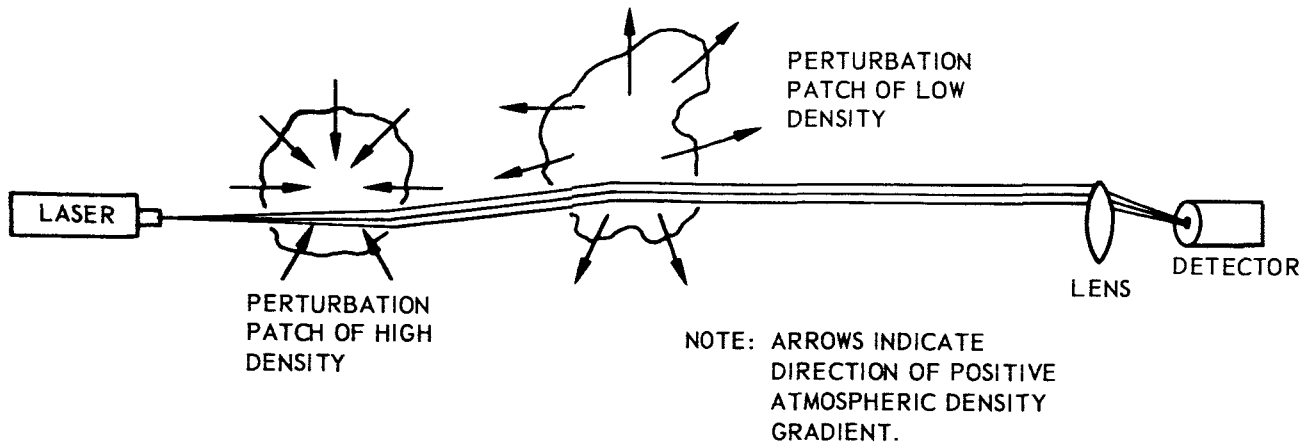
4

Figure 2-1. Beam Bending or Steering Induced by Atmospheric Perturbation Patches Which Are Much Larger Than the Beam Diameter
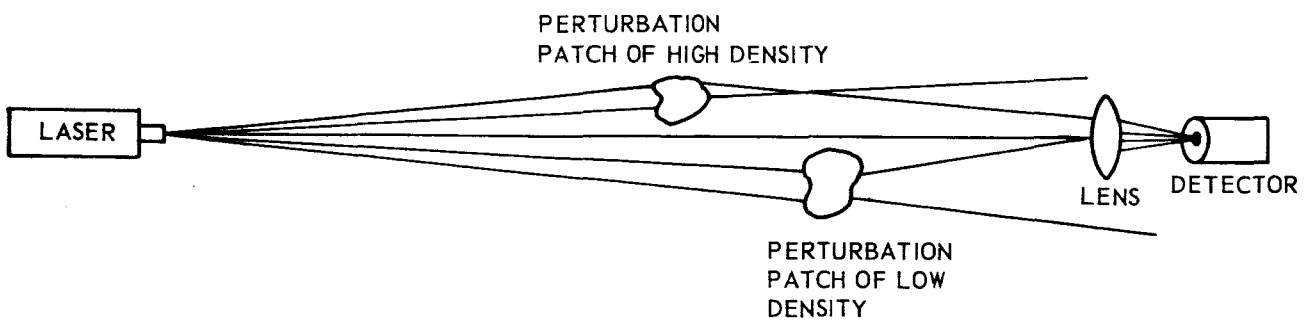
Figure 2-2. Introduction of Amplitude and Phase Distortions in the Beam Front by Atmospheric Perturbation Patches Which Are Smaller Than the Beam Diameter

5

b. Receiver angle of view - a large angle of view of the receiver will permit the receiver to collect energy over widely varying angles of arrival, thereby enhancing the collection of signal energy which has been scattered toward the receiver from the perimeter of the beam (see figure 2-2). Of course, a large receiver angle of view also enhances the collection of light originating from sources other than the transmitter.

c. Receiver aperture diameter - the greater the receiver aperture diameter, the greater is the ability of the receiver to average over a large number of the variations in amplitude and phase across the beam front. Hence, as the receiver aperture diameter is increased, the fluctuations in received signal level decrease. If the receiver diameter is large enough to collect all of the transmitted energy, then theoretically the fluctuations in received signal level cease completely.

d. Distance between transmitter and receiver (range) - as the distance between transmitter and receiver is increased, the number of scattering patches in the optical path increases. It therefore follows that the fluctuations in received signal level will increase with increasing range.

2.2 Previous Experimental Work

Several investigators have made experimental studies of laser wave propagation through the atmosphere. Hinchman and Buck (1964) reported preliminary results of an experiment which involved operating a He-Ne laser over 9- and 90-mile paths. They observed amplitude fluctuations which varied in frequency from a fraction of a cycle to several hundred cycles per second. They also observed both rapid and long-term beam bending. In a later report, Buck (1965) presented the results of this study in greater detail. Unfortunately, since the measurements over the two paths were performed at different times, no precise conclusions could be drawn about the effect of range on the statistics of the received signal.

Subramanian and Collinson (1965) performed an experiment which involved transmitting a He-Ne laser beam over 120- and 360-meter paths. They reported no detectable change in the statistics of the received signal as a function of range. However, it is to be expected that the extremely short ranges employed in this experiment might have obscured the effect of increasing range.

Edwards and Steen (1965) observed the effects of atmospheric turbulence on the transmission of incoherent visible and near-infrared radiation. They reported spectral components in the fluctuations in received signal up to several hundred cycles per second. However, range was not a parameter in these experiments, the measurements being performed over a fixed path length of about 300 meters.

Under certain conditions, the propagation of light through turbulent atmosphere is exactly analagous to the propagation of sound through a water medium which possesses a random temperature microstructure. Campanella (1965) measured the random variation in the amplitudes of sonic pulses propagated through a water medium in which was induced a nearly homogeneous random distribution of temperature perturbations. The measurements were carried out at frequencies of 480 kc and 1.42 Mc, and for transmitter to receiver separations ranging from 16 inches to 76 inches. He found, first, that the time autocorrelation of the received signal equalled the time autocorrelation of the temperature microstructure, and, second, that the variance in received signal was roughly proportional to the square of the range.

2.3 Previous Theoretical Work

A considerable amount of theoretical work has been done on the scattering of waves in random media. Bergman (1946) investigated optical scattering under the approximations of geometric optics, and predicted that the variance in amplitude fluctuations would be proportional to the cube of the range. Mintzer (1953 A and 1953 B) considered acoustic scattering in a random medium under the condition that only single scattering prevailed, and that the phases of the scattered arrivals were distributed over at least an interval of 0 to 2π. He predicted that the time autocorrelation of the received signal would equal the time autocorrelation of the refractive index of the medium, and that the variance in received signal would be directly proportional to range.

More recently, Tartarski (1961) investigated the propagation of coherent waves through turbulent atmosphere. His findings, as presented by Davis (1966), predicted that the variance in logarithmic amplitude level would be proportional to the 11/6 power of range for propagation paths horizontal to the earth surface.

3. DATA RECORDING AND PROCESSING SYSTEMS

3.1 General

Two data recording and processing systems were constructed. One of these systems was installed at the Laser Receiving Station at White Sands Missile Range, while the other was installed at the Laser Receiving Station on Ascension Island.

The purpose of these two systems was to record the signal pulse train arriving at the optical receiver, and to process the information contained in the received pulse train so as to make this information more readily amenable to post-flight analysis. Both systems are capable of:

    a. Directly recording the output of the MPT on video tape.

    b. Detecting the amplitude of each incoming pulse.

    c. Generating and recording a 2 kc tone burst for each incoming pulse, such that the initial amplitude of the tone burst is proportional to the amplitude of the pulse.

    d. Cross-correlating the periods between pulses.

    e. Generating a gate pulse train whose frequency and phase are identical with those of the signal pulse train.

In addition, the WSMR system includes equipment for:

    f. Generating five autocorrelation coefficients for each of the incoming pulses.

    g. Recording the five autocorrelation coefficients on a low noise, wide dynamic range, FM tape recording system.

3.2 Description of WSMR System

Figure 3-1 is a block diagram of the data recording and processing system installed at White Sands Missile Range. It is composed of six major subsystems:

    a. The amplification and pulse inversion subsystem.

    b. The video subsystem.

    c. The pulse period cross-correlator subsystem.

    d. The autocorrelator subsystem.

E5902

AMPLIFICATION AND PULSE INVERSION SUBSYSTEM

FROM
MPT
PRE-AMP

WSMR
INTERFACE
AMPLIFIER

50 FT. RG58

PULSE
INVERTER

MAIN
DRIVER
AMP.

VIDEO
PRE AMP

TIME-VOICE MIX SUBSYSTEM

STANDARD
TIME
SIGNAL

TIME-VOICE
MIXING
CIRCUIT

MICROPHONE

PULSE

FIRST
PULSE
STRETCHER

MPT
AGC
VOLTAGE
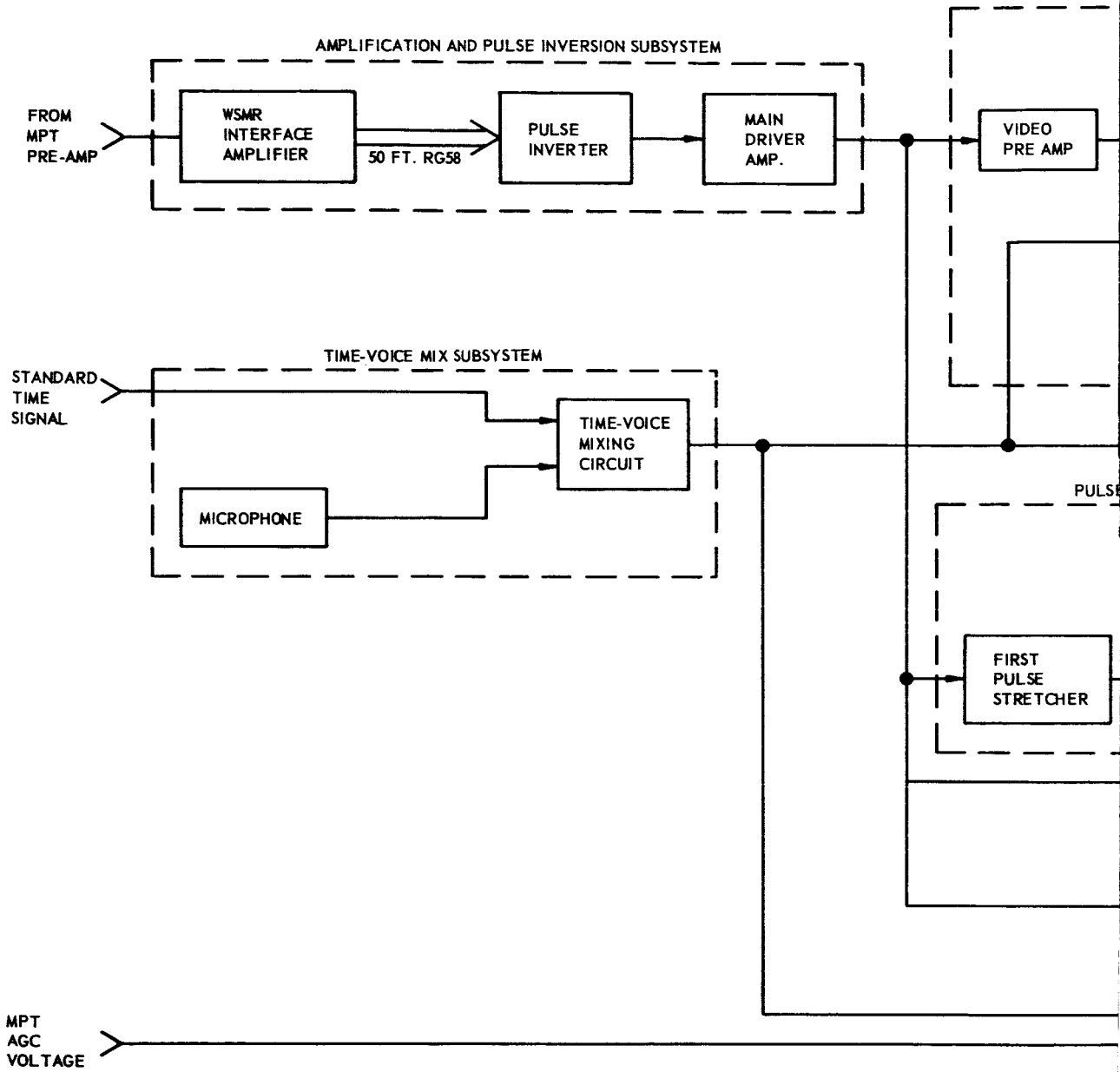
9-1

Figure 3-1. WSMR Data Recording and Processing System

e. The AM and FM audio recording subsystem.

f. The time-voice mix subsystem.

The output of the MPT preamplifier is fed into the amplification and pulse inversion subsystem. This subsystem then drives the inputs to the video subsystem, the pulse period cross-correlator subsystem, and the auto-correlator subsystem. The output of the 2-kc tone generator in the pulse period cross-correlator subsystem is recorded by one channel of the AM audio recorder, while the synchronous pulse train output of the pulse period cross-correlator is used to drive the autocorrelator gate circuit and the external sync of an oscilloscope. The five autocorrelation coefficient outputs of the autocorrelator are recorded on five channels of the FM audio recorder. The output of the time-voice mix subsystem is recorded on the audio channel of the video recorder, on one channel of the AM audio recorder, and on one channel of the FM audio recorder. The final channel of the FM audio recorder is used to record the control voltage of the AGC system for the MPT.

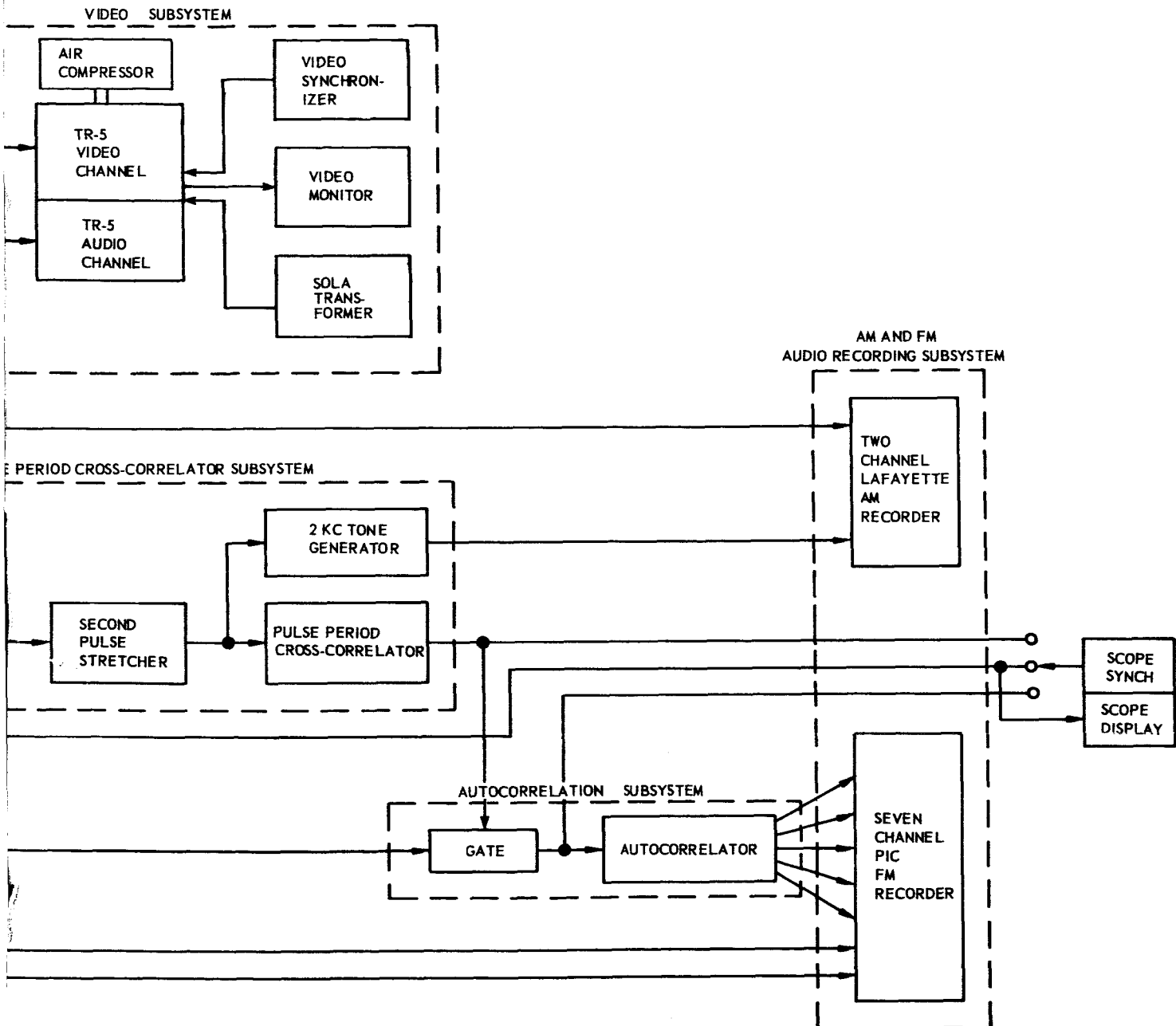The dynamic recording range of the video channel of the RCA TR-5 recorder is 10 to 1 (input levels from 0.1 to 1.0 volt). It was therefore decided to design both the pulse period cross-correlator subsystem and autocorrelator subsystem to operate over the range of 0.1 volt to 1.0 volt. The gain of the main driver amplifier is manually selected so that the average signal pulse level is approximately 0.3 volt, thereby assuring that perturbations in received signal level which are 10 db above or below the average level will be within the operating dynamic range of the video and correlation subsystems.

Figures 3-2, 3-3, 3-4, and 3-5 are photographs showing the WSMR system as it was actually installed at the Melpar Field Laboratory at White Sands. Figures 3-6 and 3-7 are views of the main driver amplifier chassis, on which are mounted the pulse inverter, main driver amplifier, video preamplifier, first pulse stretcher, autocorrelator, and autocorrelator grid bias supplies. Figures 3-8, 3-9, and 3-10 are views of the pulse period cross-correlator chassis.

3.3 Description of Ascension Island System

Figure 3-11 is a block diagram of the data recording and processing system installed at Ascension Island. It is identical to the WSMR system, except that it does not include an autocorrelator subsystem, a seven-channel FM audio recorder, or an interface amplifier. The elimination of the interface amplifier at Ascension Island was made possible by the fact that the Melpar system was housed in the same building as the NASA system; hence, interconnections between the two systems could be made directly without introducing any serious reflections or loading.
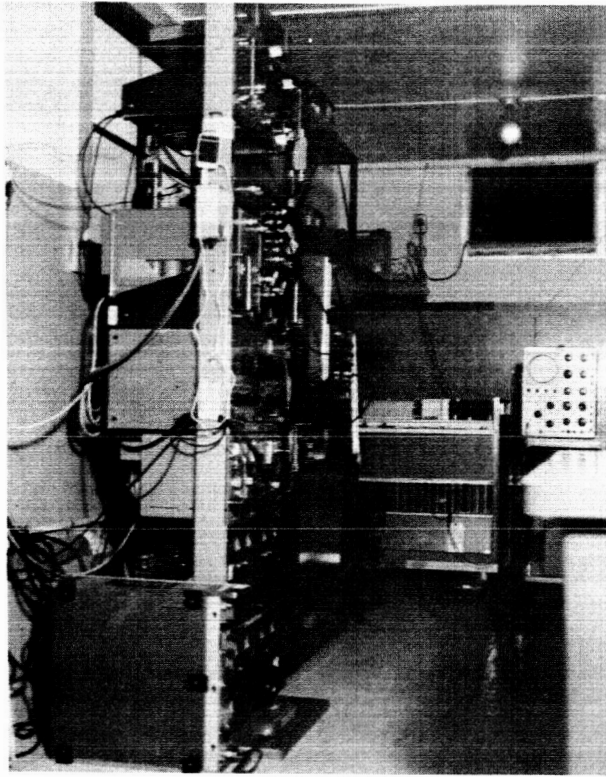
Figure 3-2. Overall View of WSMR Field Laboratory

Figure 3-3. Autocorrelator and Pulse Period Cross-Correlator Subsystem in Operation

11
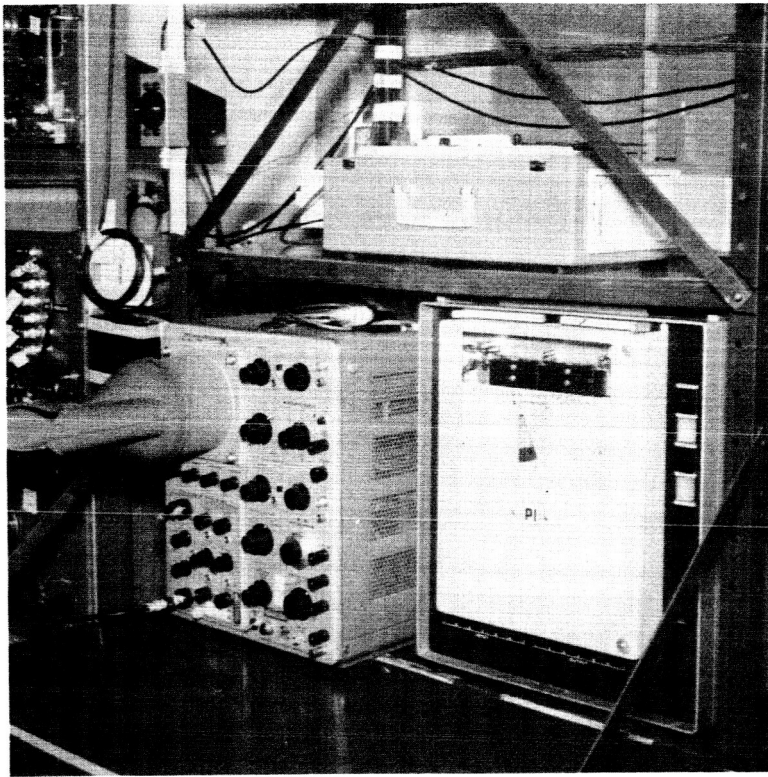
Figure 3-4. AM and FM Audio Recorders
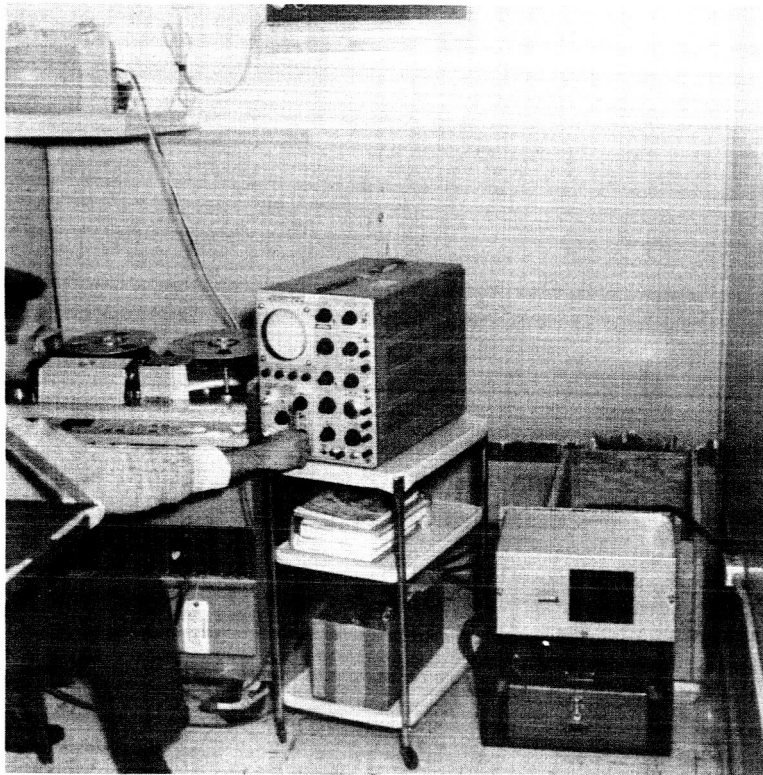
Figure 3-5. Video Recording System in Operation

12
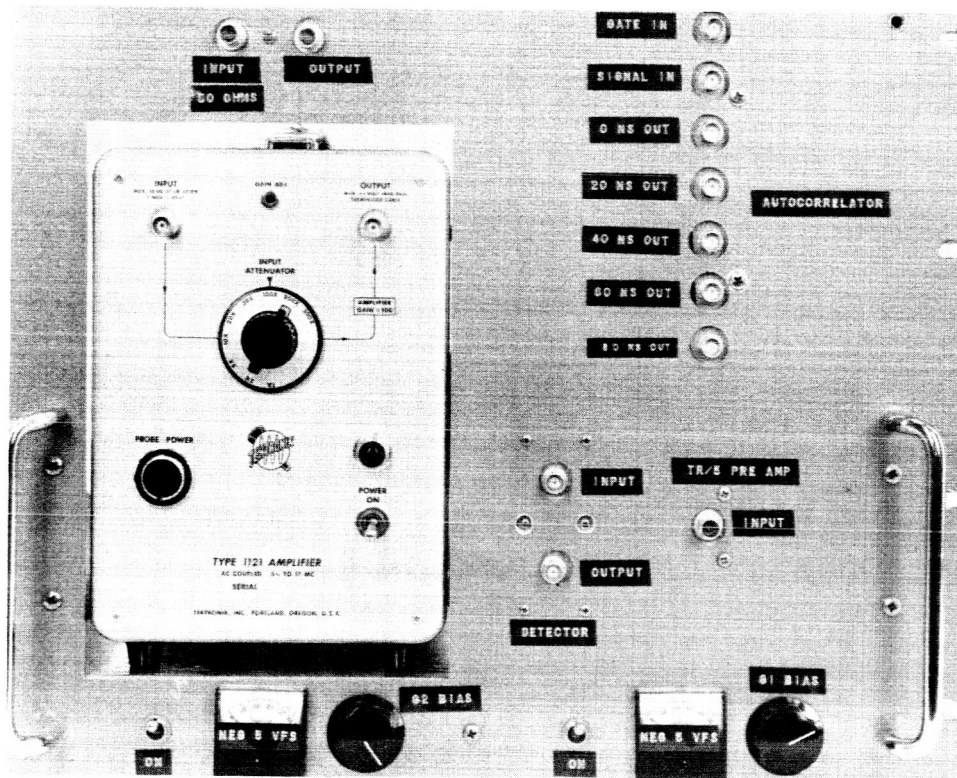
Figure 3-6. Front View of Main Driver Amplifier Chassis
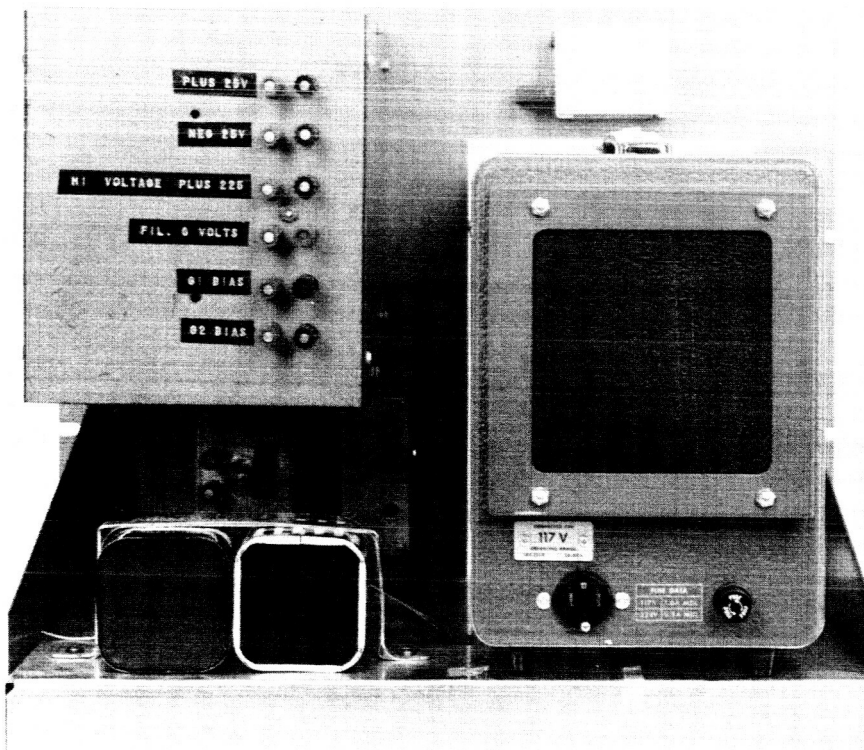
Figure 3-7. Rear View of Main Driver Amplifier Chassis
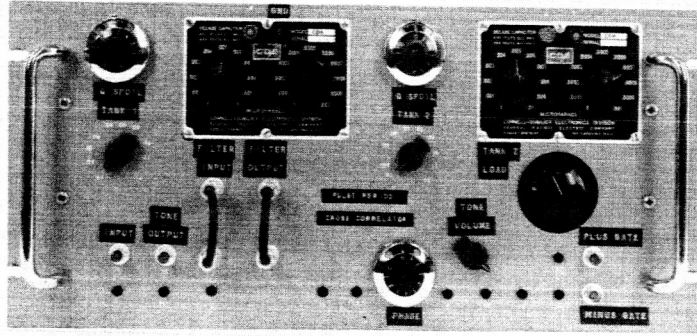
Figure 3-8. Front View of Pulse Period Cross-Correlator Chassis

5591.00100-13
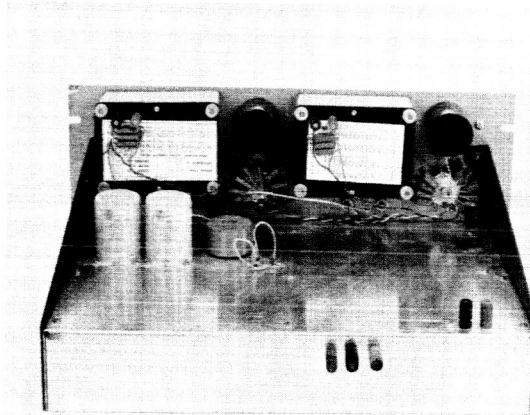
Figure 3-9. Rear View of Pulse Period Cross-Correlator Chassis

5591.00100-7
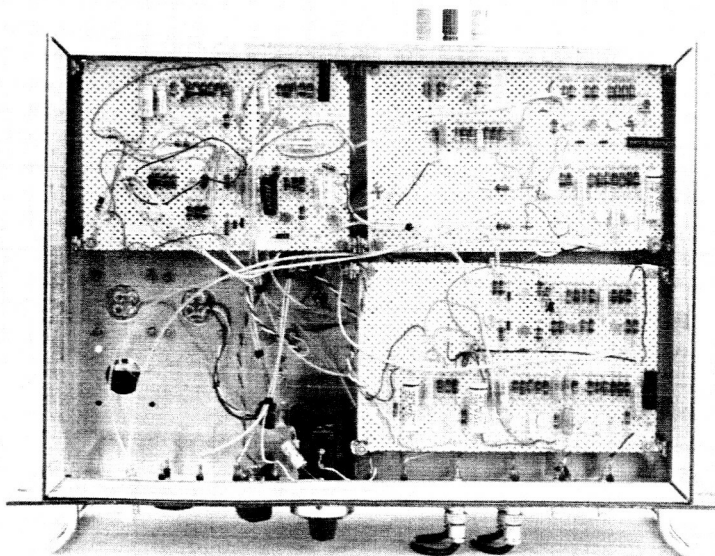
Figure 3-10. Bottom View of Pulse Period Cross-Correlator Chassis
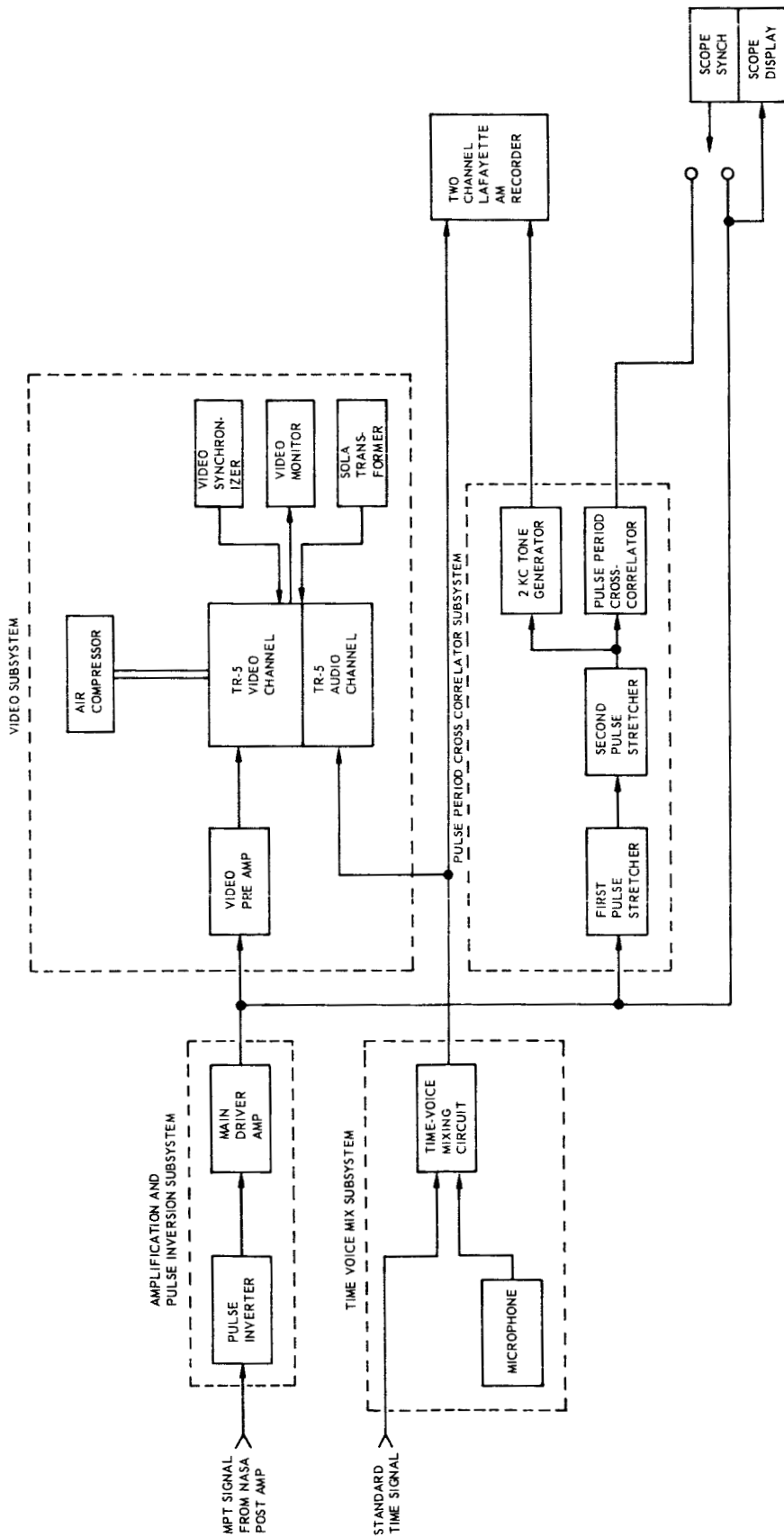
Figure 3-11. Ascension Island Data Recording and Processing System

3.4 Amplification and Pulse Inversion Subsystem

The amplification and pulse inversion subsystem comprises the WSMR interface amplifier, the pulse inverter, and the main driver amplifier.

Figure 3-12 is a schematic of the WSMR interface amplifier. This amplifier was located in the NASA field van, and tapped off the signal arriving at the NASA post-amp from the MPT preamp. The interface amplifier was carefully designed to have an output impedance of 50 ohms.

Figure 3-13 is a schematic of the pulse-inverter circuit. The purpose of the inverter is to change incoming negative pulses into positive pulses. If the incoming signal happens to consist of positive pulses, then the pulse inverter is bypassed, and the signal is connected directly to the input of the main driver amplifier.

The main driver amplifier consists of a Tektronix 1121 wideband amplifier, which has a gain of 100, and a passband from 5 cps to 17 Mcs. It also features a built-in 0 to 32 db attenuator which can be varied in steps of approximately 6 db. The main driver amplifier is capable of a 1-volt output into 93 ohms.

During system operation, the system operator monitors the output of the main driver amplifier on the oscilloscope (shown in figure 3-1), and adjusts the attenuator of the main driver amplifier so that the average output is approximately 0.3 volt. The operator then records the position of the attenuator by speaking into the microphone of the time-voice mix subsystem. These are the only functions the operator must perform during normal system operation, since the video and correlation subsystems are all designed to operate automatically with input signals 10 db above or below 0.3 volt.

3.5 Video Subsystem

3.5.1 Video Preamp

Figure 3-14 is a schematic of the video preamp. It has a high input impedance, so as not to load the output of the main driver amplifier, and a 75-ohm output impedance, in order to drive the 75-ohm cable leading to the 75-ohm "video input" terminal of the TR-5. The video preamp has a gain of approximately 1 when operated into a terminated 75-ohm line.

3.5.2 RCA TR-5 Recorder

The RCA TR-5 recorder is a general-purpose video FM recorder. It permits the recording of one channel of video information (with a bandwidth of 5.5 mcs) and one channel of audio information on the same strip of 2-inch-wide magnetic tape. The dynamic recording range of this instrument is from 0.1 volt to 1 volt. In order to provide maximum
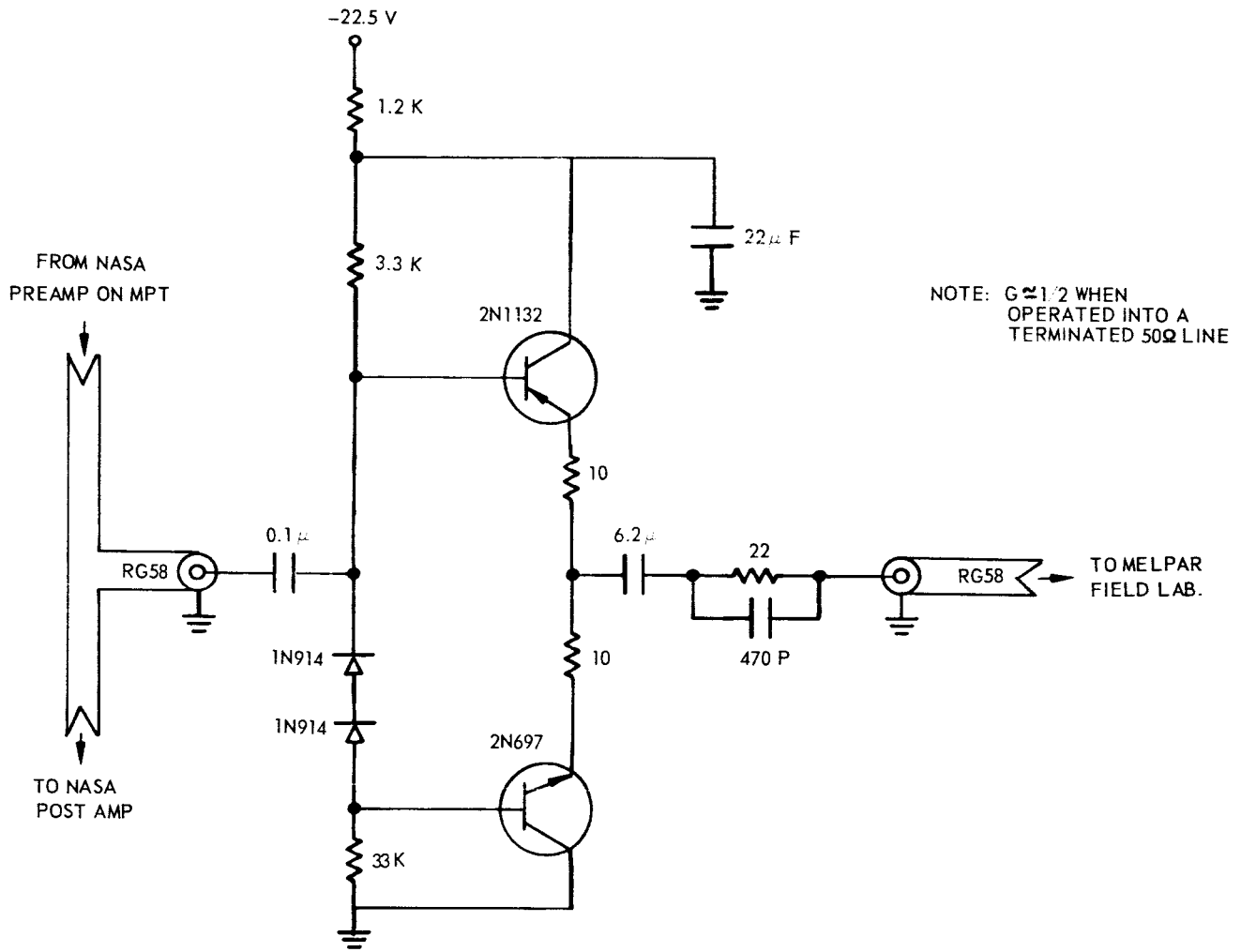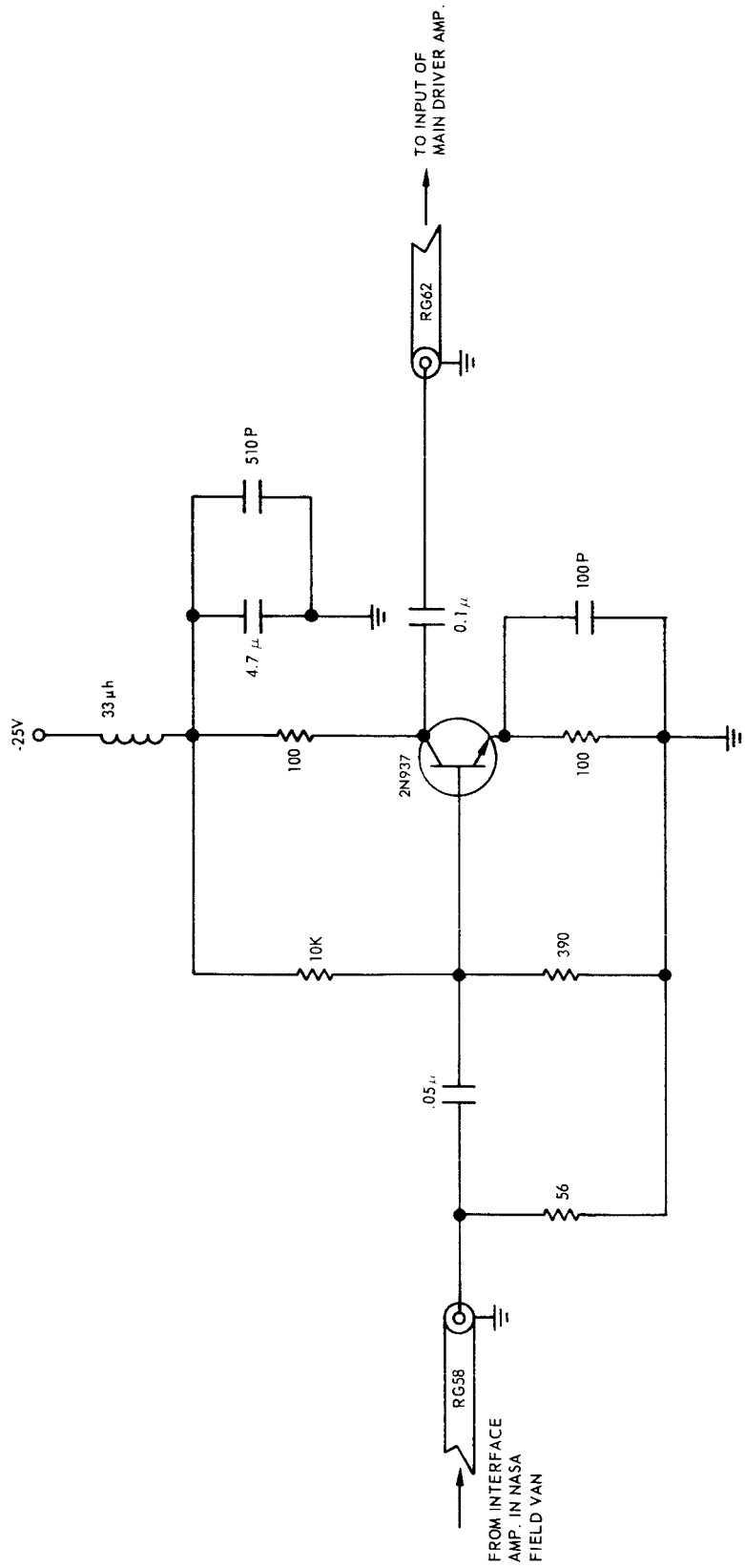
Figure 3-12. WSMR Interface Amplifier
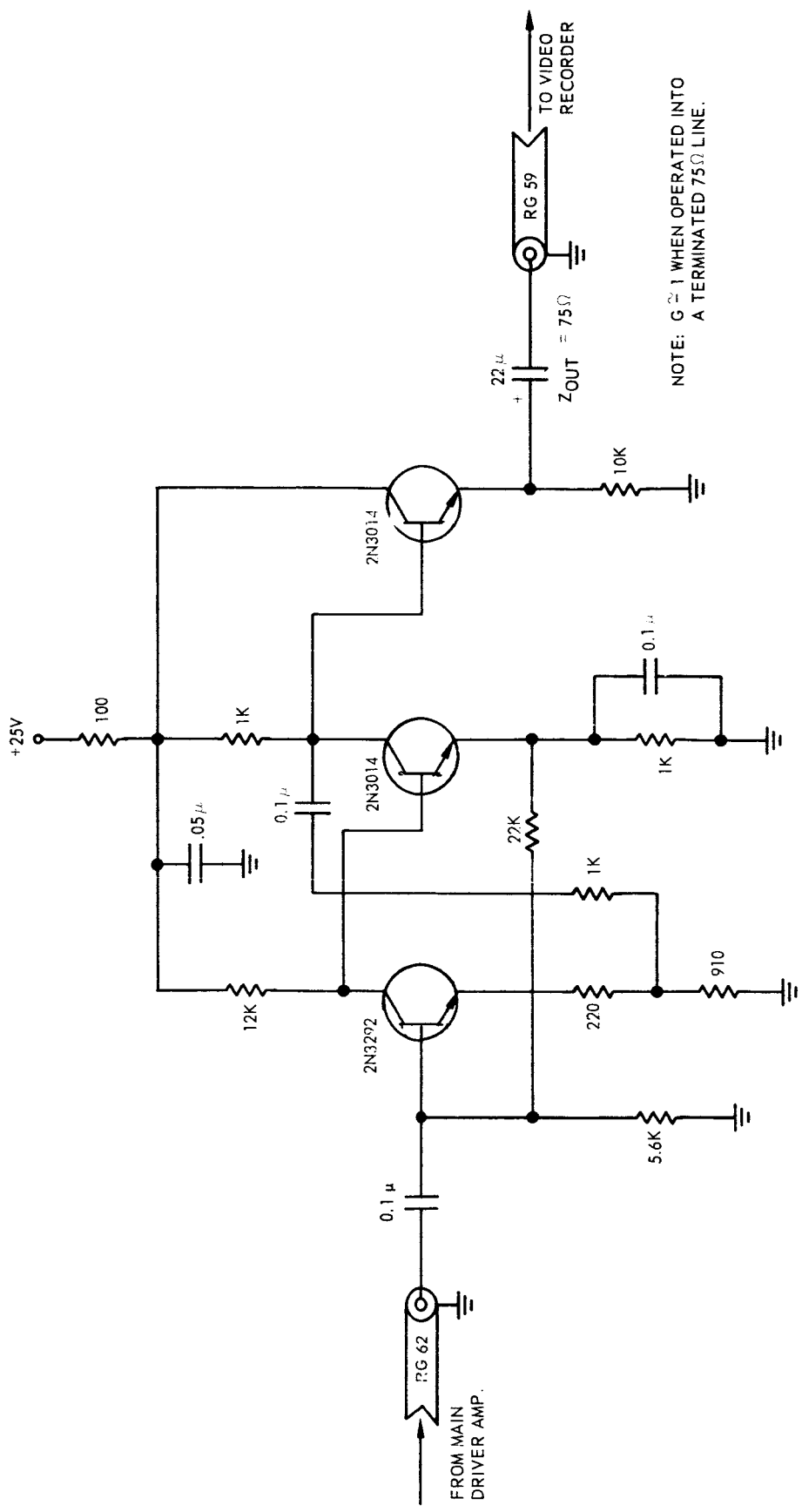
Figure 3-13. Pulse Inverter

Figure 3-14. Video Preamp

recording stability and tape life, both TR-5 recorders used in the present systems were provided with special air bearing conversion kits. The compressors shown in the video subsystems shown (figures 3-1 and 3-11) constitute part of the air bearing conversion kits.

The TR-5 was originally designed for recording television signals. In order that the instrument might be suitable for the recording and playing back sequences of 100-ns pulses, a number of modifications were necessary, as follows:

a. The magnetic headwheel of the instrument consists of four separate heads, each occupying approximately one-fourth of the circumference of the wheel. During recording, all four wheels are driven in parallel; however, during playback, the machine must switch from the head that is finishing its travel across the tape to the head that is just beginning its travel across the tape. In order to maintain continuity of signal, this switching must take place during the overlap time when both heads are scanning the tape. In addition, the switching must take place in phase with one of the horizontal sync pulses of the recorded television signal, so that the transient pulse which is generated by the switching action does not appear on the television screens of the audience. Therefore, the switching between heads is triggered by a coincidence multivibrator, which puts out a pulse in phase with the first horizontal sync pulse that occurs after the beginning of the overlap period between two adjacent heads. The beginning of the overlap period is signaled by the 4X tone wheel multivibrator, which in turn is triggered by the output of a tone wheel mounted on the headwheel. Since horizontal sync pulses would not be present in the 100-ns pulse-train data, it was decided to eliminate the coincidence multivibrator altogether and simply trigger the switching processes with the output of the 4X tone wheel multivibrator. Therefore, switching would take place precisely at the beginning of each overlap period. Specifically, the following modifications were performed within the FM Switcher, Module D-10: (1) broke connection between R147 and C81, thereby disconnecting output of 960-H from the input of the head switching circuit; (2) connected external connection no. 28 through C82 and C81 to base of Q36, thereby connecting output of the 4X tone wheel multivibrator to the input of the head switching circuit.

b. In order to maintain stable recording and playback both the head-wheel servo and capstan drive must be synchronized with some stable reference signal. The source of this reference signal is chosen by the "Internal-External" switch on the Reference Generator Module. During recording, the instrument is synchronized with either the vertical sync pulses of the incoming television signal (switch in "Internal" position) or by the vertical sync pulses from the 60-cps station master clock (switch in "External" position). During playback, the instrument is synchronized with either an internal oscillator (switch in "Internal" position), or by the vertical sync pulses from the 60-cps station master clock (switch in "External" position). In order to provide maximum stability during recording and playback of the 100-ns pulse data, a special 240-cps video synchronizer was acquired (see section 3.5.4). In order to permit the recorder to be synchronized with

this special video synchronizer, and in order that the recorder not load the output of the synchronizer, the following modifications were performed in the Reference Generator, Module D-16: (1) added 1.5-uf capacitor across C10 in vertical multivibrator; (2) disconnected R43 from R44, and shorted R44; (3) connected common side of A section of S1 directly to C11 and C1; and (4) grounded both throw poles of B section of S1.

3.5.3 Video Switch Pulse Gating Circuit

Figure 3-15 is a schematic of the video switch pulse gating circuit.

When the FM switcher of the TR-5 switches from one head to the next during playback, a switch pulse is generated at the output of the recorder. This video switch pulse can be extremely annoying when the recorded signal itself is a sequence of pulses. The purpose of the video switch pulse gating circuit is to prevent the video switch pulse from appearing at the output. The circuit achieves its purpose by simply shorting the output during the time the video switch pulse occurs.

With the modifications described in section 3.5.2, part (a), the FM switcher is triggered by the 4X tone-wheel multivibrator. Therefore, the video switch pulse occurs in phase with the output of the 4X tone wheel multivibrator. Therefore, in order to gate out the video switch pulse, the video switch pulse gating circuit is also triggered by the output of the 4X tone wheel multivibrator (collector of transistor Q-36, Reference Generator, Module D-16).

It will be noted that the video switch pulse gating circuit does not appear in either the WSMR or Ascension Island systems (figures 3-1 and 3-11). Since this circuit is needed only for laboratory analysis of recorded pulse data, it was not incorporated into the field systems.

3.5.4 Other Video Subsystem Components

The video synchronizer is a 240-v cps tuning-fork oscillator, Melpar model no. 925, which exhibits a long-term stability of 1 part in 10^5. It is powered by a 22.5-volt battery.

The video monitor is an RCA model AGOO5J New Vista television set. It is used as a television display for the video output of the TR-5 recorder during playback of the alignment tape. It also provides a source of video signals for aligning the recording sections of the TR-5. The set was modified for use as a video monitor by installing a connection from the input to the video strip inside the set to a BNC output jack on the back of the set.

The Sola transformer is a Sola Corporation model 23-25-230-3, 3-kVA, isolation-regulation transformer. Its purpose is to provide the TR-5 with distortion-free, constant-voltage, line power while operating in the field.
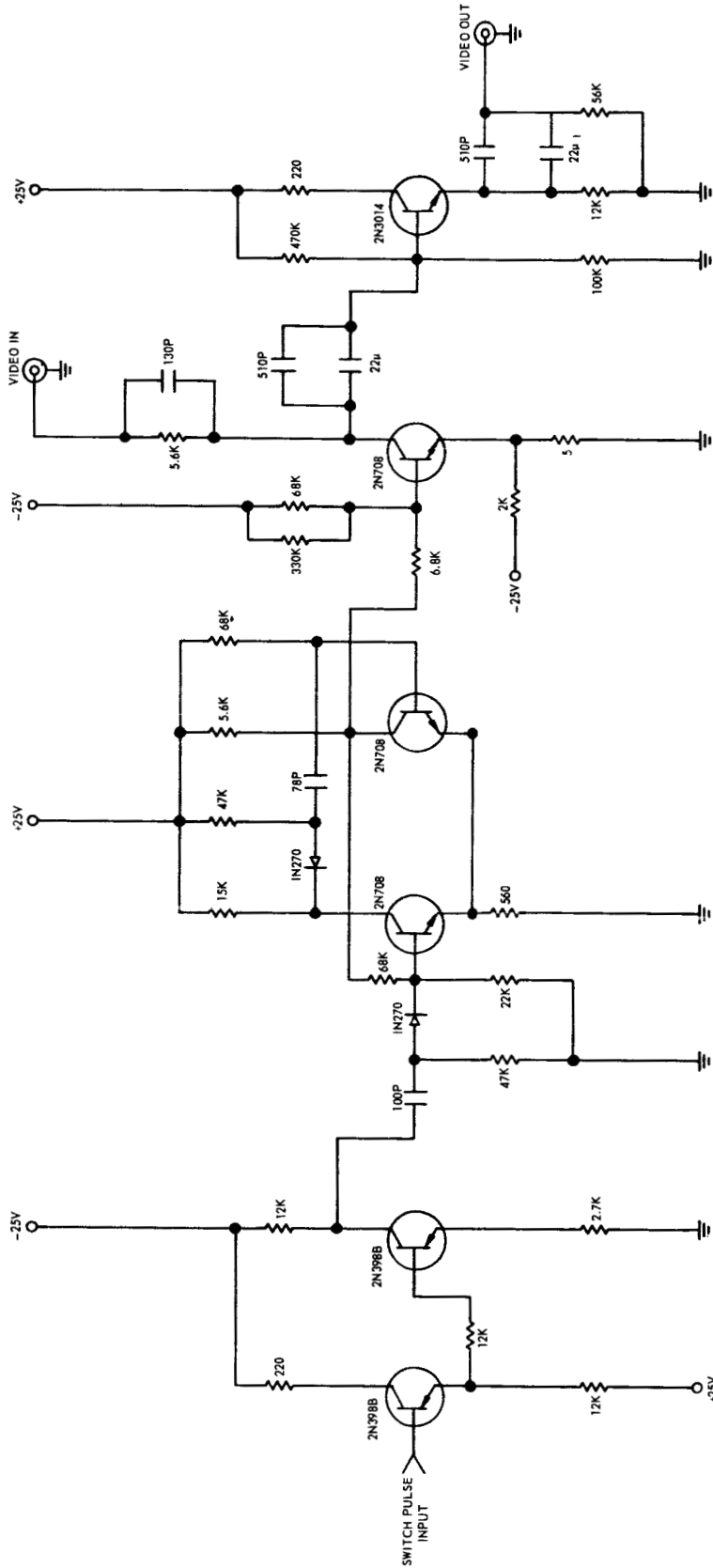
NOTES 1. "VIDEO IN" TERMINAL IS DRIVEN BY A TERMINATED 75Ω
LINE FROM THE "VIDEO OUT" TERMINAL OF THE TR-5

2. "SWITCH PULSE IN" TERMINAL IS DRIVEN BY THE OUT-
PUT OF THE 4X TONE WHEEL MULTIVIBRATOR (COL-
LECTOR OF TRANSISTOR Q-36) IN THE REFERENCE
GENERATOR MODULE (D-16).

3. "VIDEO OUT" TERMINAL HAS A 75Ω OUTPUT IMPEDANCE.

Figure 3-15. Switching Transient Gating Circuit

3.6 Autocorrelator Subsystem

3.6.1 Theoretical Considerations

The autocorrelation function, $\phi_{ff}(\tau)$, for a square integrable function, $f(t)$, can be represented by

$$\phi_{ff}(\tau) = \int_{-\infty}^{+\infty} f(t) \, f(t+\tau) \, dt \qquad (3\text{-}1)$$

Since $\phi_{ff}(\tau)$ is clearly symmetric about $\tau = 0$, it may be rewritten as

$$\phi_{ff}(\tau) = \int_{-\infty}^{+\infty} f(t) \, f(t-\tau) \, dt \qquad (3\text{-}2)$$

Finally, if $f(t) = 0$ for $t < 0$, the autocorrelation function becomes

$$\phi_{ff}(\tau) = \int_{0}^{+\infty} f(t) \, f(t-\tau) \, dt \qquad (3\text{-}3)$$

For example, suppose $f(t)$ is given by

$$f(t) = H \left[u(t) - u(t-T) \right] \qquad (3\text{-}4)$$

that is, $f(t)$ is a square pulse H units high of T seconds duration. Then, the autocorrelation function corresponding to $f(t)$ is given by

$$\phi_{ff}(\tau) = H^2(T - |\tau|) \text{ when } \quad |\tau| \leq T \qquad (3\text{-}5)$$
$$= 0 \qquad \text{ when } \quad |\tau| \geq T$$

Now, let $f(t)$ be a Gaussian pulse, given by

$$f(t) = A \exp\left[- \frac{(t-\mu)^2}{2\sigma^2} \right] \qquad (3\text{-}6)$$

Then the corresponding autocorrelation function is

$$\phi_{ff}(\tau) = A^2 \sigma \sqrt{\pi} \; \exp\left[- \frac{\tau^2}{4\sigma^2} \right] \qquad (3\text{-}7)$$

which is seen to be a Gaussian pulse centered at the origin, and having a standard deviation which is $\sqrt{2}$ times the standard deviation of $f(t)$. Figure 3-16 illustrates the Gaussian pulse and its autocorrelation function under the conditions $A = 1$, $\sigma = 1$, and $\mu = 4$.

The purpose of the autocorrelator in the data recording and processing system is to detect multipath arrivals of Gaussian signal pulses. The two-arrival case can be represented by

$$g(t) = A \exp\left[- \frac{(t-T_1)^2}{2\sigma^2}\right] + B \exp\left[- \frac{(t-T_1-T)^2}{2\sigma^2}\right] \qquad (3\text{-}8)$$

where T represents the delay in arrival of the second pulse relative to the first. The autocorrelation function for this double Gaussian pulse is given by

$$\phi_{gg}(\tau) = (A^2+B^2)\ \sqrt{\pi}\ \sigma\ \exp\left[- \tau^2/4\sigma^2\right]$$
$$+ AB\ \sqrt{\pi}\ \sigma\ \exp\left[- \frac{(\tau+T)^2}{4\sigma^2}\right] + AB\sqrt{\pi}\ \sigma\ \exp\left[- \frac{(\tau-T)^2}{4\sigma^2}\right] \qquad (3\text{-}9)$$

which is seen to be a two-sided double Gaussian pulse, centered at the origin, and with secondary maxima at $\tau = \pm T$. Figure 3-17 illustrates the double Gaussian pulse and its autocorrelation function under the conditions $A = 1$, $B = 0.5$, $\sigma = 1$, $T_1 = 4$, and $T = 6$.
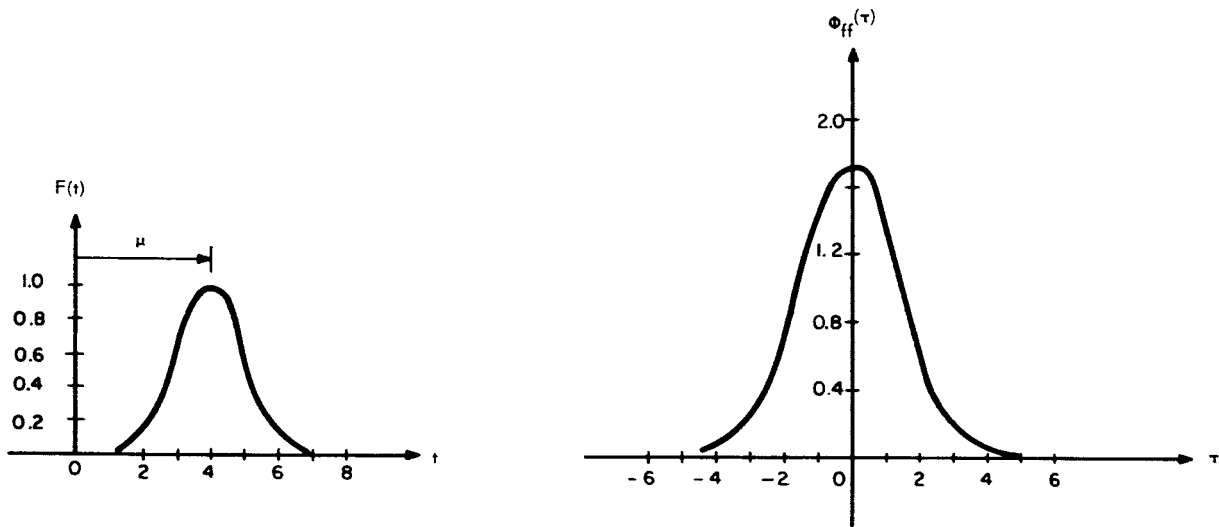
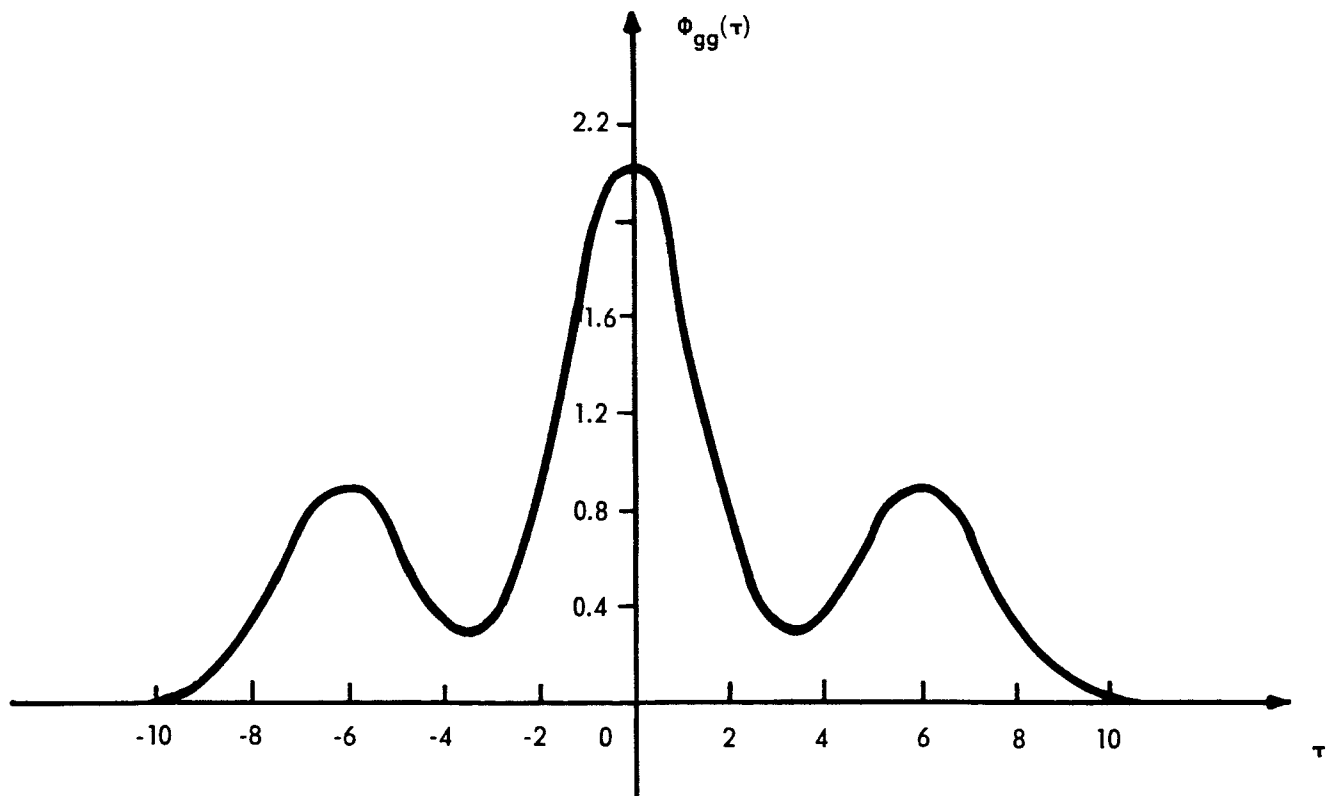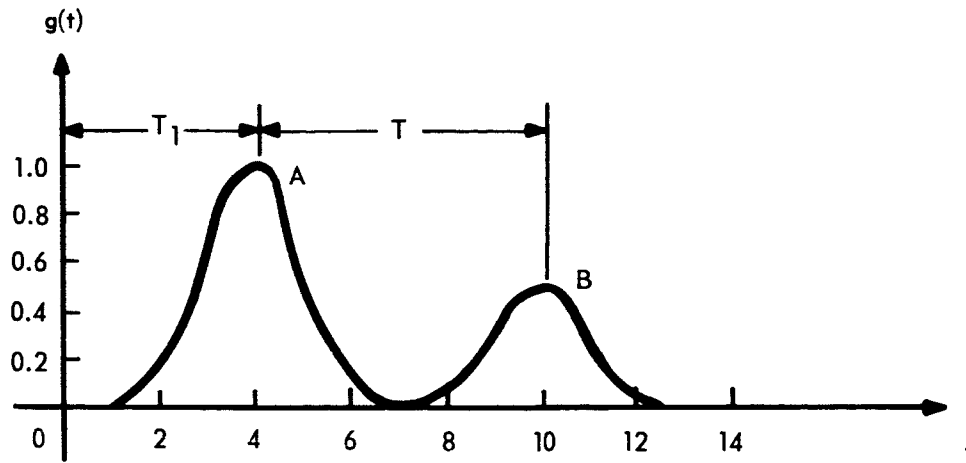Figure 3-16. Gaussian Pulse and Corresponding Autocorrelation Function

Figure 3-17. Double Gaussian Pulse and Corresponding Autocorrelation Function

3.6.2 General Description of Autocorrelator

The pulses emitted by the hand-held laser transmitter are approximately Gaussian in shape, and have a pulse width on the order of 100 nanoseconds. It would be extremely difficult to resolve multiple arrivals of these pulses for which the delay time between arrivals was less than 20 nanoseconds. On the other hand, the theoretical considerations presented in section 1 would indicate that delay times greater than 80 nanoseconds are extremely improbable. Therefore, the delay times (arguments) for the five autocorrelation coefficient outputs of the autocorrelator were chosen as 0, 20, 40, 60, and 80 nanoseconds.

Figure 3-18 is a block diagram of a theoretical autocorrelator. This device performs the mathematical operation described in equation 3-3 for τ = 0, 20, 40, 60, and 80 nanoseconds.

Figure 3-19 is a block diagram of the autocorrelator which was actually constructed. The performance of this device is identical to that of the theoretical autocorrelator, with two exceptions:

a. Only positive input signals are autocorrelated. This exception is not important when the input signals are positive pulses.

b. The integrators of the practical autocorrelator have finite storage times ($\sim$4 microseconds) that are long compared to the duration time of the individual signal pulses ($\sim$100 nanoseconds), but that are short compared to the pulse repetition rate (100 pps). Therefore, each incoming signal pulse is individually autocorrelated, and the autocorrelation coefficient outputs for a particular pulse are not functions of the autocorrelation coefficients of any previous pulses.

The principal problem area in the development of this practical auto-correlator was the pulse multiplying circuits. The first requirement of any multiplier is that its output be proportional to the product of two inputs. This requirement necessitates that the output be zero when either or both of the two inputs are zero. Hence, if some active element having two control terminals is to be used as a multiplier, the element must be operated near its cutoff point with respect to both of the control terminals. The 7587 nuvistor tetrode chosen as the multiplying element exhibits a square-law characteristic when operated near cutoff with respect to either grid; therefore, a compensating square-root circuit was provided so that the output of each multiplier is essentially linearly proportional to both of its inputs.

The incoming signal (shown in Figure 3-19 as a 100-nanosecond 1-volt square pulse) enters the autocorrelator at the gate circuit driver amplifier. The purpose of this emitter-follower amplifier is to present a high impedance load to the signal source. The signal then passes into the gate circuit. The purpose of the gate circuit is to permit the free passage of signal pulses while preventing the passage of noise pulses. After passing through the
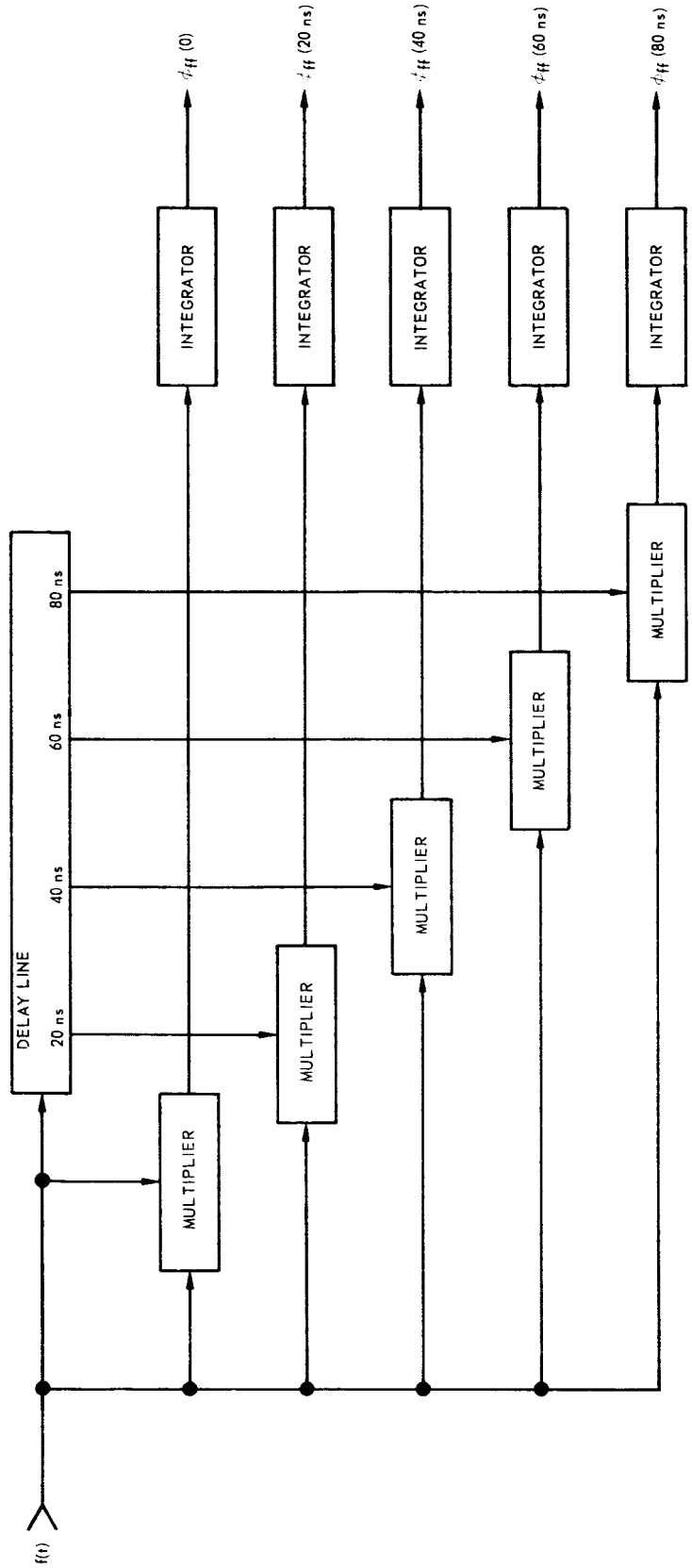
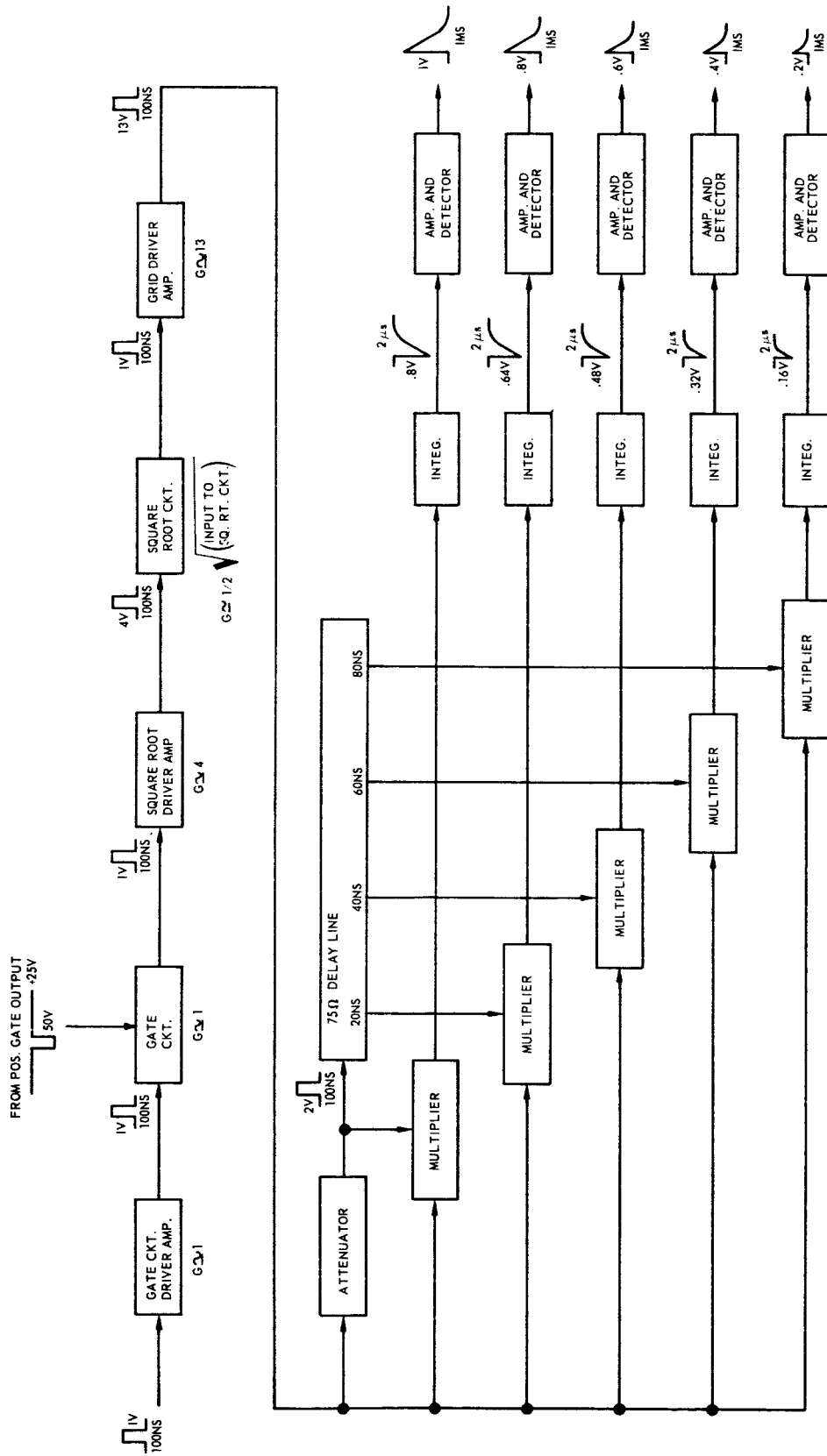Figure 3-18. Theoretical Autocorrelator Block Diagram

Figure 3-19. Practical Auto Correlator Block Diagram

square-root driver amplifier and square-root circuit, the signal is amplified to a high level by the grid driver amplifier. At this point part of the signal is attenuated and fed to the delay line, where it is tapped off at various delay points and fed to the low level control grids of the multipliers. The main output of the grid driver amplifier is fed directly to the high level screen grids of the multipliers. The multiplier outputs are then fed to the integrators, which in turn produce output pulses whose heights are proportional to the integral of the multiplier outputs. Finally, in order to permit the recording of the integrator outputs by audio FM machines, the integrator output pulses are stretched by the amplification and detection circuits. Calibration of the entire autocorrelator is achieved by feeding a train of 100-nanosecond 1-volt square pulses into the autocorrelator, and then adjusting the gain control potentiometers on the amplification and detection circuits so that the five outputs are proportional to the corresponding theoretical values.(equation 3-5).

Figures 3-20, 3-21, 3-22, and 3-23 are photographs of the exterior and interior of the autocorrelator. Figures 3-24, 3-25, 3-26, 3-27, and 3-28 are schematic diagrams of the various autocorrelator circuits. Figure 3-29 illustrates the waveforms appearing at various test points in the autocorrelator for a 100-ns 1-volt square-pulse input. Figure 3-30 illustrates the relative response of the autocorrelator outputs as a function of input pulse height. Figure 3-31 compares the actual autocorrelator outputs with the theoretically predicted autocorrelation function for a double Gaussian pulse input.

3.7 Pulse Period Cross-Correlator Subsystem

General Description

The purpose of the pulse period cross-correlator subsystem is threefold:

a. To provide a 2-kc tone burst each time a signal pulse arrives.

b. To detect the periodicity and phase of the signal pulse train in the presence of noise pulses.

c. To provide a gate pulse train precisely in phase with the signal pulse train. This gate pulse train is then used to actuate the autocorrelator gate circuit, and to trigger an oscilloscope display.

Figure 3-32 is a block diagram of the pulse period cross-correlator subsystem. After being stretched to millisecond lengths by the first and second pulse stretchers, the signal is fed to both the Zero Phase Filter (ZPF) preamp, and the 2-kc tone generator. Within the tone generator, the pulses are used to drive a 2-kc tuned tank. The output of the tone generator is an exponentially damped 2-kc wave with a time constant of about 6 milliseconds.
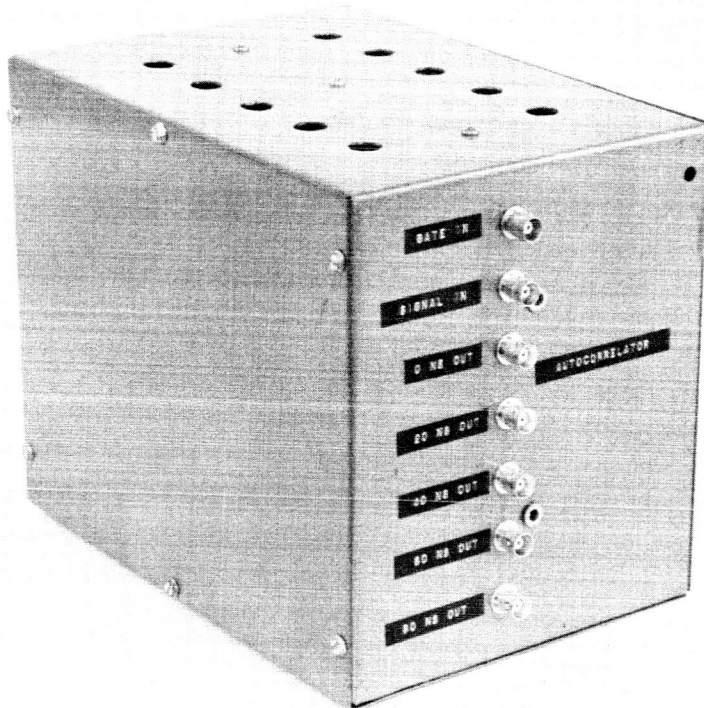
Figure 3-20. Front View of Autocorrelator

5591.00100-8
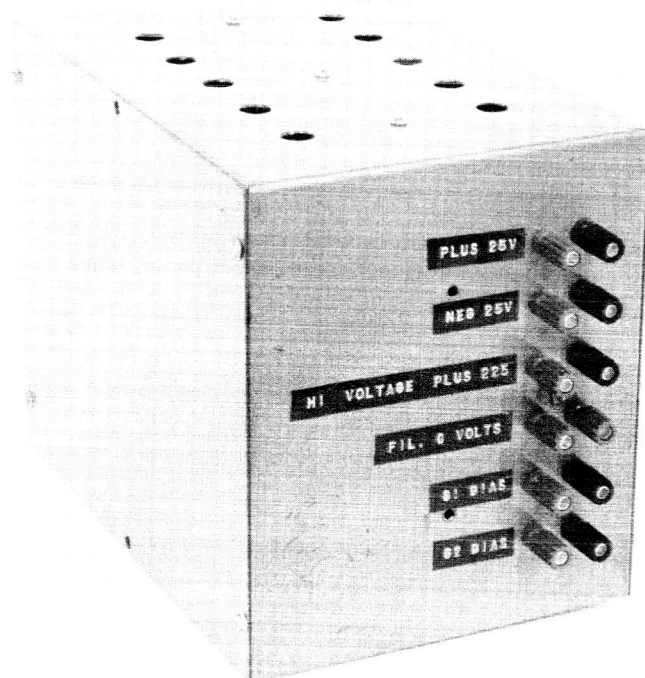
Figure 3-21. Rear View of Autocorrelator
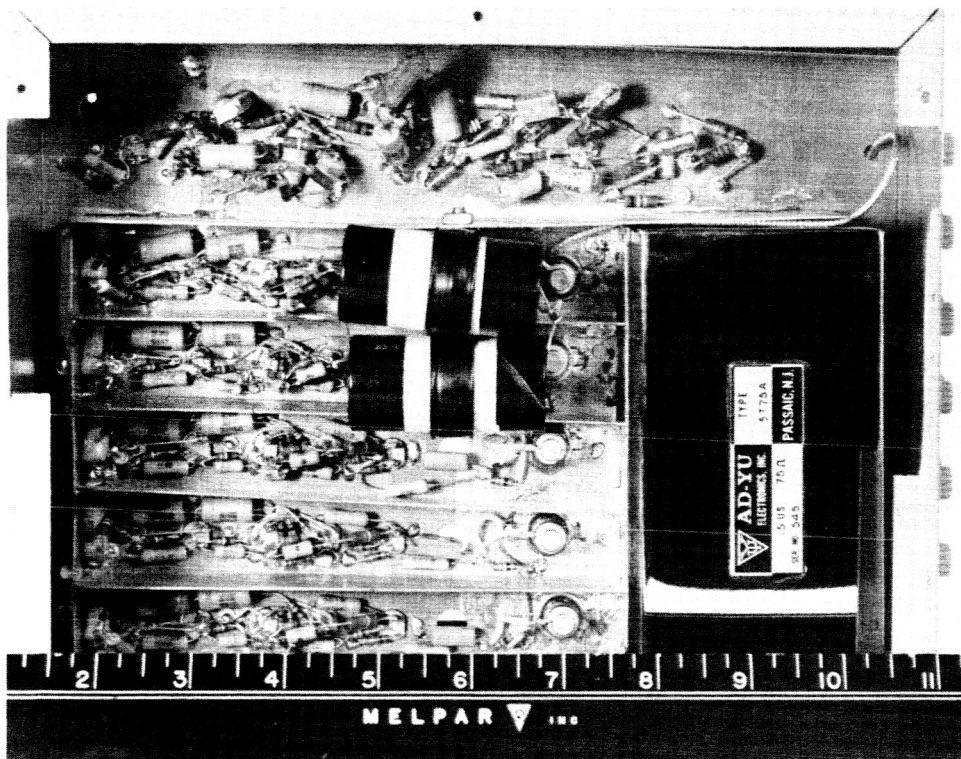
Figure 3-22. Right Side Interior View of Autocorrelator
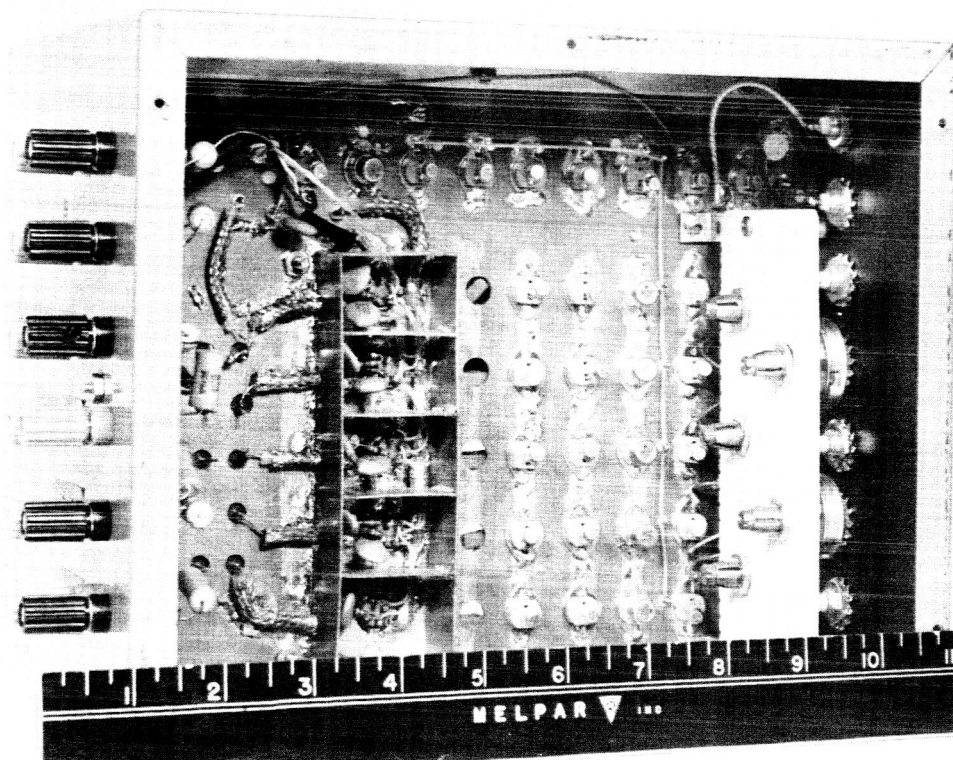
Figure 3-23. Left Side Interior View of Autocorrelator
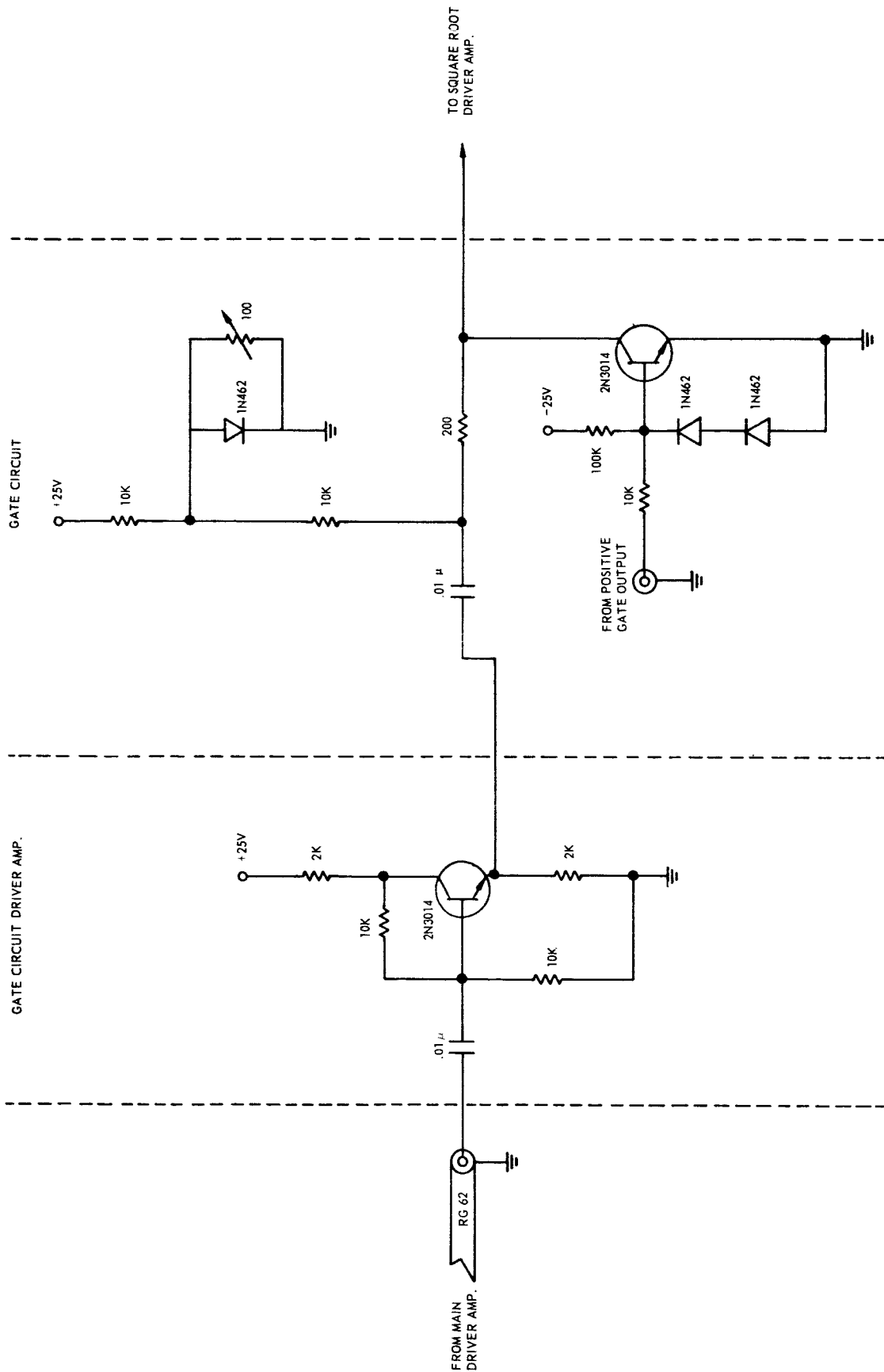
Figure 3-24. Gate Circuit Driver Amplifier and Gate Circuit
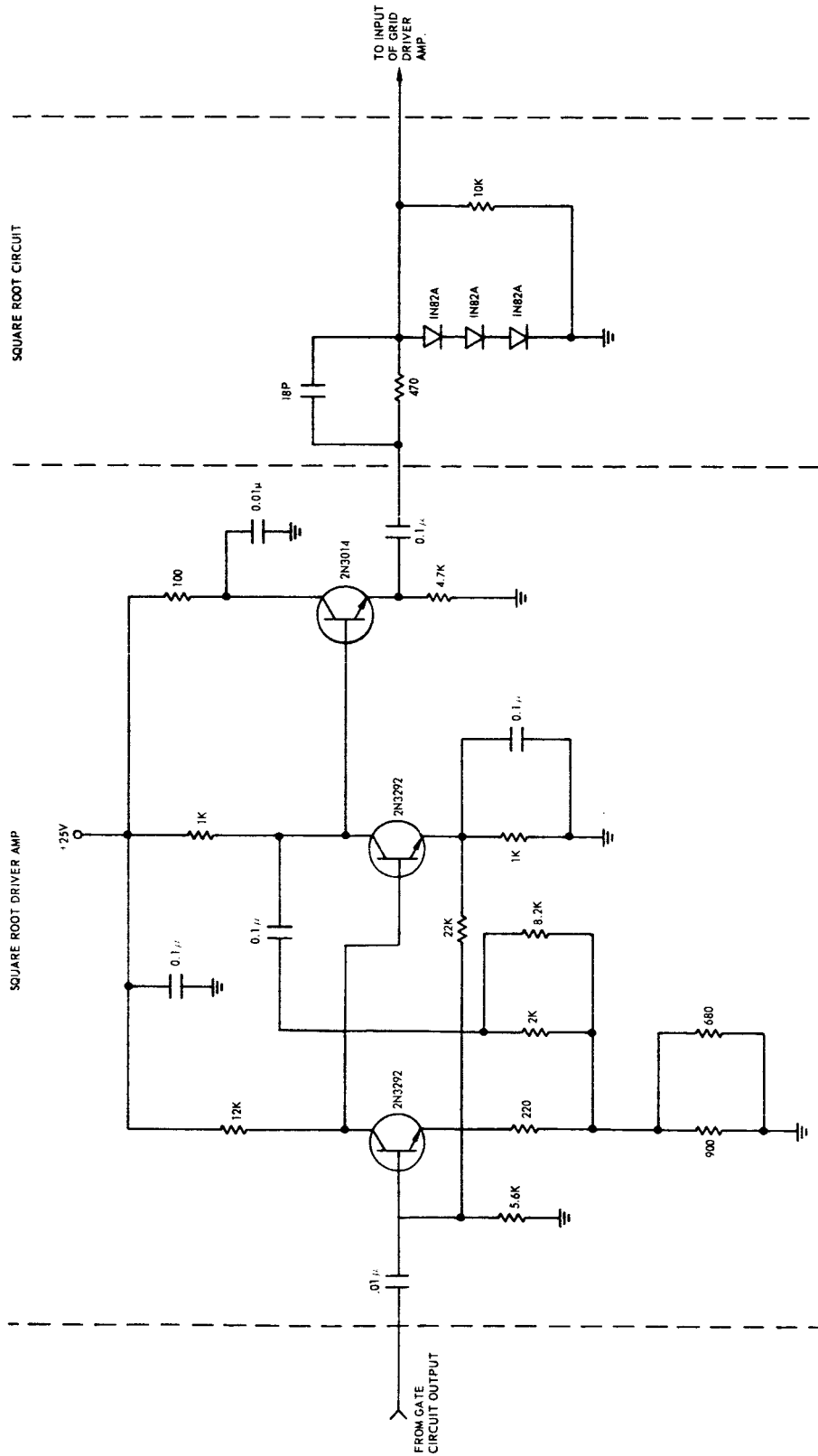
Figure 3-25. Square-Root Driver Amplifier and Square-Root Circuit
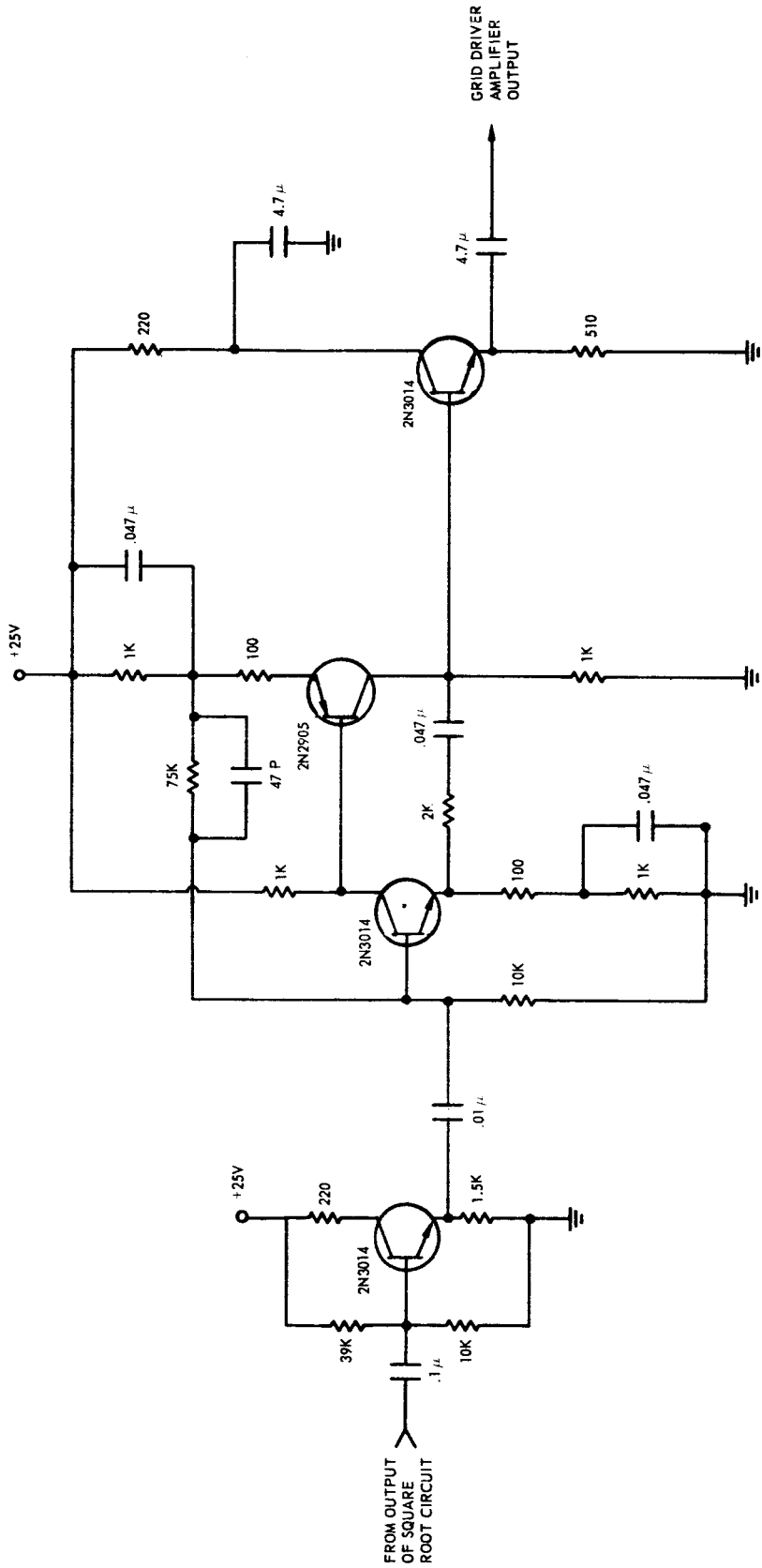
Figure 3-26. Grid-Driver Amplifier
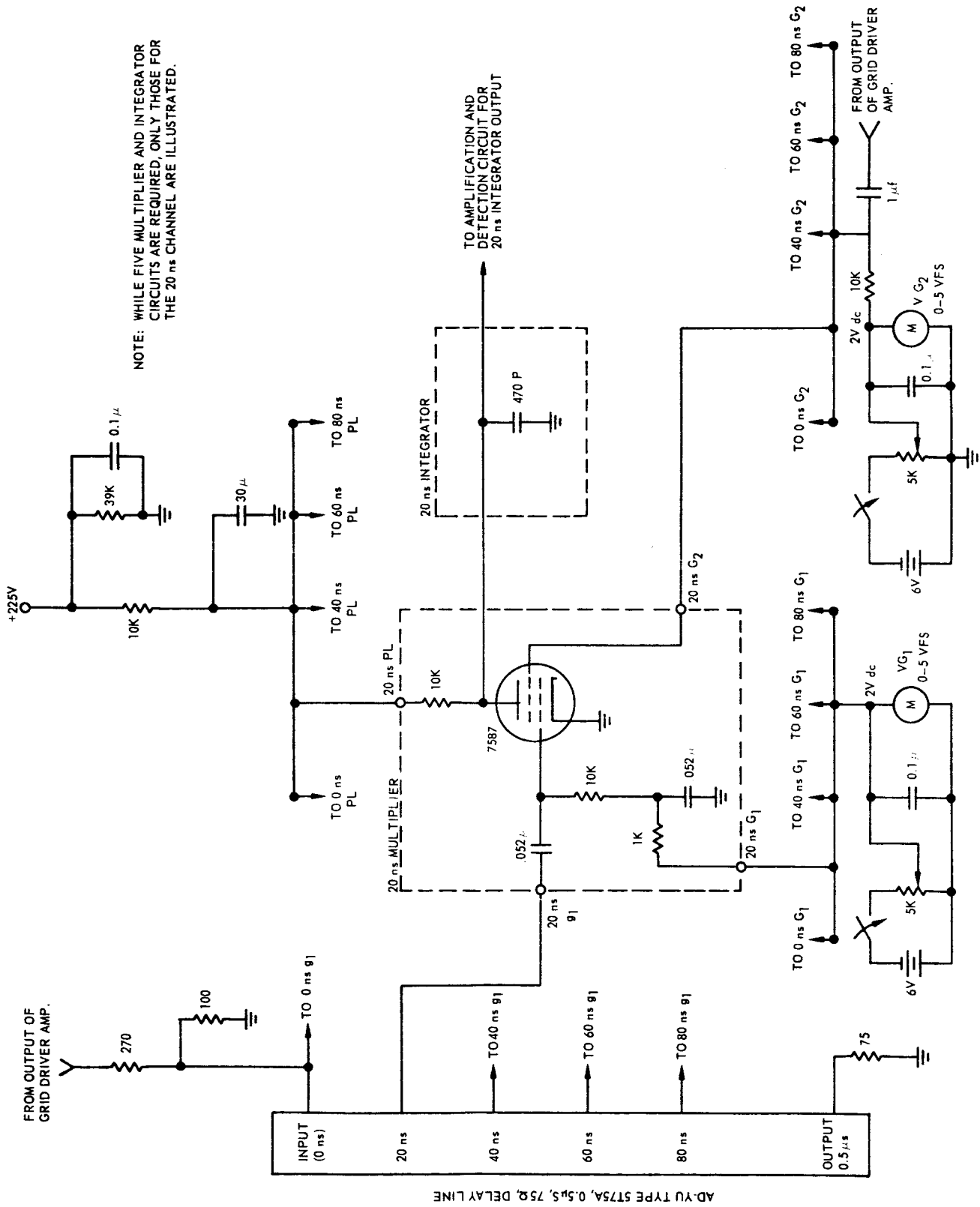
Figure 3-27. Delay-Line, Multiplier, and Integrator Circuits
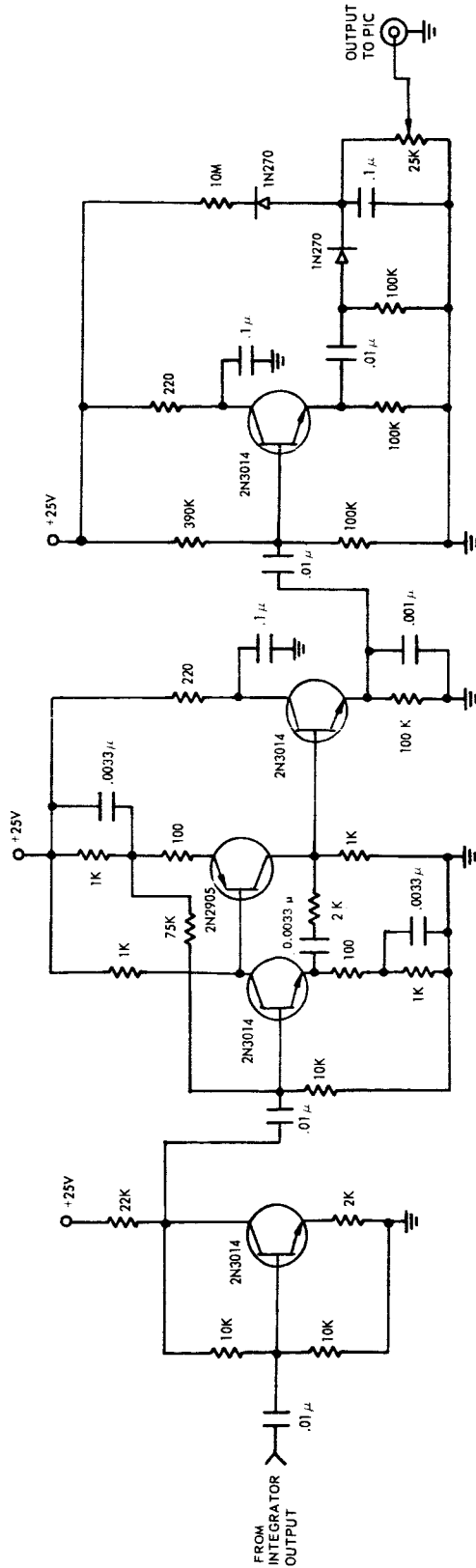
Figure 3-28. Integrator Output Amplification and Detection Circuit
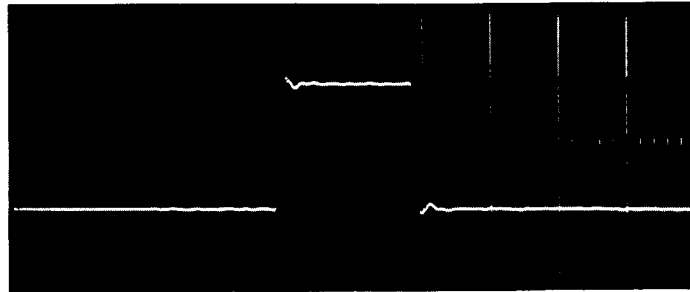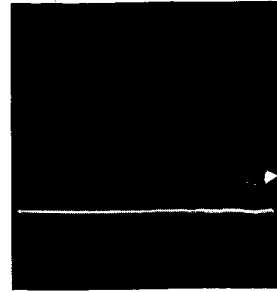
INPUT TO AUTOCORRELATOR
0.5 V/CM; 50 NS/CM

OUTPUT O
0.5 V/CM; 5
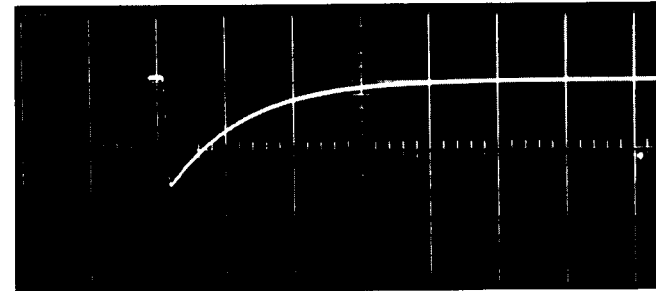
OUTPUT OF 0 NS INTEGRATOR
0.5 V/CM; 1 μS/CM

39-1
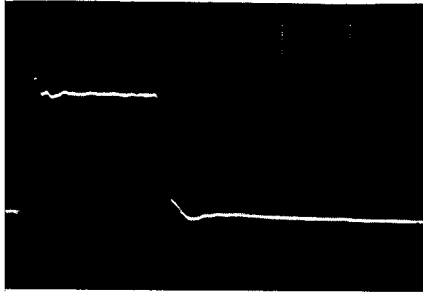
F SQUARE ROOT CIRCUIT
50 NS/CM
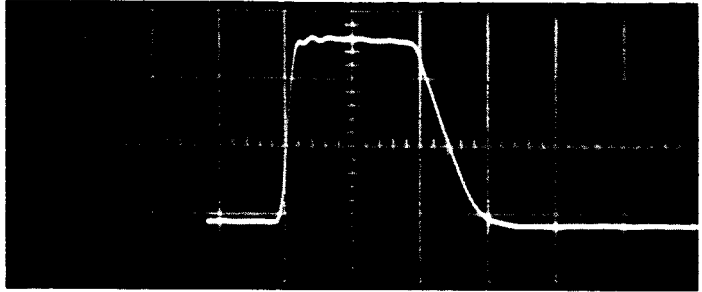
OUTPUT OF GRID DRIVER AMPLIFIER
5 V/CM; 50 NS/CM
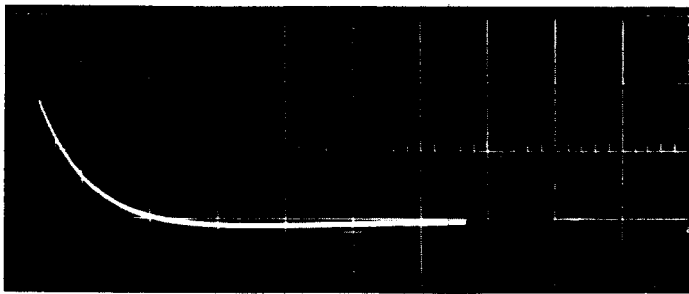
OUTPUT OF 0 NS AMPLIFIER AND
DETECTOR 0.5 V/CM; 2 MS/CM

Figure 3-29. Waveforms at Autocorrelator Test Points for a 100-ns, 1-Volt,
Square Pulse Input

OUTPUT PULSE HEIGHT
(db, RELATIVE TO 1 V)

-14   -12   -10   -8   -6   -4   -2   0

INPUT PULSE
HEIGHT
(db, RELATIVE TO 1 V)

- 4

0 NS CHANNEL ———————————→   - 8

20 NS CHANNEL ———————————→   -12

40 NS CHANNEL ———————————→   -16

60 NS CHANNEL ———————————→   -20

80 NS CHANNEL ———————————→   - 24

- 28

-32
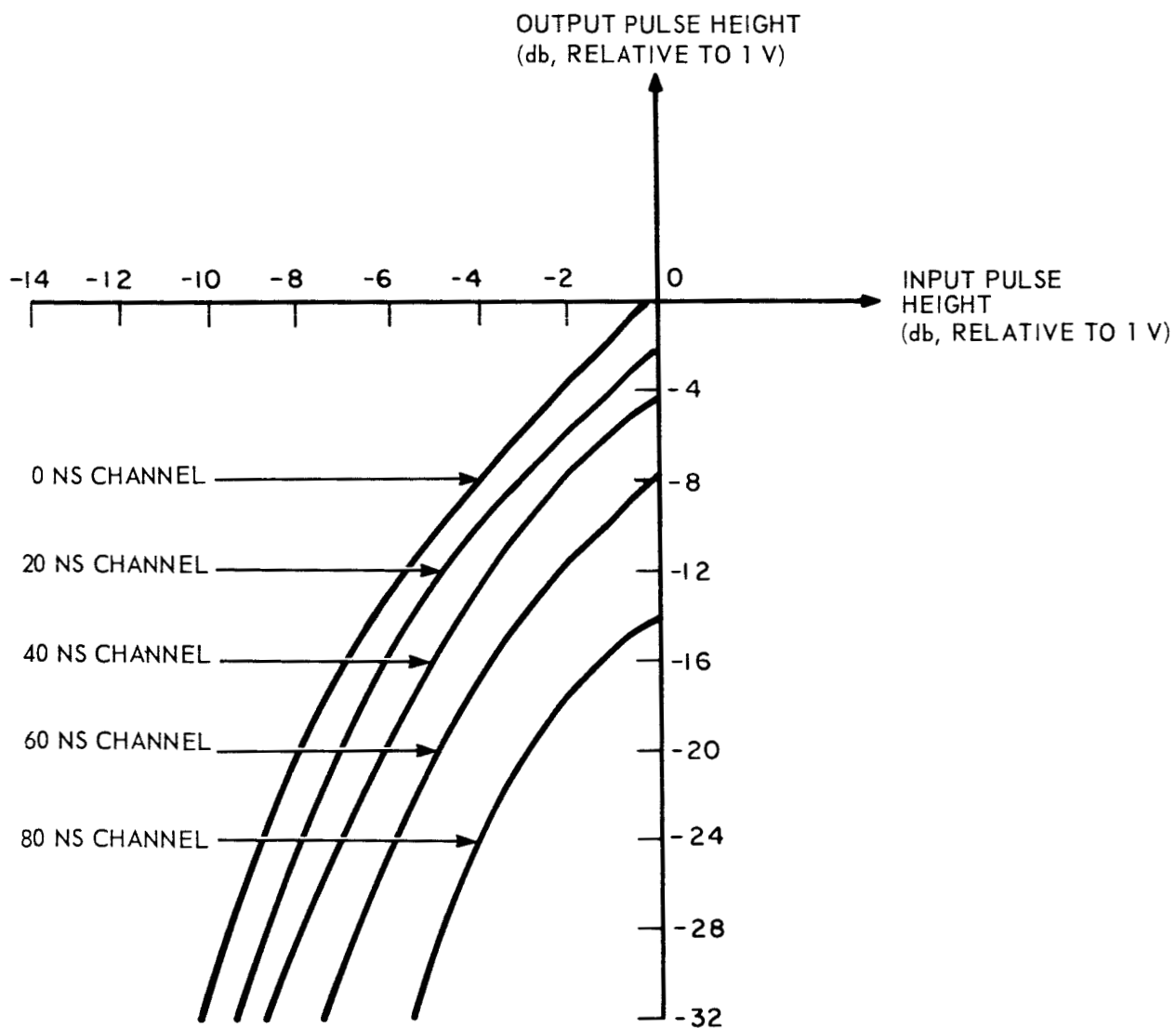
NOTE: IDEALLY, THE SLOPE OF EACH OF THE
CURVES WOULD BE 2 db OUTPUT ATTENUATION
FOR 1 db INPUT ATTENUATION.

Figure 3-30.   Relative Response of the Autocorrelator Outputs as a Function of Input
Pulse Height

40
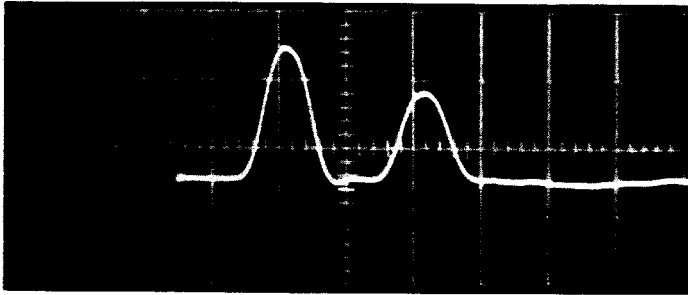
DOUBLE GAUSSIAN PULSE INPUT
TO AUTOCORRELATOR 0.5 V/CM;
50NS/CM
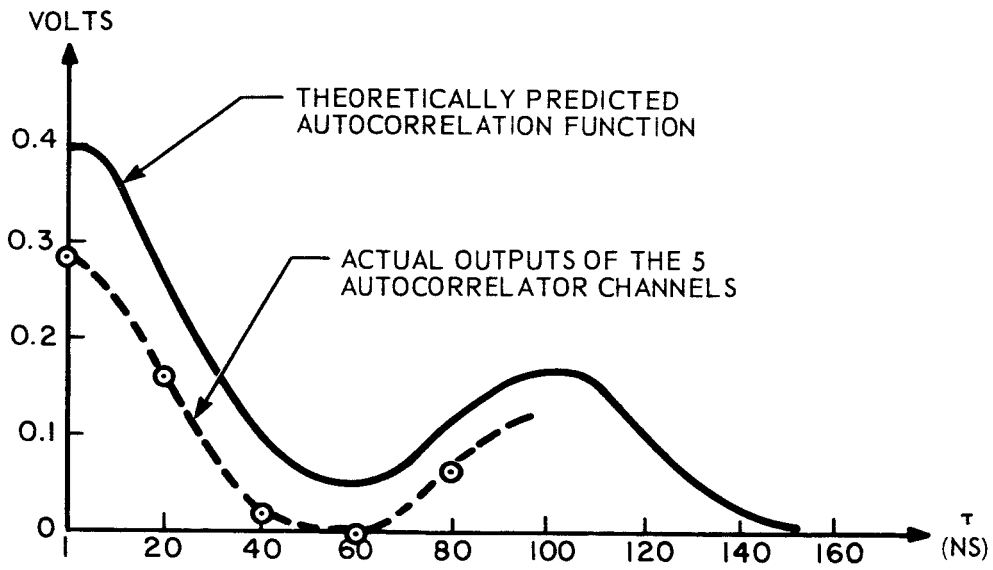
Figure 3-31.   Theoretical and Experimental Autocorrelation of a Double Gaussian
Pulse

E5745
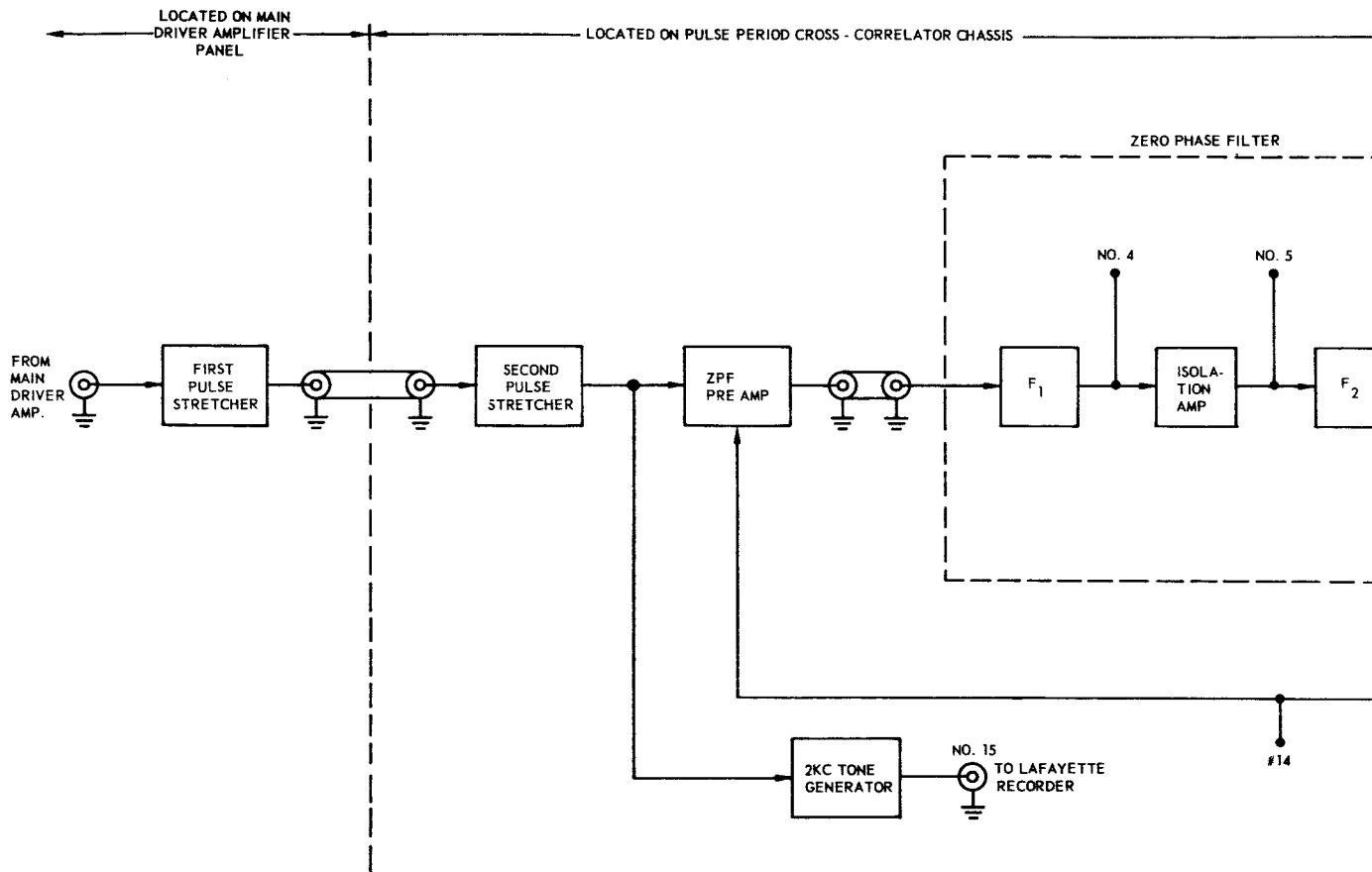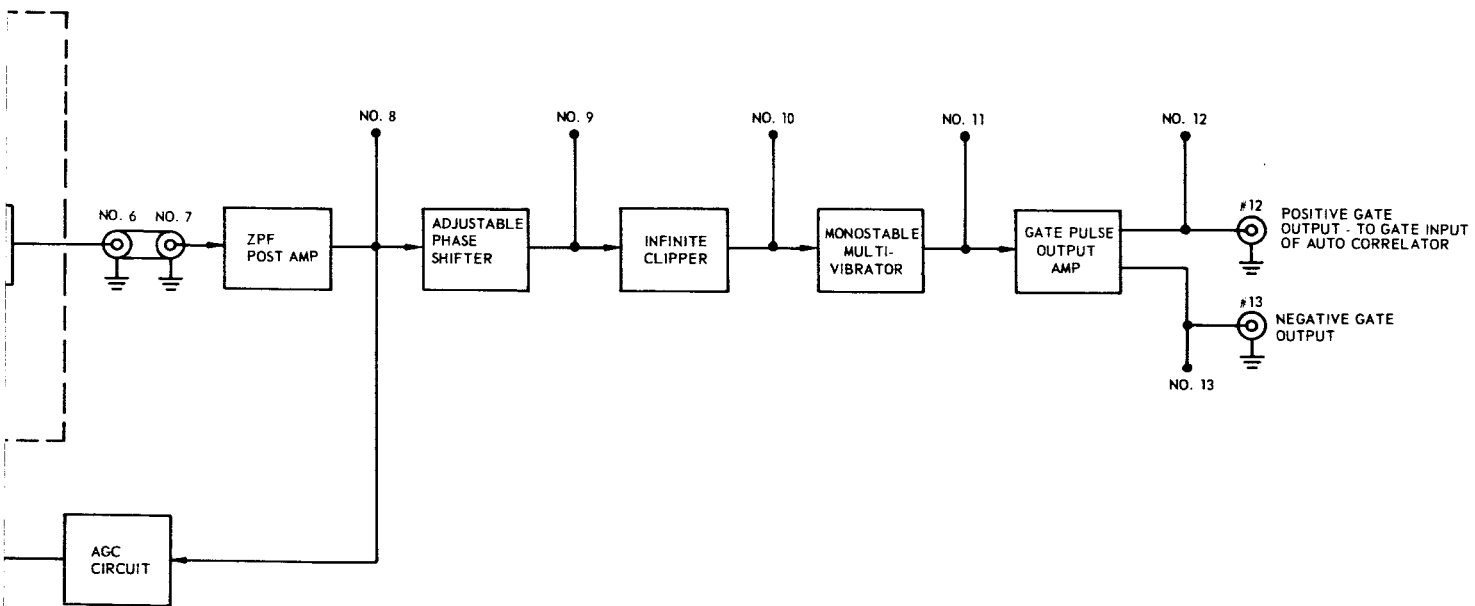
LOCATED ON MAIN
DRIVER AMPLIFIER
PANEL
———— LOCATED ON PULSE PERIOD CROSS - CORRELATOR CHASSIS ————

ZERO PHASE FILTER

NO. 4   NO. 5

FROM
MAIN
DRIVER
AMP.

| FIRST PULSE STRETCHER | | SECOND PULSE STRETCHER | | ZPF PRE AMP | | F_1 | | ISOLA-TION AMP | | F_2 |

| 2KC TONE GENERATOR |

NO. 15
TO LAFAYETTE
RECORDER

#14

42-1

Figure 3-32. Block Diagram for Pulse Period Cross-Correlator Subsystem

42

The output of the zpf preamp is fed to the zero phase filter, which retains only the fundamental component of the stretched pulse train (i.e., the harmonic component whose frequency is that of the pulse repetition rate and whose phase coincides with that of the pulse train). In this manner any randomly spaced noise pulses are filtered out. The output of the zero phase filter is fed to the zpf postamp, which in turn drives both the adjustable phase shifter and the AGC circuit in the feedback loop. The purpose of the AGC circuit is to adjust the gain of the zpf preamp so that the signal level entering the zero phase filter is always about 1 volt. The purpose of the adjustable phase shifter is to remove any slight phase difference between the incoming signal pulse train and the sinusoidal output of the zero phase filter. The output of the adjustable phase shifter is fed to the gate pulse generating circuitry, which consists of an infinite clipper, a monostable multivibrator, and a gate pulse output amplifier.

The most critical part of the pulse period cross-correlator subsystem is the zero phase filter. It is absolutely essential to the operation of this subsystem that the zero phase filter be properly tuned to the pulse repetition rate, and that there be no time variation in the relative phase between the output of the zero phase filter and the signal pulse train (any constant phase difference between these two signals can be removed by the adjustable phase shifter). Three different hand-held laser transmitters were constructed for the Laser Communicator Experiment. Each exhibited a different pulse repetition rate, ranging from 80 pps to over 100 pps. In addition, the specifications for these transmitters were such that the pulse repetition rate for any one transmitter could vary with time over a 2-cycle bandwidth. Therefore, it was necessary to design the zero phase filter such that:

    a. Its center frequency could be manually varied from 75 to 120 cps.

    b. For any given center frequency, the filter would exhibit an essentially zero phase characteristic over a 2-cps bandwidth.

Figure 3-33 is a pole-zero plot of an ideal bandpass zero phase filter, centered at ω_0. It consists of a double pole at $s = -2\sigma_0 + j\omega_0$, and a zero at $s = \sigma_0 + j\omega_0$. The angle of the transfer function of the filter at $\omega = \omega_0 + \Delta$ is $\Theta - 2\phi$, where Θ is the angle of the zero and ϕ is the angle of one of the poles. Clearly, for small Δ,

$$\Theta \simeq \frac{\Delta}{\sigma_0}$$

$$\phi \simeq \frac{\Delta}{2\sigma_0} \qquad\qquad (3\text{-}10)$$

Hence the angle of the transfer function of the filter is essentially zero in the neighborhood of ω_0:

$j\omega$

Φ Θ

$\omega_0 + \Delta$

ω_0

σ_0

$2\sigma_0$

DOUBLE POLE AT $s = 2\sigma_0 + j\omega_0$

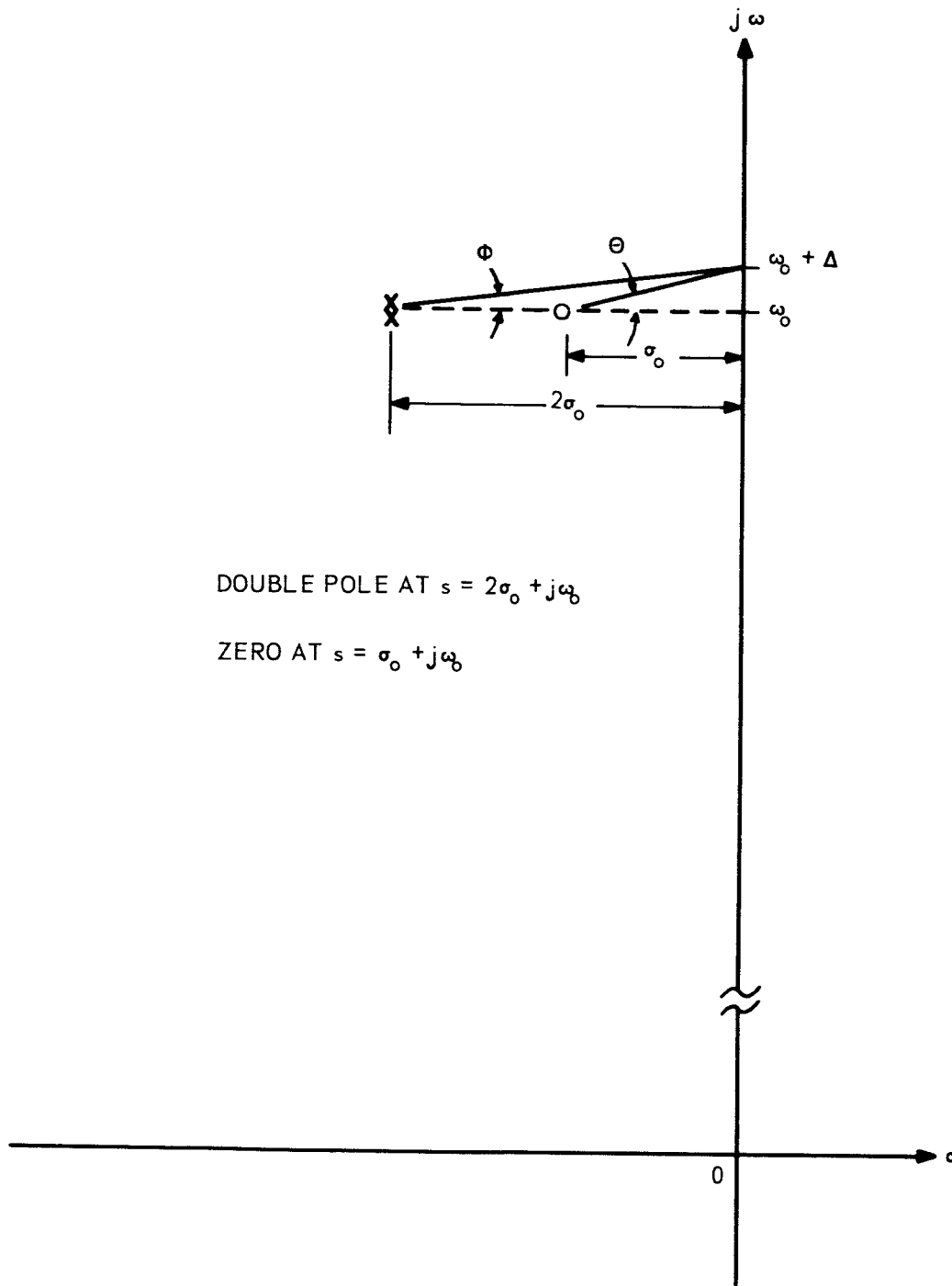ZERO AT $s = \sigma_0 + j\omega_0$

σ

0

Figure 3-33. Pole-Zero Plot of Ideal Zero Phase Filter in the Neighborhood of ω_0

$$\Theta - 2\phi \simeq \frac{\Delta}{\sigma_0} - 2 \frac{\Delta}{2\sigma_0} = 0 \qquad\qquad (3\text{-}11)$$

It is also apparent that, for large Δ (i.e., for ω's far from ω_0), the zero is effectively canceled by one of the poles, and the ideal zero phase filter behaves essentially like a single pole. Figure 3-34 compares the magnitude and phase functions of a zero phase filter with those of a single pole.

In practice, the pole-zero plot of the ideal zero phase filter in the neighborhood of ω_0 can be synthesized by two networks, F_1 and F_2, acting in cascade. Figures 3-35 and 3-36 are simplified schematics of these networks, while Figures 3-37 and 3-38 are pole-zero plots of the transfer functions of the two networks (it is assumed that R_{L-1} is much greater than the resonant impedance, R_0, of T_1). These figures also illustrate the relationships between the various circuit parameters and the location of the poles and zeroes in the s-plane.

Figures 3-39, 3-40, and 3-41 are schematic diagrams of the first and second pulse stretchers and the 2-kc tone generator. Figure 3-42 is a schematic of the zpf preamp and zero phase filter. In actual operation the values of the two variable capacitors in the zero phase filter are chosen so that the resonant frequencies of the two tank circuits coincide with the pulse repetition rate of the particular hand-held laser transmitter which is being used. The Q-Spoil controls are then set so that the first tank has a Q of 10 and the second tank has a Q of 20. Finally, the Tank 2 Load control is set so that the total load resistance in series with the second tank equals the resonant impedance of the second tank circuit. These values give rise to an overall Q of 5 for the zero phase filter, and insure essentially zero phase over a 2-cps bandwidth.

Figure 3-43 is a schematic diagram of the zpf post amp and adjustable phase shifter, figure 3-44 is a schematic diagram of the AGC circuit, and figures 3-45 and 3-46 are schematic diagrams of the gate pulse generating circuitry.

3.8 Time-Voice Mix Subsystem

The purpose of the time-voice mix subsystem is to permit alternate recording of voice commentary and a standard time signal on the same data channel.

Figure 3-47 is a schematic diagram of the time-voice mixing circuit. The system operator selects either voice recording or time recording by mannual operation of the switch. The amplifier noted in the schematic is a Lafayette Radio Co. model 99-9037 transistor amplifier, powered by a 9-volt dry cell.
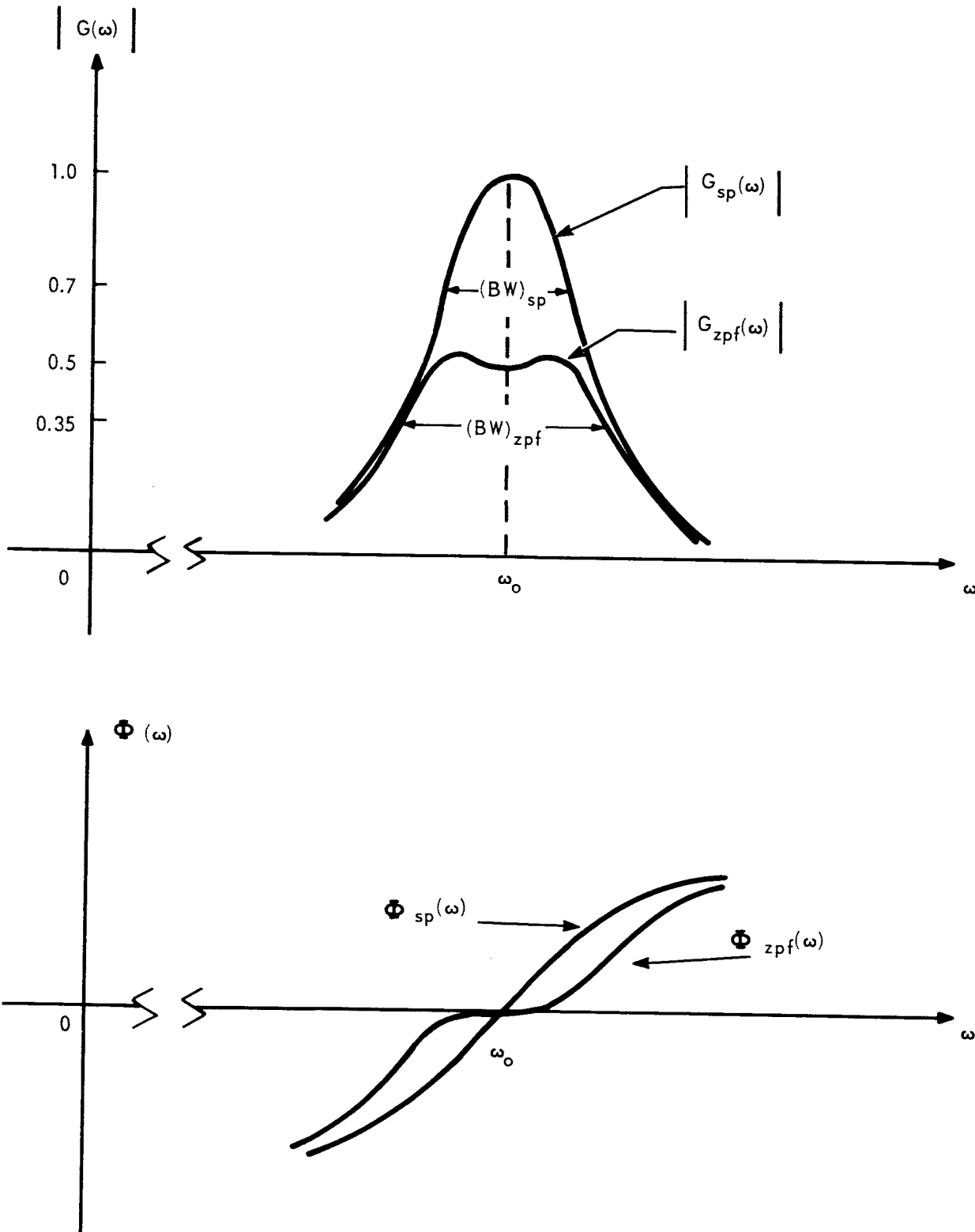
Figure 3-34. Comparison of Magnitude Function, Bandwidth, and Phase Function
in the Neighborhood of ω_O for Ideal Zero-Phase Filter (Double-Pole
at $S = 2\sigma_O + j\omega_O$, Zero at $S = -\sigma_O + j\omega_O$, and Single-Pole Located at
$S = -2\sigma_O + j\omega_O$)

46
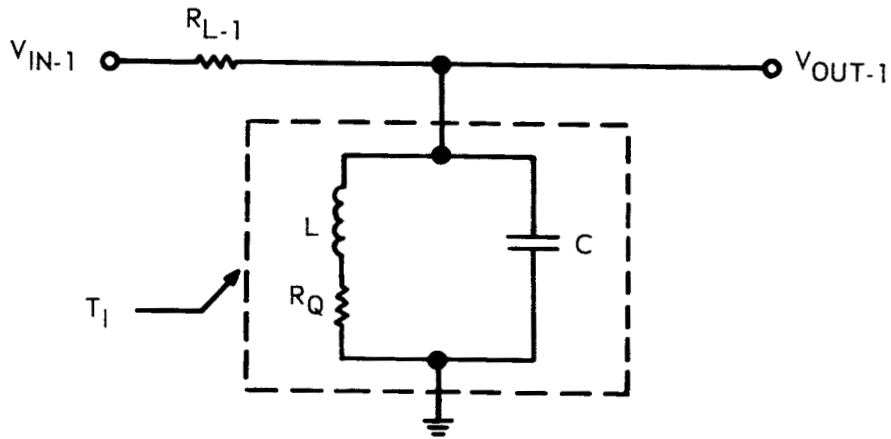
Figure 3-35. Simplified Schematic of F_1
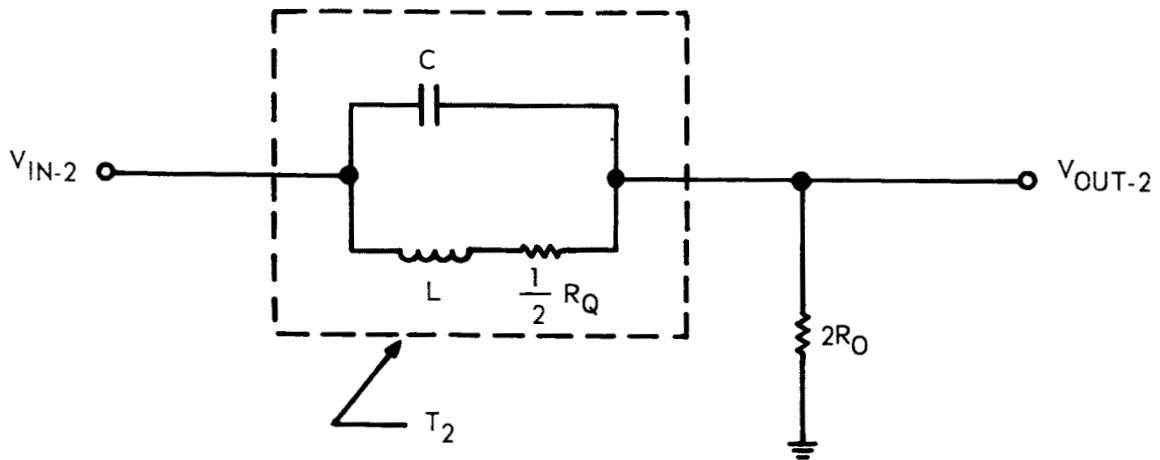
Figure 3-36. Simplified Schematic of F_2

POLES AT $s = -\dfrac{R_Q}{2L} + j\omega_0$

ZERO AT $s = -\dfrac{R_Q}{L}$

$\omega_0 = \sqrt{\dfrac{1}{LC}}$

$\dfrac{R_Q}{2L}$

$\dfrac{R_Q}{L}$

$\dfrac{R_Q}{2L}$

$j\omega$

σ

0

$-\omega_0$
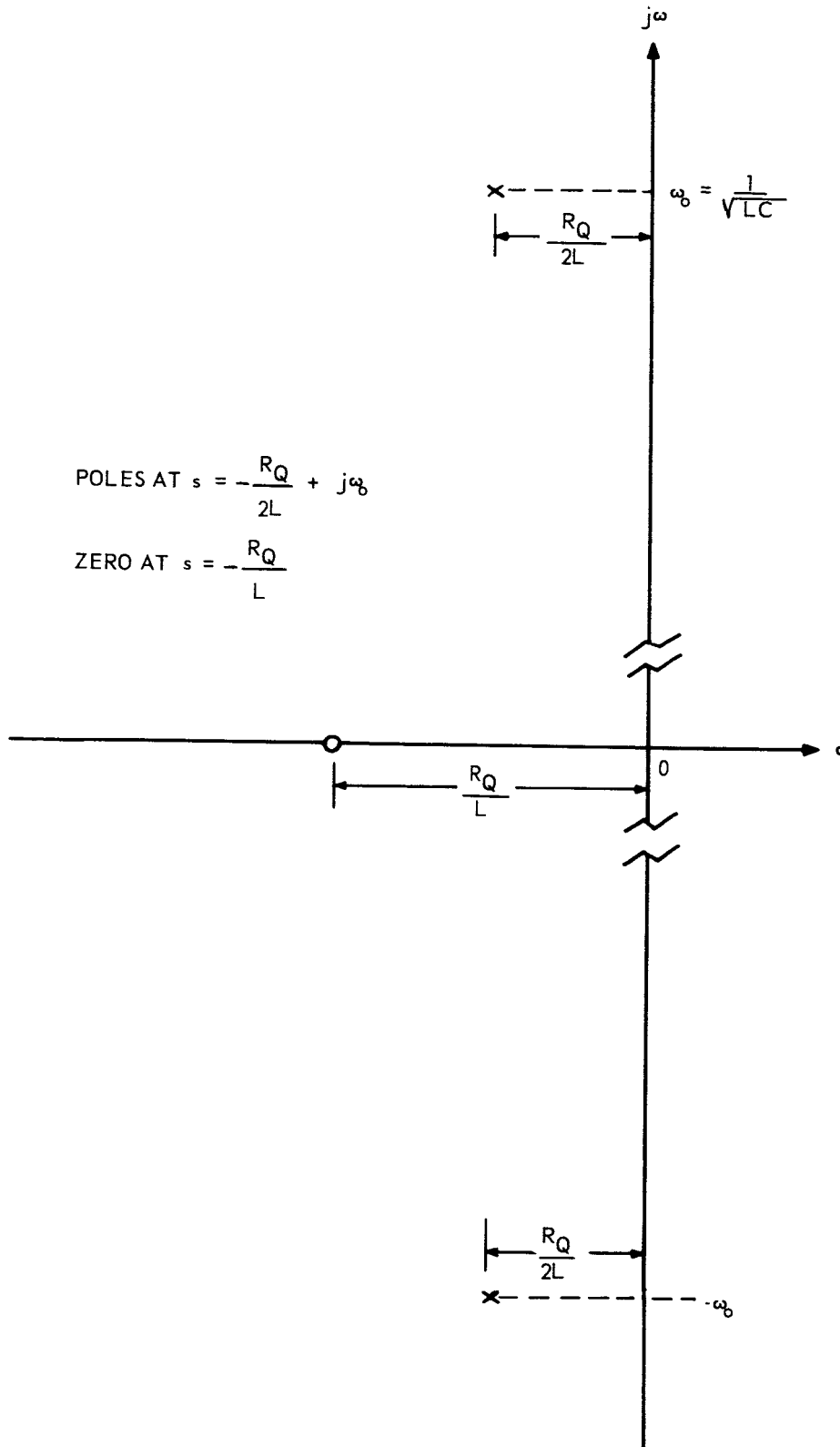
Figure 3-37. Pole-Zero Plot of Simplified F_1

$$\omega_o = \frac{1}{\sqrt{LC}}$$

$$\frac{R_Q}{4L}$$

$$\frac{RQ}{2L}$$

POLES AT $s = -\dfrac{R_Q}{2L} + j\omega_o$

ZEROS AT $s = -\dfrac{R_Q}{4L} + j\omega_o$

$$\frac{R_Q}{2L}$$

$$\frac{R_Q}{4L}$$

$$-\omega_o$$
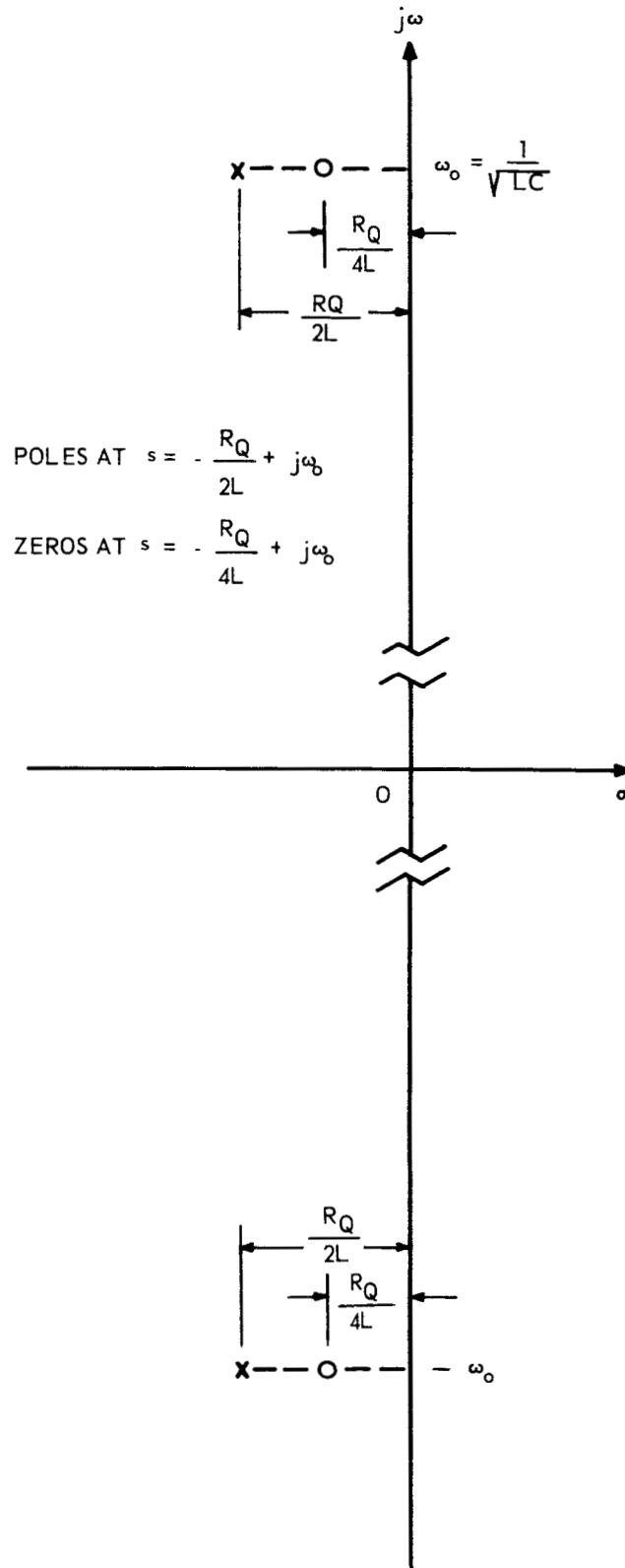
Figure 3-38. Pole-Zero Plot of Simplified F_2

Figure 3-39. First Pulse Stretcher

E5747

FROM FIRST
PULSE STRETCHER
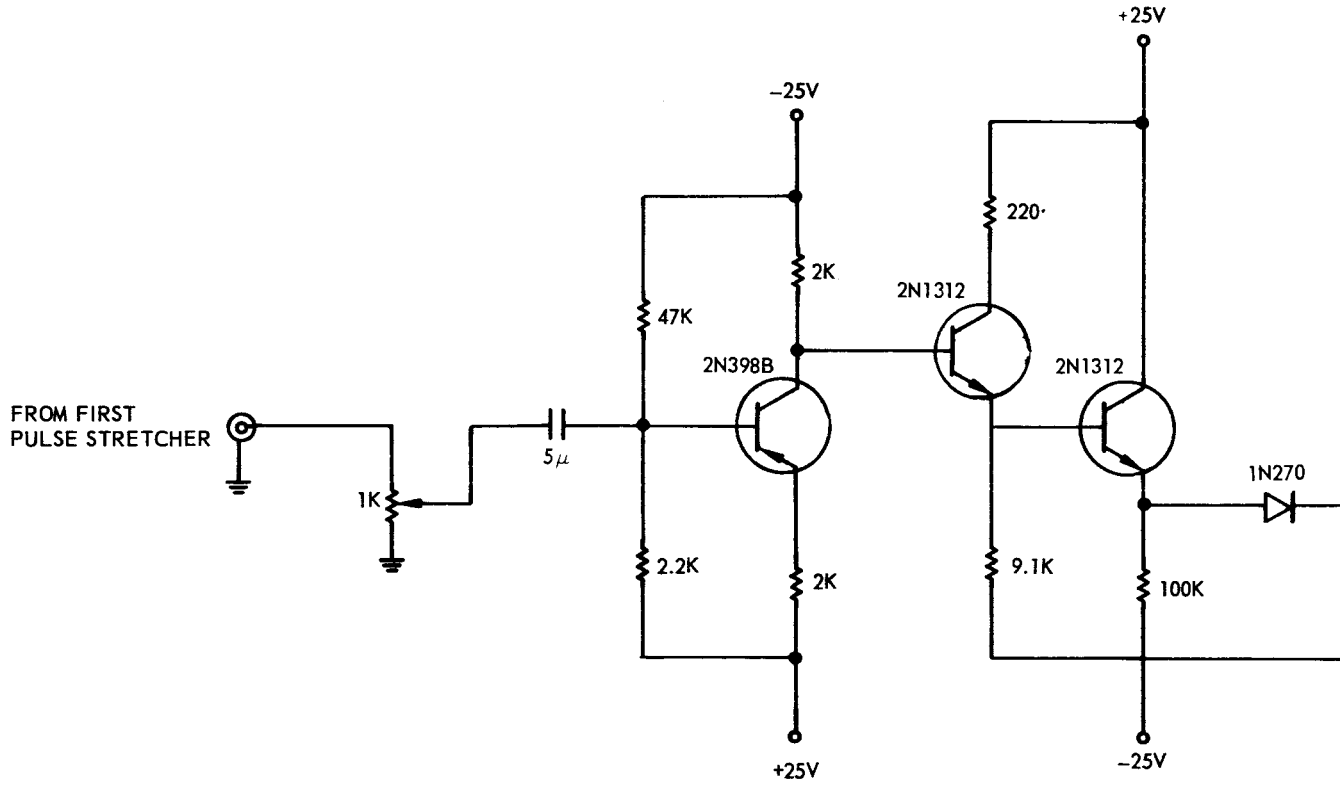
51-1
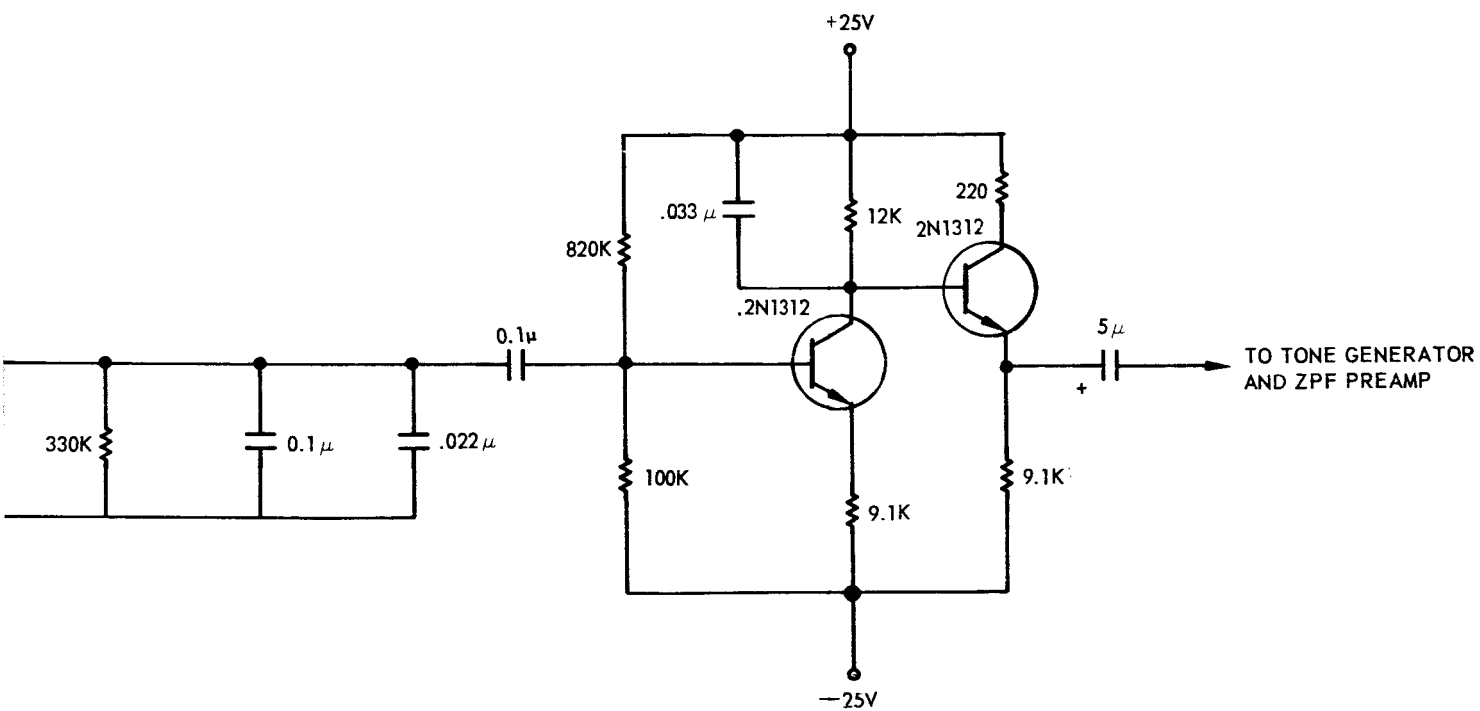
Figure 3-40. Second Pulse Stretcher
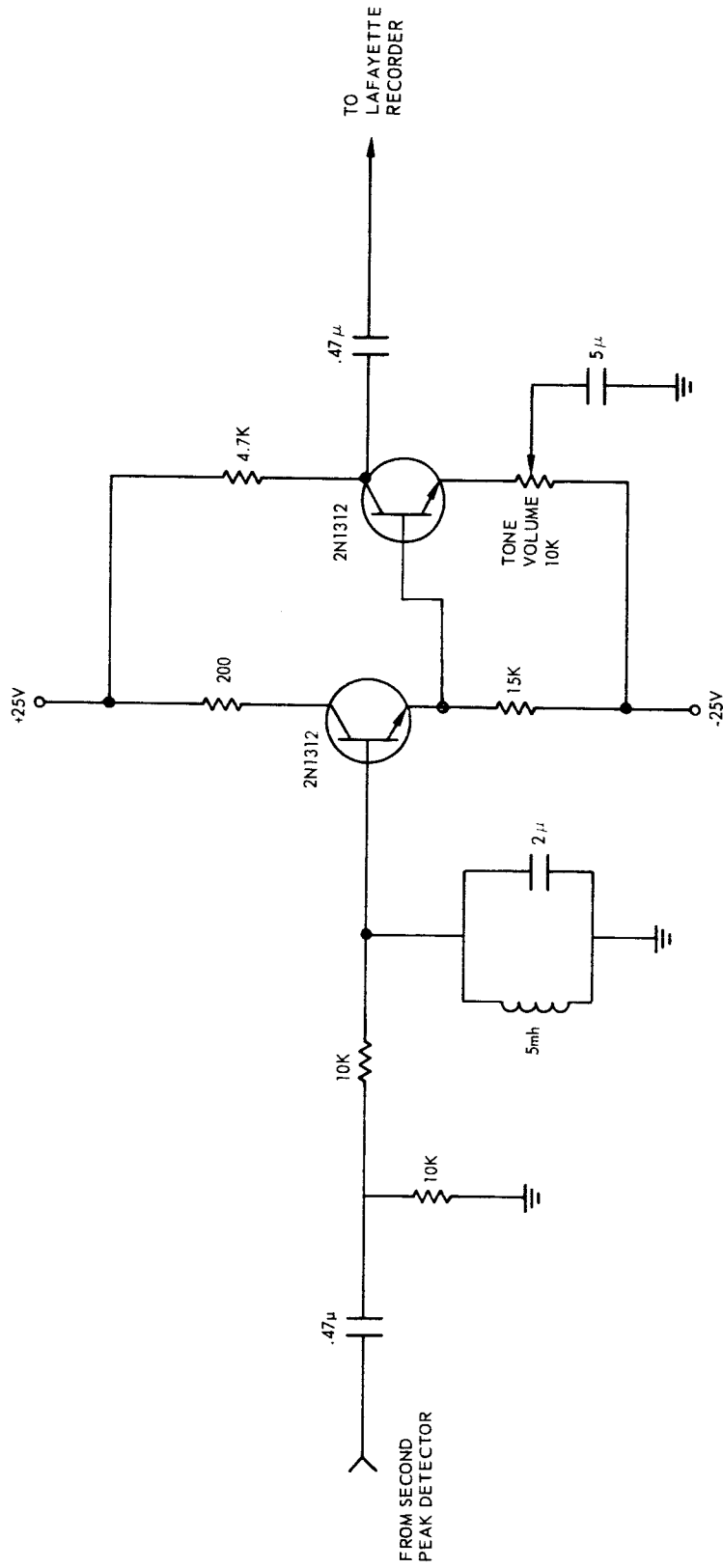
Figure 3-41. 2-KC Tone Generator
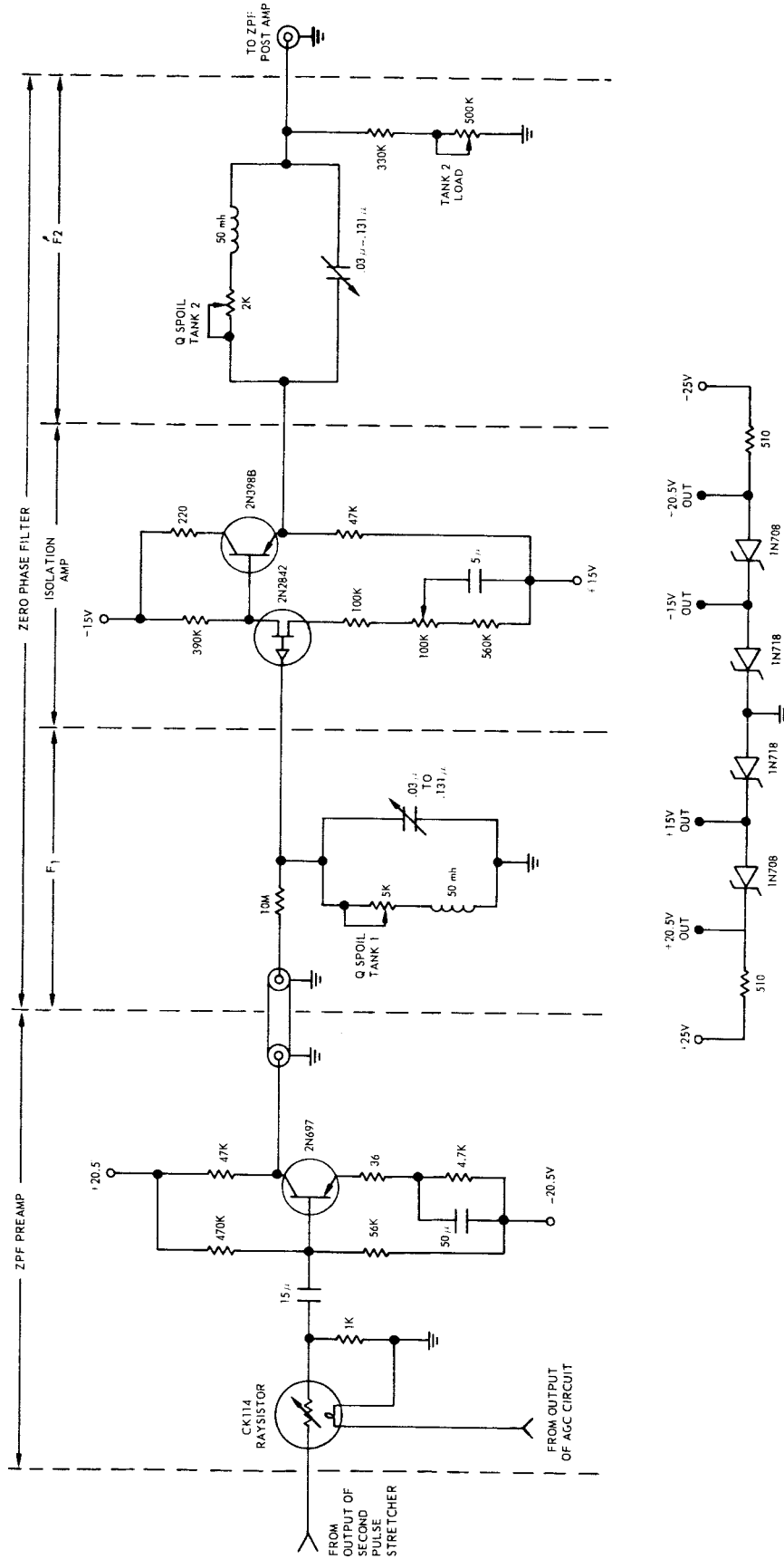
Figure 3-42. ZPF Preamp and Zero-Phase Filter
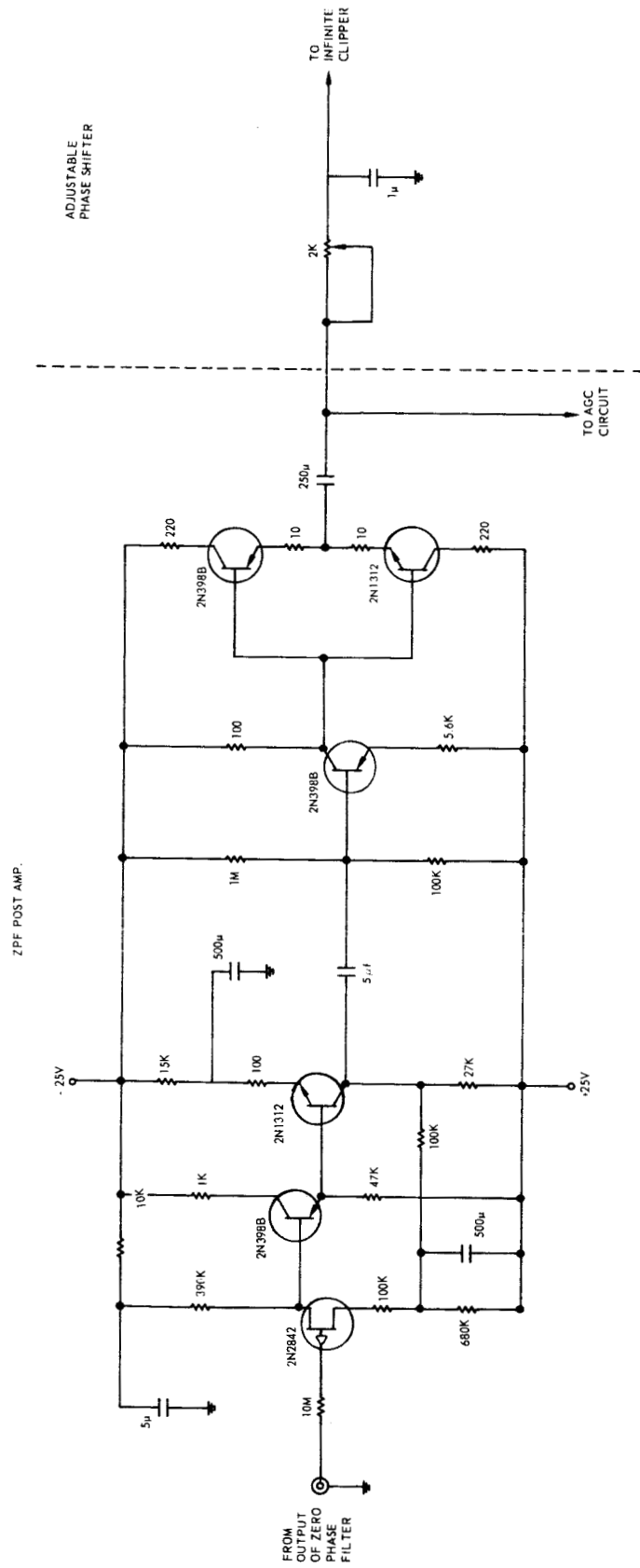
Figure 3-43. ZPF Postamp and Adjustable Phase Shifter
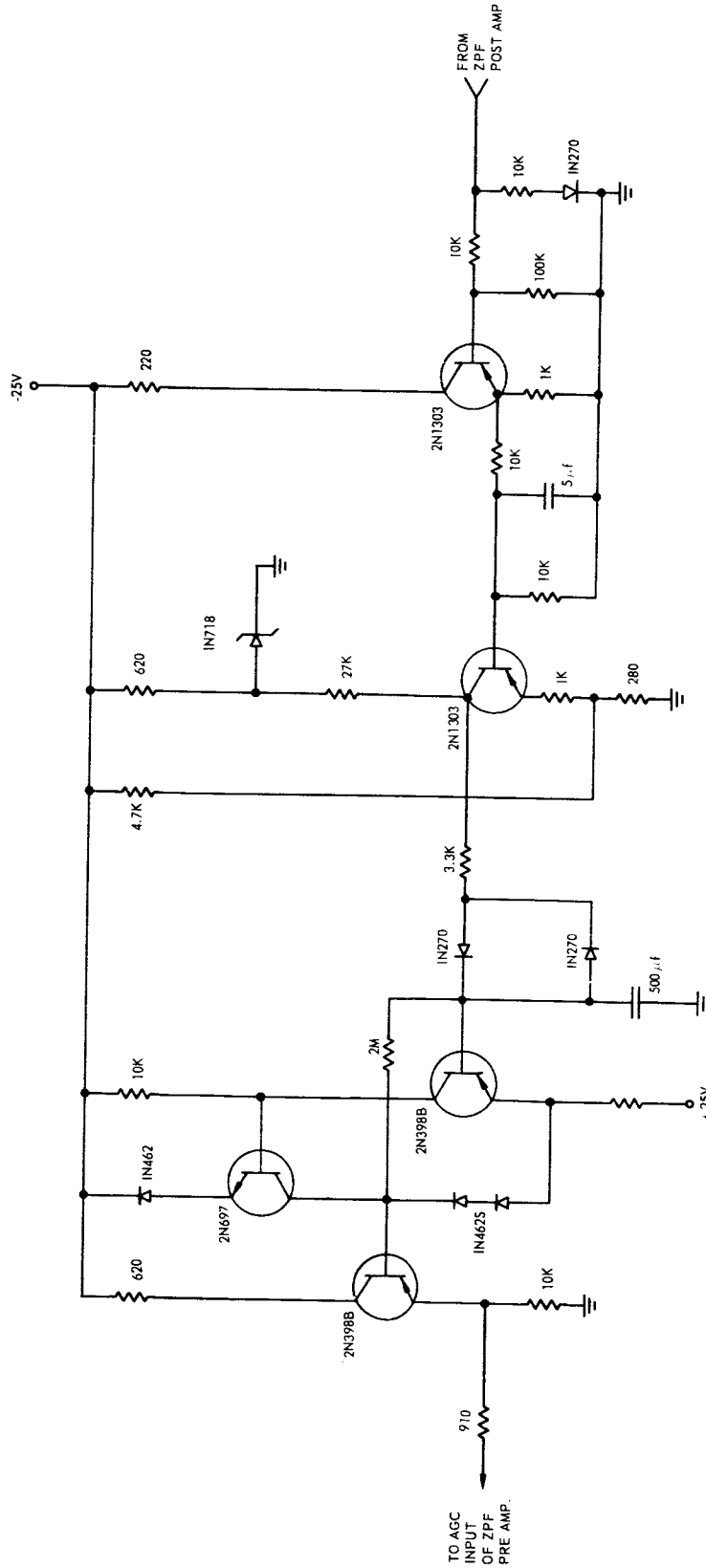
Figure 3-44. AGC Circuit
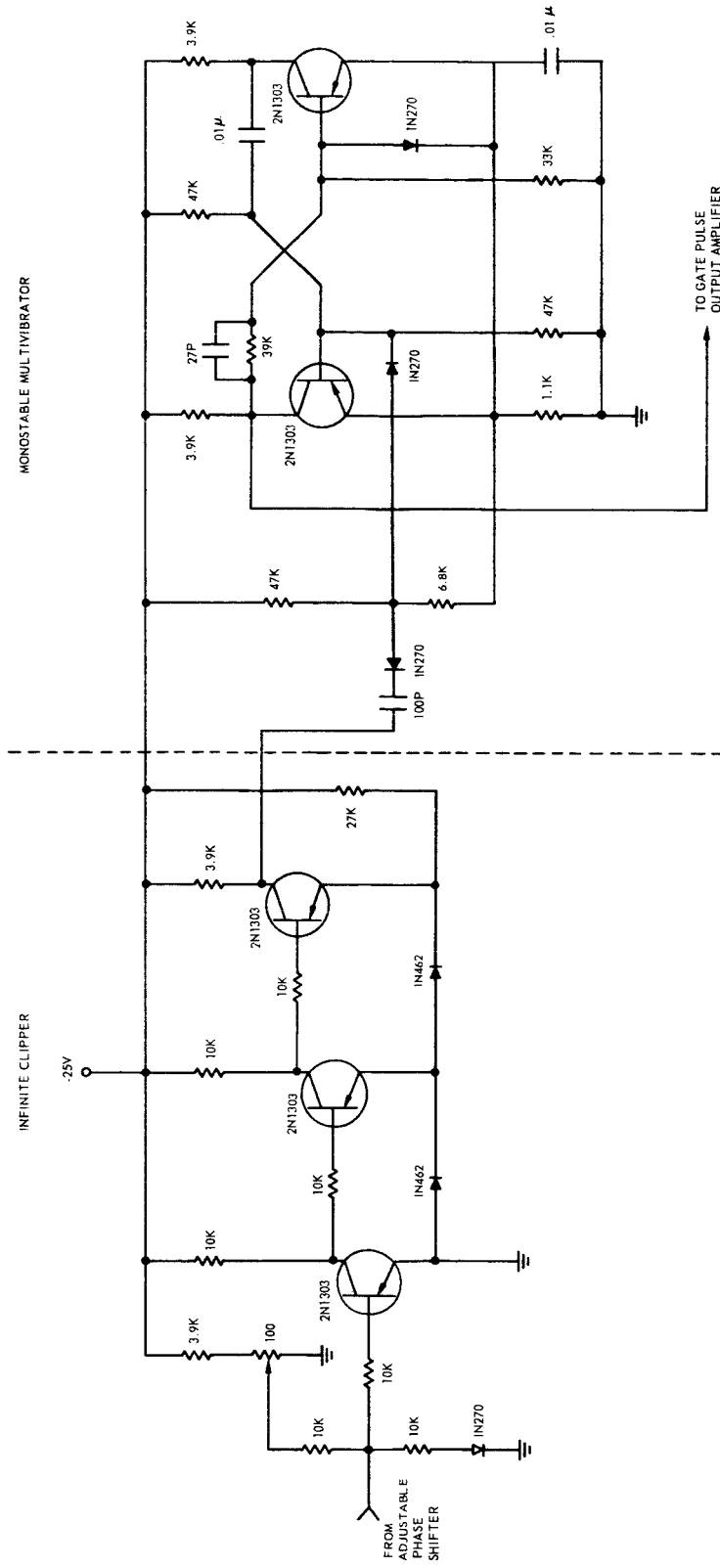
Figure 3-45. Infinite Clipper and Monostable Multivibrator
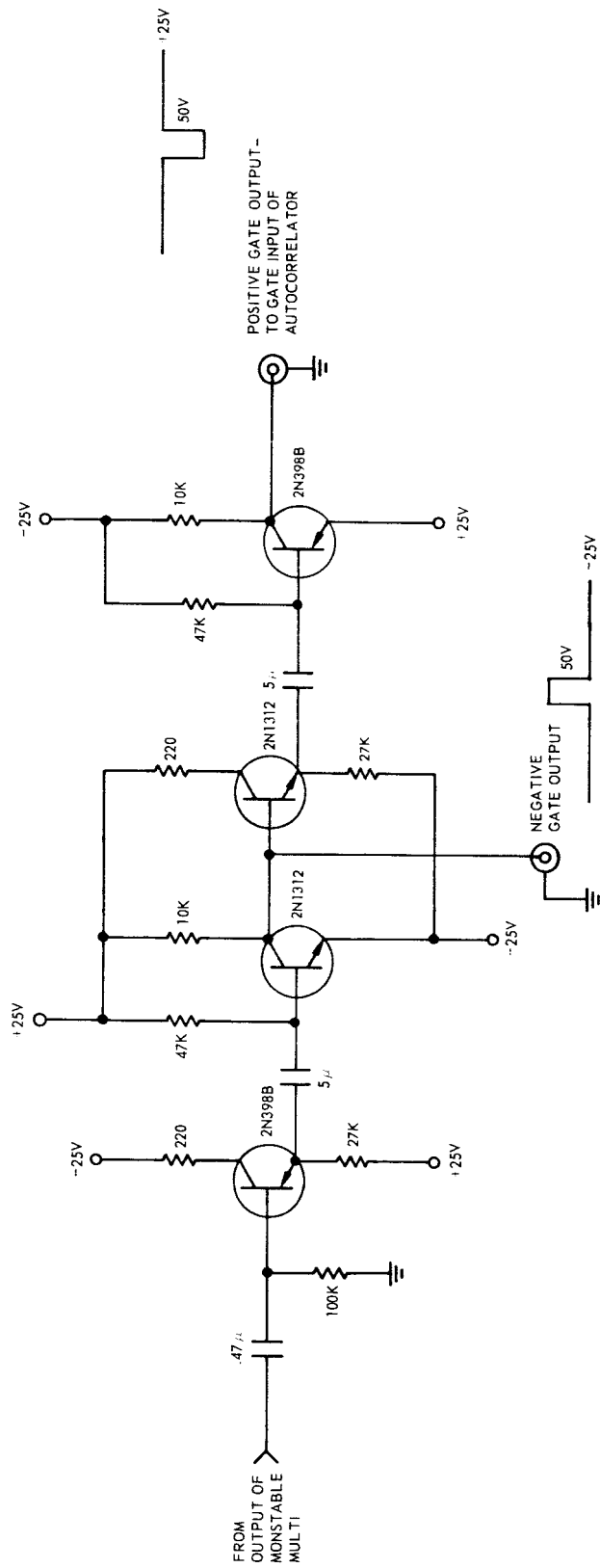
Figure 3-46. Gate Pulse Output Amplifier
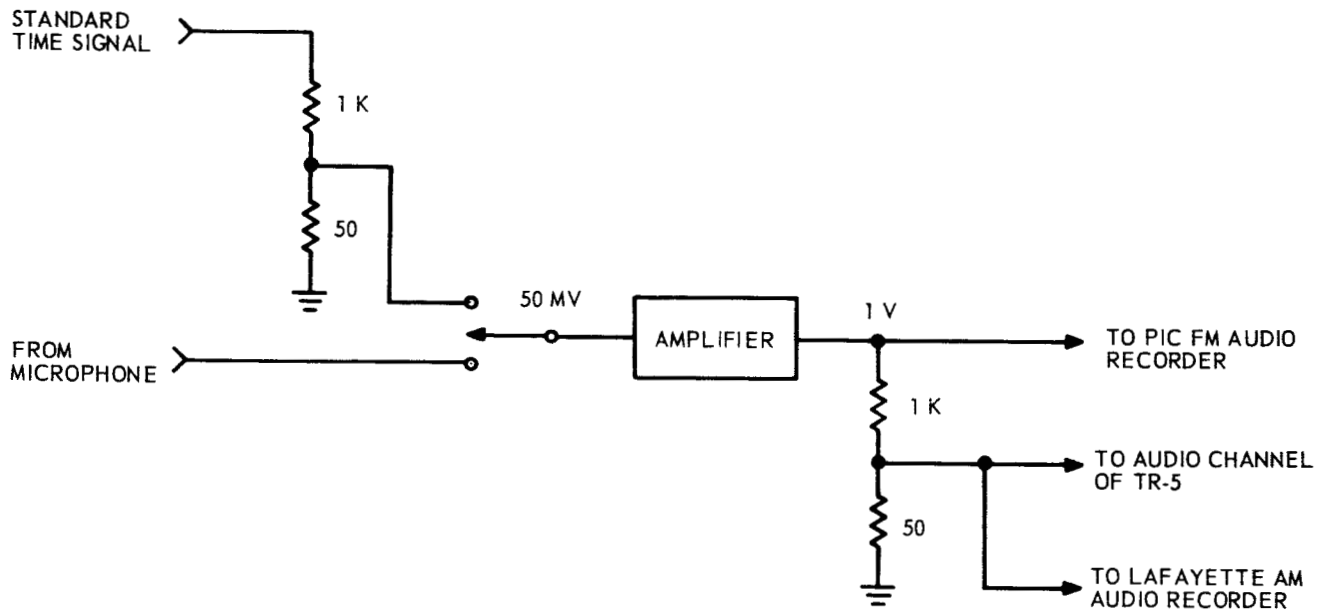
Figure 3-47. Time-Voice Mixing Circuit

The time-voice mix circuit generates two different levels of output; one at about 1 volt to drive one channel of the PIC FM audio recorder, and one at about 50 millivolts to drive both the audio channel of the TR-5 video recorder and one channel of the Lafayette AM audio recorder.

3.9 AM and FM Audio Recording Subsystem

The AM recorder used in this subsystem is a Lafayette Radio Co. model RK600A two-channel recorder. The recorder is operated at 7.5 inches per second. One channel of the recorder is driven by the output of the time-voice mixing circuit, while the other channel is driven by the output of the tone generator. In addition, the audio amplification and speaker system of the second channel is driven by the tone generator, so that the system operator perceives a distinct, audible tone whenever the signal from the hand-held laser transmitter is being received.

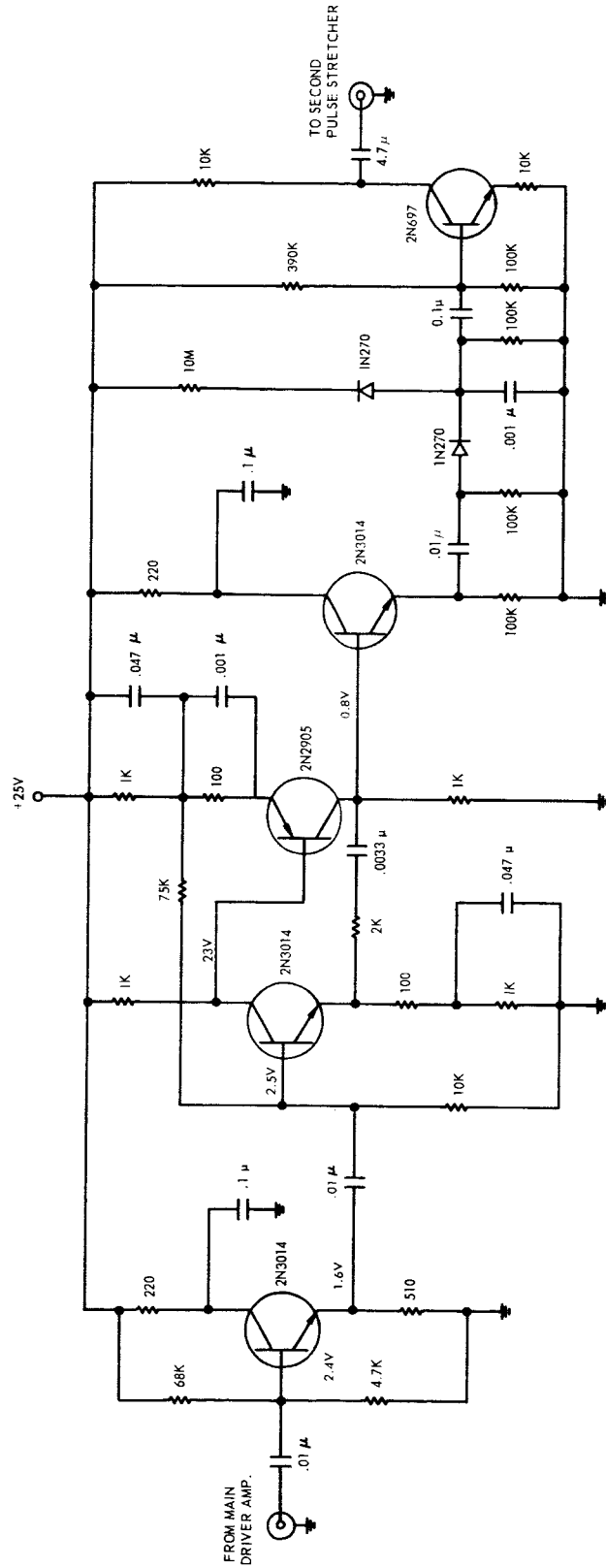The FM audio recorder used in this subsystem is a Precision Instruments Corporation model PS207-A3M seven-channel recorder. All seven channels are adapted for FM recording and playback of nominal 1 volt rms signals at a tape speed of 15 inches per second. Under these conditions, the frequency range of each channel is from dc to approximately 2.5 kc, and the dynamic recording range is approximately 40 db. Five channels of the recorder are used to record autocorrelation coefficients, one channel is used for recording the output of the time-voice mixing circuit, and the last channel is used to record the MPT AGC voltage.

4. FIELD ACTIVITIES DURING THE FLIGHT OF GT-7

4.1 WSMR Laser Communicator Site

On 26 November 65, the WSMR data recording and processing system (described in section 3.2) was shipped from the Melpar plant in Falls Church to the White Sands Missile Range. The system was accompanied by a senior scientist and a senior engineering technician, who were responsible for installing and operating the system at the WSMR Laser Communicator site. By 2 December 65, the WSMR data recording and processing system was completely installed and operating in the field.

Poor weather and the failure of the beacon laser to operate properly prevented any attempts at laser communication between WSMR and the space capsule during the first week of the flight of GT-7 (4 December 65 through 11 December 65). On 12 December 65, the beacon laser was operating properly, the weather was relatively clear, and an attempt at laser communication was made during orbital pass no. 119. Although the astronauts were unable to see the WSMR beacon for any significant lengths of time, they were able to observe one or two flashes from it. By aiming the hand held laser transmitter in the general direction of the flashes, one of the astronauts attempted to transmit laser pulses in the low pulse rate mode. However, a careful analysis of all of the recordings made during this pass showed conclusively that no detectable energy from the laser transmitter was received at the Laser Communicator Site. From 13 December 65 until the end of the flight of GT-7 (18 December 65), all attempts at laser communication between WSMR and the space capsule were precluded either by bad weather or by the engagement of the astronauts in other activites.

On 14 December 65, a hand-held laser transmitter was employed in a static transmission experiment between T-5 mountain and the WSMR Laser Communicator Site. The optical path between transmitter and receiver was approximately 11 miles long, and passed directly over the central WSMR base facilities. The transmitter was aimed by hand and was operated in both the low and high pulse rate modes. Transmitted energy was definitely received at the WSMR site during this static test in both modes of operation; however, the gain of the main driver amplifier was set too high, and all of the recording and processing systems were overdriven. Therefore, no useful data was recorded or processed during this test. On 16 December 65, another attempt was made to obtain low pulse rate (80 pps) transmission data from T-5 mountain. In this test, the transmitter was placed on a concrete ledge, aimed by hand, and then fixed in position by stones wedged underneath the transmitter casing. Severe fluctuations in received signal strength were observed during this test, and it was extremely difficult to adjust the gain of the main driver amplifier so that the excursions in signal strength remained within the 10-to-1 dynamic range of the recording and processing systems. It was finally decided to simply record the data with the gain of the main driver amplifier set to give an average signal level of about 0.3 volt.

On 18 December 65, the WSMR data recording and processing system was disassembled. Those pieces of the system which were needed for post-flight system calibration and data analysis were crated and shipped to the Melpar plant in Falls Church. The remaining parts of the system (consisting primarily of the video recording subsystem, racks and shelves, field supplies, and hand tools) were left in the Melpar field laboratory at White Sands.

4.2 Ascension Island Laser Communicator Site

On 14 November 65, the Ascension Island data recording and processing system (described in section 3.3) was shipped by NASA aircraft from Friendship Airport (Baltimore) to Ascension Island. The system was accompanied by an electronic engineer, who was responsible for installing and operating the system at the Ascension Island Laser Communicator Site. By 29 November 65, the system was completely installed and operating in the field.

The failure of the beacon laser to operate properly prevented any attempt at laser communication between Ascension Island and the space capsule during all but one of the orbital passes which had been assigned for this purpose. During the one assigned pass for which the beacon laser was operating, a heavy cloud cover precluded optical transmission in any form. Therefore, no laser communication data were received, recorded, or processed at the Ascension Island Laser Communicator Site.

On 18 December 65, the entire Ascension Island data recording and processing system was crated and shipped back to the Melpar plant in Falls Church.

5. POST-FLIGHT STUDIES AND EXPERIMENTS

5.1 General

Initial inspection of the T-5 mountain experiment data at the Melpar laboratories in Falls Church, Virginia, showed that the fluctuations in received signal strength had exceeded the 10-to-1 dynamic range of the recording system by a wide margin. It was estimated that over some portions of the data, the fluctuations in received signal were on the order of 100 or 1000 to 1. At the time, there appeared to be three possible mechanisms that could account for these severe fluctuations:

    a. Gross perturbations in atmospheric index of refraction.

    b. Variations in the energy distribution across the beam front induced by random scattering in the atmosphere and resonant modes in the diode laser cavities.

    c. Intermittent or faulty operation of the hand-held laser transmitter.

In order to determine which of these three mechanisms was indeed the cause of the observed excursions in received signal level, it was decided to ship the hand-held transmitter that had been used in the T-5 mountain experiments to the Melpar laboratories. If laboratory tests showed that the fluctuations were primarily attributable to atmospheric perturbations, and if sections of recorded data could be found in which the fluctuations in signal strength had been roughly within the dynamic range of the recorders, then those sections of data would be statistically analyzed.

5.2 Repair of Hand-Held Laser Transmitter

When the hand-held laser transmitter arrived at the Falls Church laboratories it was found to be in faulty operating condition. The power output of the laser diodes was somewhat erratic, and occasionally sparking could be heard within the interior of the transmitter. When operated from an external power supply, the case of the transmitter was found to be at 300 volts dc potential with respect to the positive terminal of the external supply. Eventually, the instrument simply ceased to operate altogether.

Upon careful examination of the interior circuitry it was discovered that:

    a. The wire leading from the positive terminal of the power source to the No. 2 terminal of the power transformer had become pinched between two parts of the case assembly, and was hence sporadically at case potential.

    b. The case of the RCA 40255 regulation transistor at the 300-volt output terminal of the power supply was touching the mounting screw of the 10-volt plug receptacle. This screw in turn was touching the case of the transmitter. Therefore, since the case of the transistor was at 300 volts, the case of the transmitter became elevated to 300 volts.

Apparently, a spark would occasionally pass from the transmitter case to the pinched wire described in (a) above. Whenever this spark occurred, the 300-volt output of the power supply was momentarily grounded, and the laser diodes would fail to operate. Eventually, the connection between the transmitter case and the pinched wire permitted an amount of current to flow that was sufficient to burn out one of the 2N2878 power transistors.

All of the above difficulties were quickly remedied, and the transmitter was then found to be in excellent working order. It was not clear, however, whether the transmitter had been operating sporadically during the T-5 mountain experiments.

5.3 Measurement of Beam Power Stability

In this experiment, measurements were performed to determine the power output stability of each of the four laser diodes acting individually, and of all four diodes acting in concert. The purpose of these measurements was first to ascertain that the hand-held laser transmitter was operating properly after the repairs described in section 5.2 had been performed; and second, to determine whether inherent instabilities in output power could possibly account for the fluctuations in the T-5 mountain experiment data.

Figure 5-1 shows the experimental arrangement that was used for making the beam power stability measurements. In order to measure the power output stability of only one of the beams, the other three beams were masked. Figure 5-2 gives typical tone generator outputs for each beam acting individually, and for all four beams acting in concert. It can be seen that the power output of the four beams acting in concert is quite stable, exhibiting fluctuations on the order of 10 to 20 percent. The individual beam power outputs are not so stable as the four acting in concert, and occasionally exhibit fluctuations as severe as 2 or 3 to 1. However, it was readily noted that even fluctuations this severe could not possibly account for the 100-to-1 fluctuations observed in the T-5 mountain experiment data.

5.4 Measurement of Transverse Beam Pattern

In this experiment, the cross-sectional beam pattern of one of the laser diodes was photographed. The purpose of the experiment was to determine the size of any irregularities in the distribution of energy across the beam front which had been induced by higher order modes in the diode laser cavity.

Figure 5-3 shows the experimental arrangement which was used for photographing the beam pattern of the upper-left laser diode of the hand-held laser transmitter. With no film in the camera, and with the camera back and lens shutter open, the MPT tube was used as a detector to align the camera with the laser beam. Then the camera was loaded with Polaroid type 413 infrared film, and the lens was adjusted to give a full-size image of the beam pattern on the film.
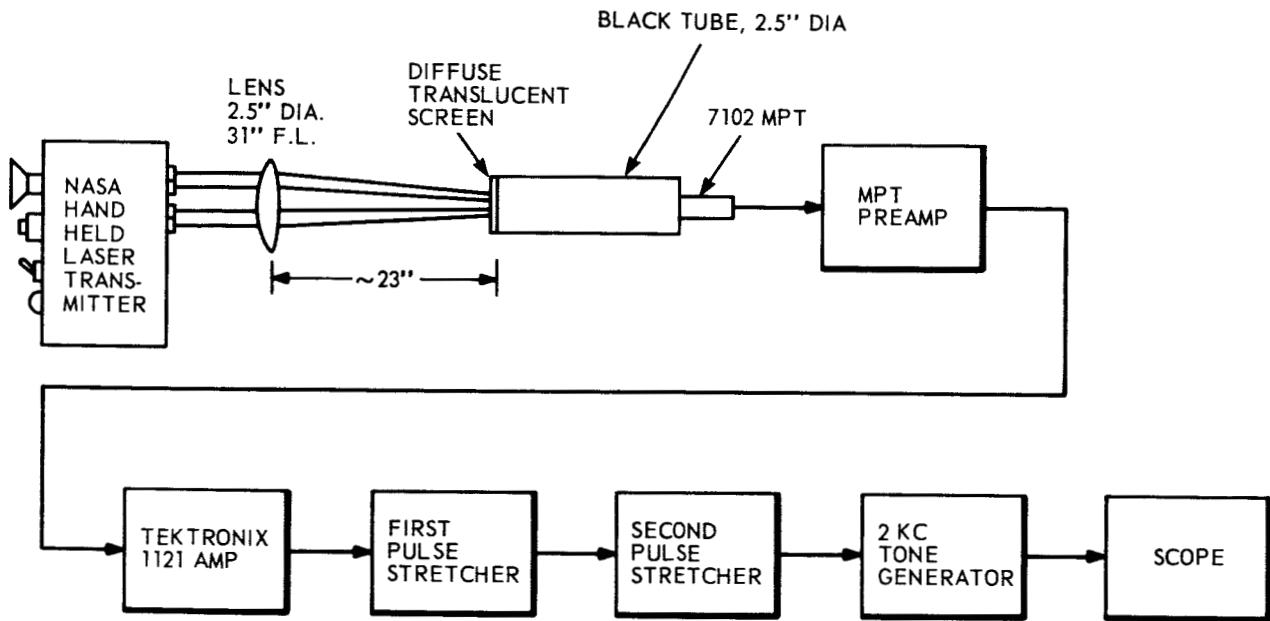
Figure 5-1. Experimental Arrangement for Measuring Beam Power Stability of
the NASA Hand-Held Laser Transmitter
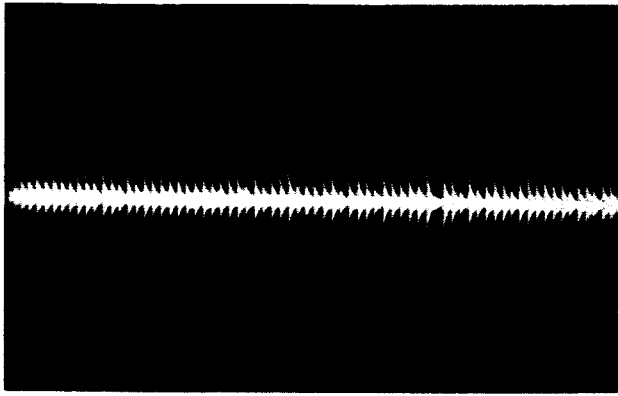
UPPER LEFT BEAM
0.05 V/CM; 100 MS/CM
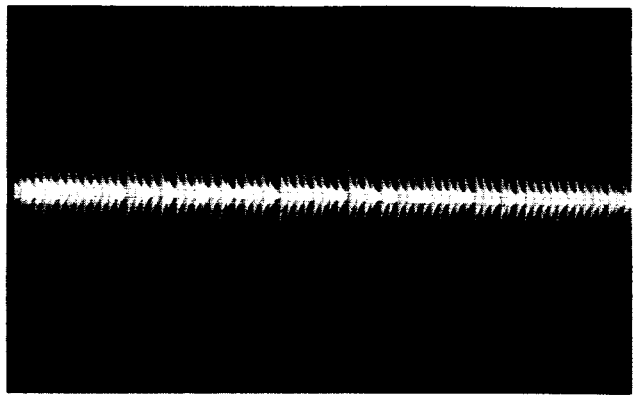
UPPER RIGHT BEAM
0.05 V/CM; 100 MS/CM

LOWER RIGHT BEAM
0.05 V/CM; 100 MS/CM

LOWER LEFT BEAM
0.05 V/CM; 100 MS/CM

ALL FOUR BEAMS
0.05 V/CM; 100 MS/CM

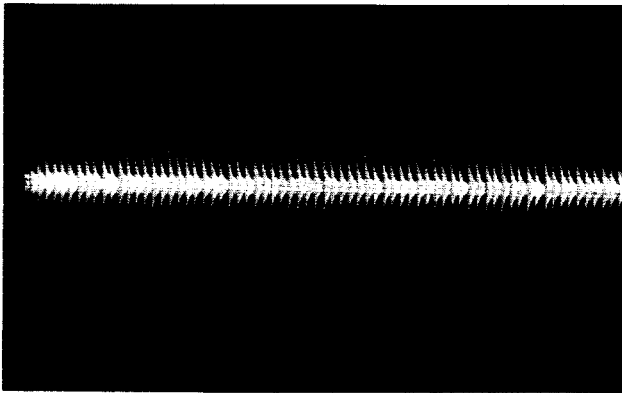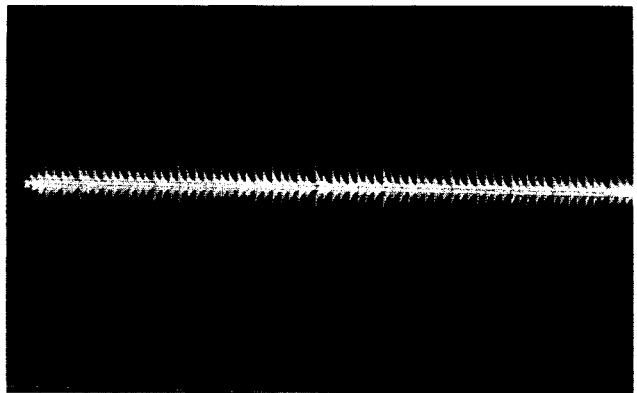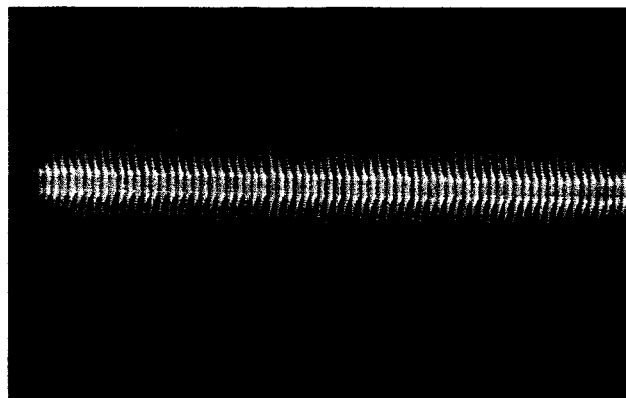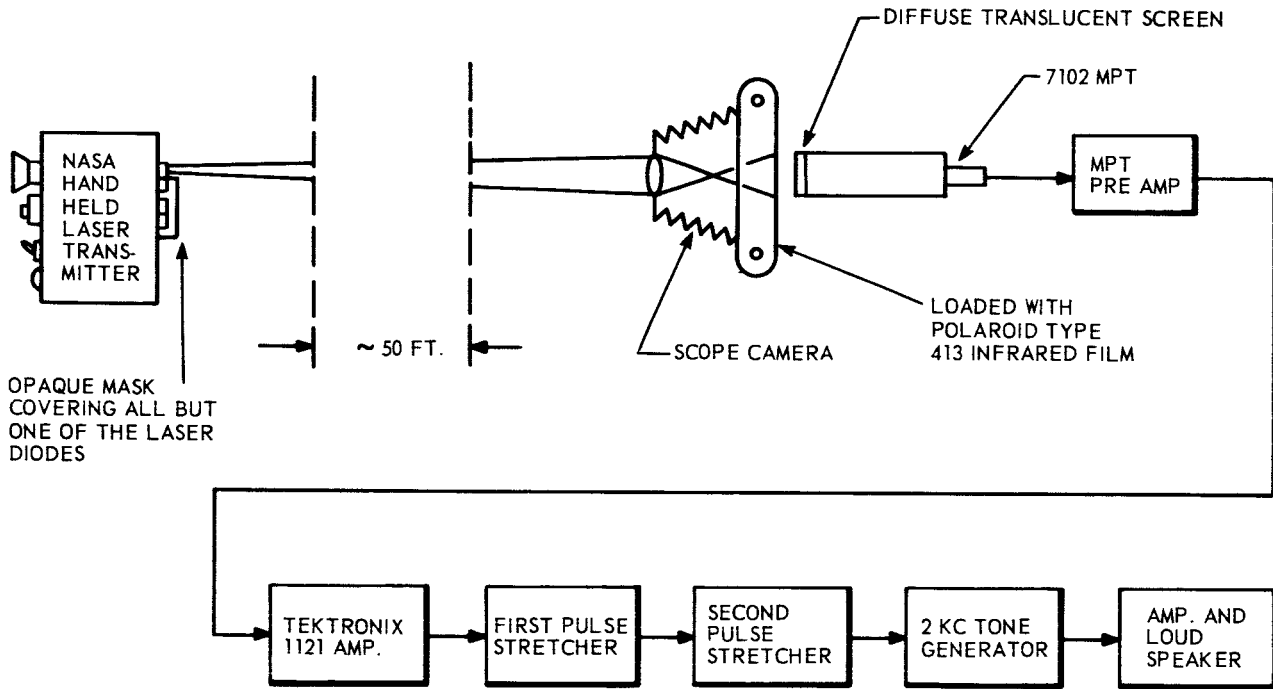Figure 5-2.   Beam Power Stability Data for NASA Hand-Held Laser Transmitter   65

Figure 5-3. Experimental Arrangement for Photographing the Beam Pattern of
the NASA Hand-Held Laser Transmitter

Figure 5-4 shows two of the beam pattern photographs taken during this experiment. Since the pulse repetition rate of the transmitter was about 80 pps, the image in the upper photograph (shutter speed 1/75 second) most probably was impressed by only one pulse, while the image in the lower photograph (shutter speed 1/25 second) was most probably impressed by two pulses. The fact that a large number of such photographs exhibited essentially identical beam patterns led to the conclusion that the beam pattern of a particular laser diode is probably constant in time.

The distance between maxima in the horizontal direction across the pattern is about 3/8 inch, while the distance between maxima in the vertical direction across the beam is about 1/8 inch. Since the distance between transmitter and camera was about 50 feet (600 inches), it can be concluded that horizontal maxima are spaced by about 0.6 milliradian, while vertical maxima are spaced by about 0.2 milliradian.

No attempt was made to photograph the beam pattern induced by all four beams acting in concert. It is to be presumed that, at long distances from the transmitter, the patterns would tend to overlap randomly, thereby lessening the probability of sharp, distinct maxima and minima. However, assuming that the single-diode pattern is the worst possible case, it can be concluded that beam bending or steering (induced by either atmospheric effects or motion of the transmitter) of as little as a few tenths of a milliradian could cause the portion of the beam illuminating the receiver to change from a maximum to a minimum, thereby inducing fluctuations in the received signal which could not be explained on the basis of normal atmospheric degradation of a uniform beam front.
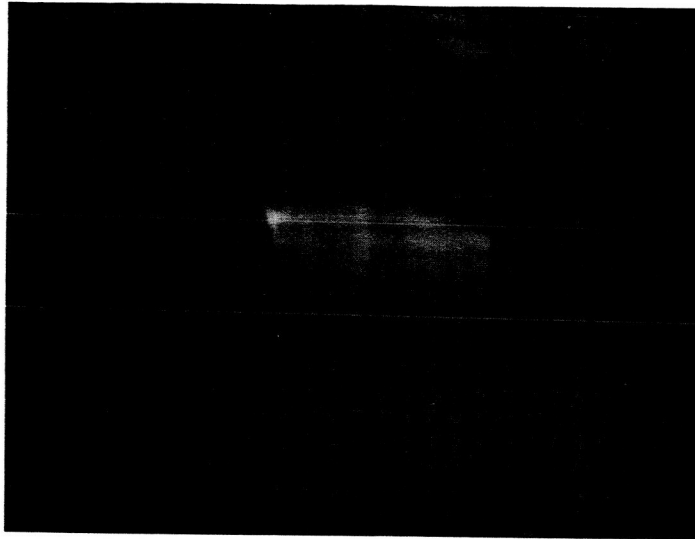
SHUTTER SPEED = 1/75 SEC.
ONE PULSE
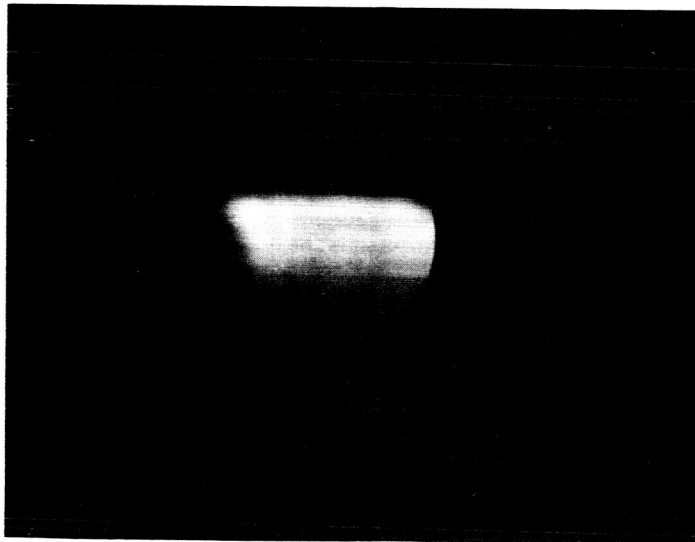
SHUTTER SPEED = 1/25 SEC.
TWO PULSES

Figure 5-4. Photographs of Beam Pattern of Upper Left Beam of NASA Hand-Held
Laser Transmitter

5.5 Propagation Experiments Over a 1000-Foot Path

In this experiment, a model of the T-5 mountain experiment was set up over a 1000-foot outdoor optical link at the Falls Church laboratories. The hand-held laser transmitter was mounted on a tripod at the outer edge of the laboratory parking lot, and was carefully aimed up to an optical receiver mounted on the roof of the laboratory. The receiving system was identical to the receiving system illustrated in figure 5-1, except that (a) the translucent screen shown in figure 5-1 was replaced by a circular aperture about 3/4 inch in diameter, and (b) the output of the tone generator was recorded on one channel of the Lafayette AM audio recorder described in section 3.9. The 3/4-inch dimension of the aperture was chosen so that the solid angle (centered at the transmitter) subtended by the receiver in the model experiment would be approximately equal to the solid angle subtended by the 36-inch receiver used in the T-5 mountain experiment, thereby insuring that the percentage of total beam area subtended by the receivers in the two experiments would be roughly equal.

The purpose of this experiment was to determine whether signal fluctuations in excess of the 10-to-1 dynamic range of the pulse detection system could be observed when the transmitter was rigidly mounted, accurately aimed, and known to be operating properly. It was found that, during both evening and nighttime operation of the experiment, signal fluctuations having ratios far greater than 10 to 1 could be readily observed, and that the envelope patterns of these signals were quite similar in character to the envelope patterns of the T-5 mountain experiment data. This experiment did not prove that the T-5 experiment was valid, but it did show that atmospheric effects could cause wide fluctuations in the received signal level as the sum of instrumentally induced fluctuations was small compared to observed 1000-foot measurements. It was concluded that the T-5 data could be valid, and therefore worthy of analysis.

5.6 Analysis of T-5 Mountain Experiment Data

Figure 5-5 illustrates approximately 3 seconds of the tone-generator output recorded during the T-5 mountain experiments. The total 3-second data strip was broken into 4 strips of equal length, with strip 2 following strip 1 in time, strip 3 following strip 2, etc. This particular segment of data was chosen for detailed analysis because approximately 70% of the signal pulses recorded during this segment were within the dynamic range of the pulse detection system. The horizontal division marks represent about 0.1 second in time. The vertical scale is in arbitrary units, with the upper and lower limits of the peak detection system being represented by approximately 7.6 divisions and 0.6 division respectively.

Table 5-1 presents the number of pulses n, average pulse signal level X, variance in pulse signal level $\overline{(\Delta X)}^2$, standard deviation in pulse signal level σ_X, and signal-to-noise ratio S/N, for each strip individually and for all four strips taken together. For the purposes of this analysis, it was assumed that the value of each pulse height had been correctly recorded

E6186

STRIP NO. 1
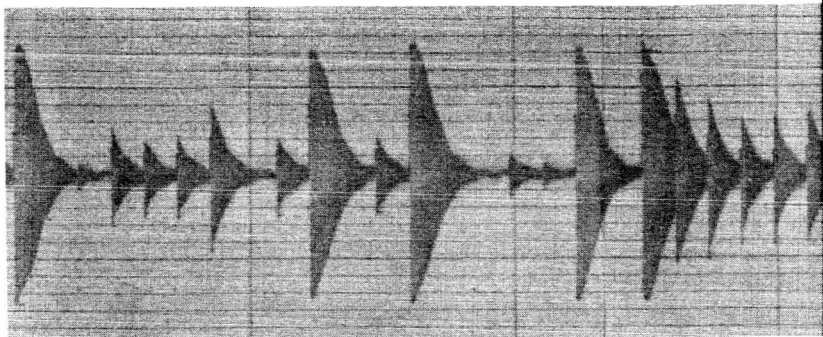
STRIP NO. 2
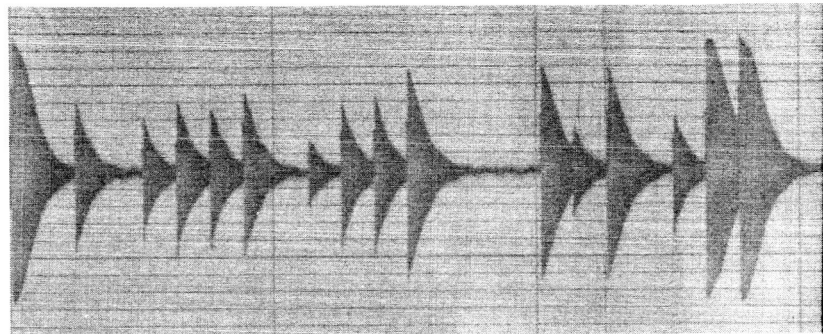
STRIP NO. 3
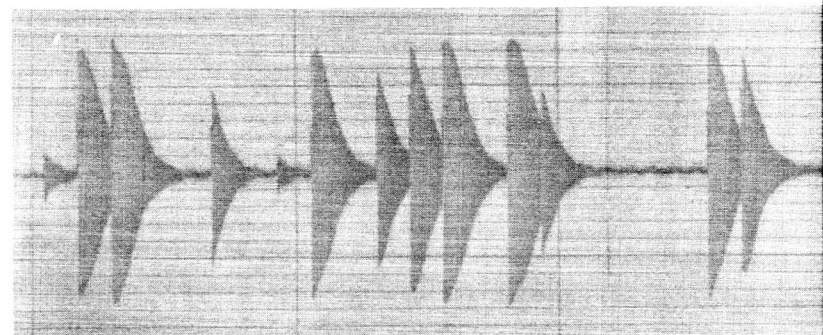
STRIP NO. 4
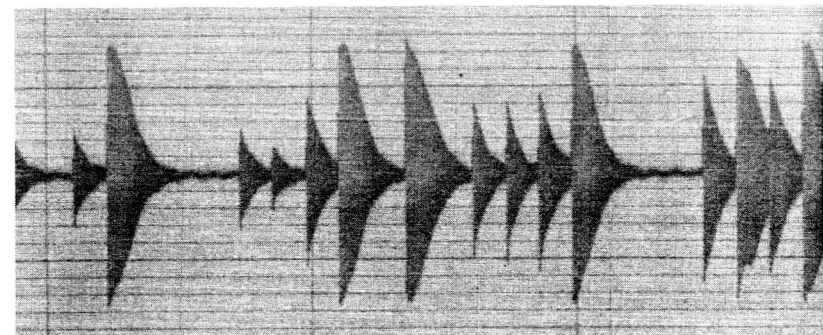
70-1
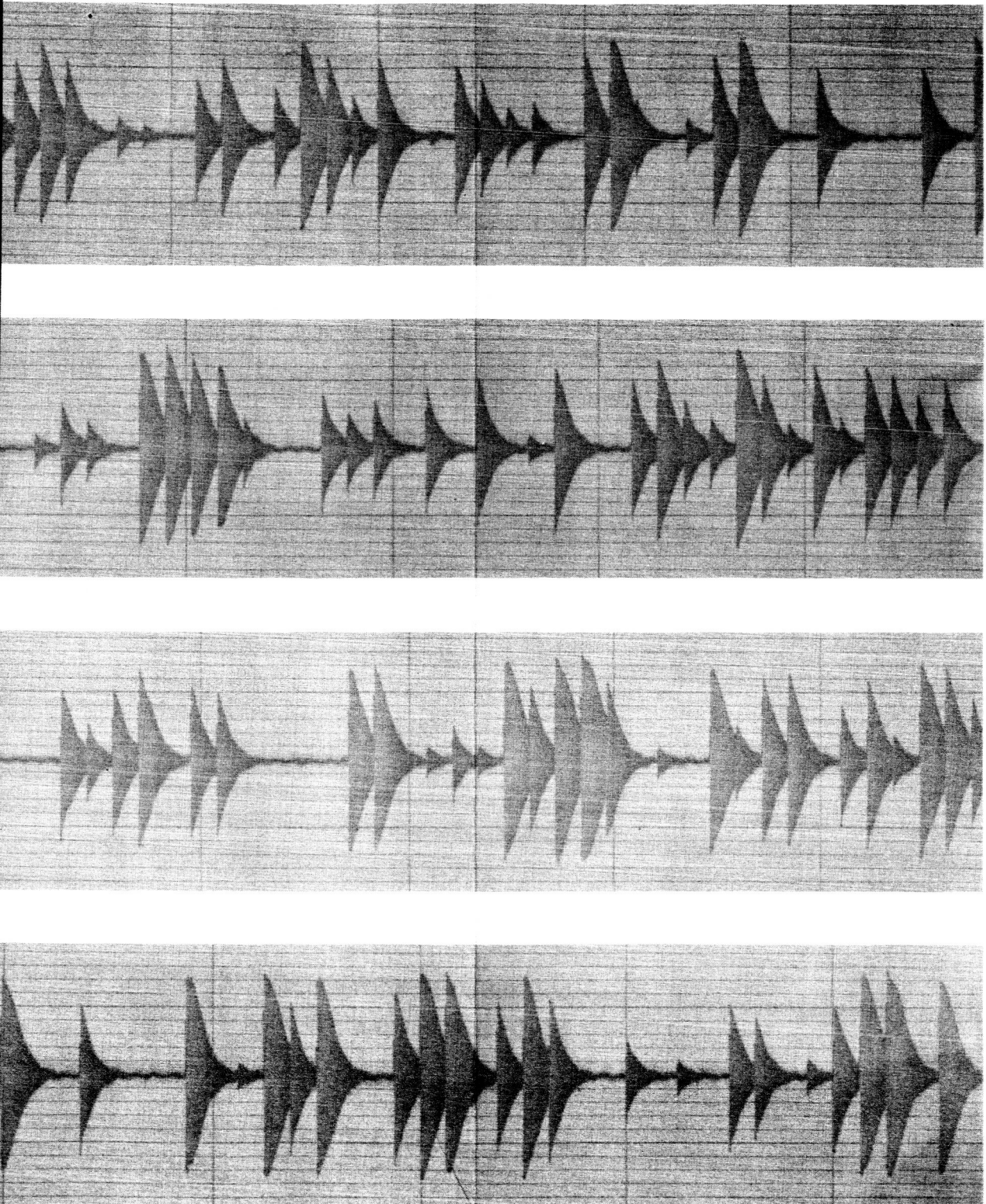
HORIZONTAL SCALE: 0.1 SECOND/DIVISION

Figure 5-5. Tone Generator Output, T-5 Mountain Experiment Data

70

on the strip chart (i.e., no attention was paid to the fact that a pulse that had been recorded with a height of 7.6 units (as limited by saturation of the peak detector) might actually have represented a pulse of much greater height. In computing the signal-to-noise ratio, it was further assumed that the pulses represented uniformly spaced samples of receiver output for a constant transmitter output. Under this assumption, the signal-to-noise ratio is given by the ratio of average signal level $\bar{X}$ to rms noise level σ_X.

TABLE 5-1

PARAMETERS OF T-5 MOUNTAIN EXPERIMENT DATA

	n	$\bar{X}$ (units)	$\overline{(\Delta X)^2}$ (units)^2	σ_X (units)	S/N
Strip 1	63	3.5	6.2	2.5	1.4
Strip 2	62	3.7	5.8	2.4	1.5
Strip 3	63	3.7	8.0	2.8	1.3
Strip 4	63	3.7	8.9	3.0	1.2
Overall	251	3.7	7.1	2.7	1.4

Figure 5-6 is a graph of the cumulative distribution function F(x) for the entire 3-second data segment, where

$$F(x) = P\left\{X < x\right\} \qquad (5\text{-}1)$$

that is, where F(x) is the probability that a pulse height will be less than x. The validity of the data points shown in this figure was not affected by the limited dynamic range of the pulse detection system.

Figure 5-7 is a graph of the probability density function f(x) for the entire 3-second data segment, where

$$f(x) = \frac{dF(x)}{dx} \qquad (5\text{-}2)$$

The data points for this graph were obtained by direct differentiation of the smoothed F(x) curve in figure 5-6, as opposed to a partitioning of the actual pulse height data.

It is interesting to note that figure 5-6 gives a value of 3.7 for the median pulse height, which happens to coincide with the value of 3.7 given in table 5-1 for the overall average pulse height. However, an examination of the probability density function in figure 5-7 reveals that
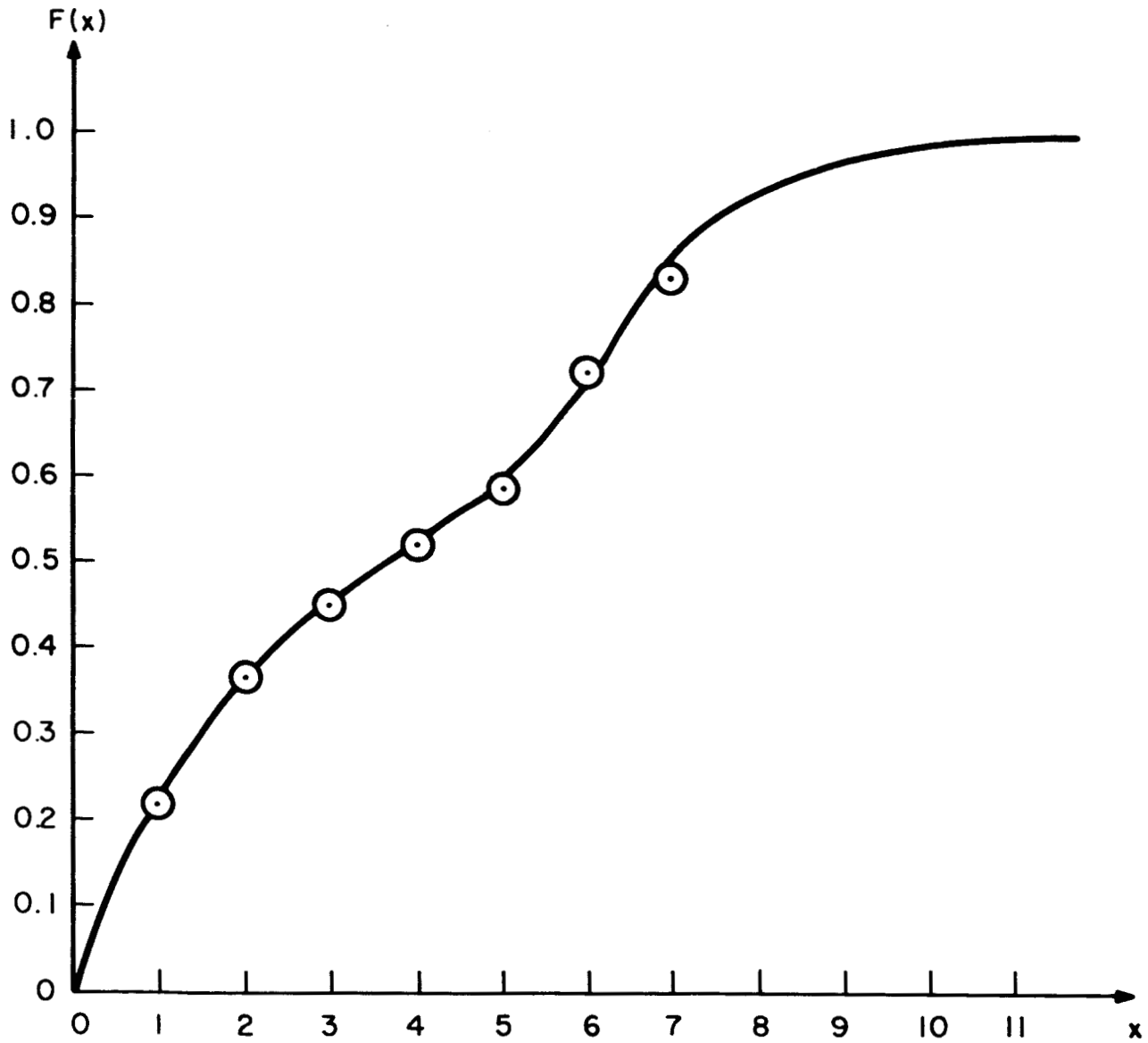
Figure 5-6. Cumulative Distribution Function, T-5 Mountain Experiment Data
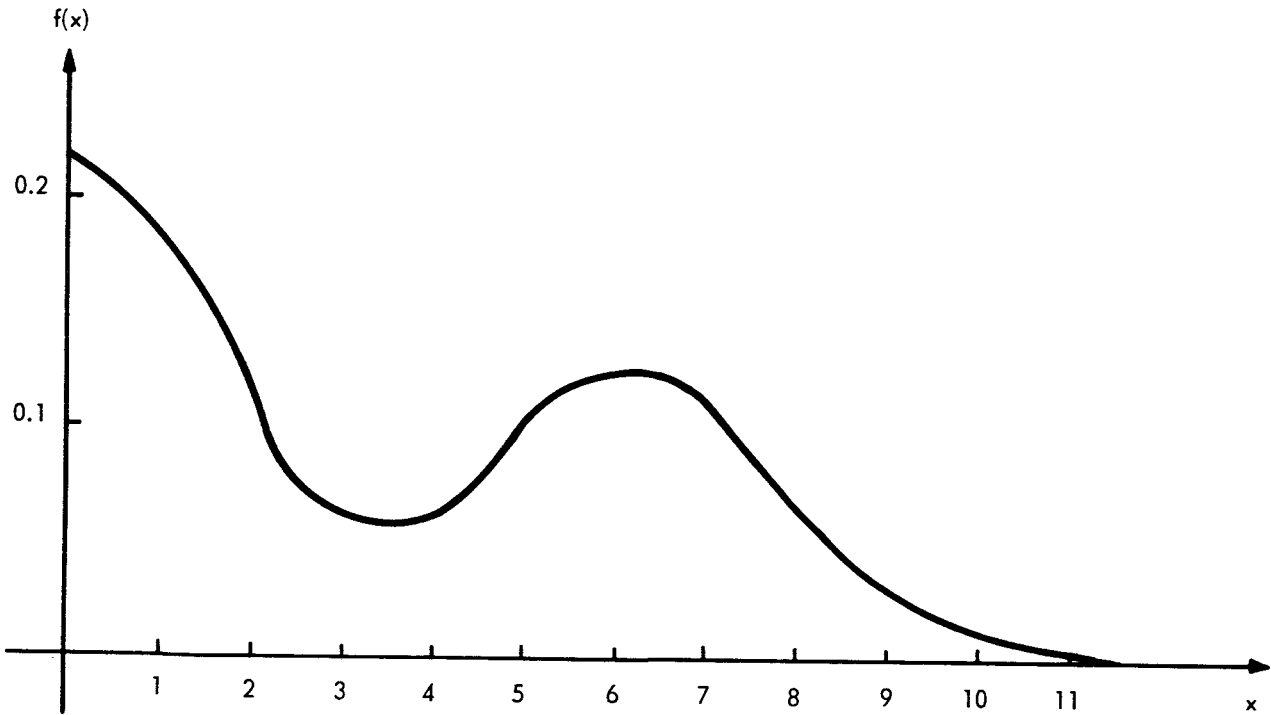
Figure 5-7. Probability Density Function, T-5 Mountain Experiment Data

pulses having heights of 3.7 occurred infrequently, and that instead, the density function is weighted heavily in favor of either low-height pulses or pulses having heights on the order of 5 units. This double maximum appearing in figure 5-7 might be attributable to a slight back and forth bending of the beam such as would cause the receiver to be alternately illuminated by a maximum and a minimum in the inherent transverse beam pattern (see section 5.4).

Any quantitative analysis of the harmonic content of the data presented in figure 5-5 would be necessarily limited to frequencies below 40 cps by virtue of the fact that the pulse repetition rate was only 80 pps. Because of this severe limitation, no extensive spectral analysis of these data was performed.

6. CONCLUSIONS AND RECOMMENDATIONS FOR FURTHER STUDIES

6.1 Analysis of GT-7 Laser Communicator Experiment

In January 1965 a meeting was held at the NASA Manned Spacecraft Center in Houston to review the GT-7 Laser Communicator Experiment. The following four problem areas were pinpointed at that meeting:

a. Beacon lasers - these high-powered gas lasers proved to be rather unreliable in the field. The principal problem with the beacon laser at WSMR was leaks in the anode assembly, while the main difficulty at Ascension Island was cracking of the laser tubes induced by the formation of bubbles in the water jacket cooling system.

b. Tracking systems - severe tracking errors between the tracking radar and the optical pedestal were encountered at both WSMR and Ascension Island.

c. Lack of prominent landmarks - the astronauts pointed out that it was impossible to visually acquire Ascension Island from the capsule, because the island is not surrounded by prominent landmarks. This same problem was true to some degree with the Laser Communicator site on the island of Kauai.

d. Hand-held transmitter sighting telescope - the field of view of the sighting telescope in the hand-held laser transmitter was much too small. Furthermore, the blue-green filter in the reticle of this telescope, which was designed to aid the astronauts in acquiring the blue-green beacon laser, proved to be a hinderance because it obscured the overall landscape, thereby obliterating the prominent landmarks which were so essential to visual acquisition of the beacon.

The post-flight data analysis of section 5 underscored two additional problem areas:

a. Transverse beam pattern - the cross-sectional beam pattern of the hand-held laser transmitter might have induced fluctuations in the received signal which would not have been induced by normal atmospheric degradation of a uniform beam front.

b. Limited dynamic range of the TR-5 - based on the large excursions in received signal level observed in the T-5 mountain experiment data, it would appear that the 10-to-1 dynamic range of the TR-5 video recorder severely limits the usefulness of this instrument for the direct recording of atmospheric propagation data.

6.2 Recommendations for Future Spacecraft Laser Communication Experiments

The following recommendations might apply to any future space-to-earth laser communication experiments:

a. Receiver Site - the receiver sites should be located in areas that have generally clear skies. In addition, the areas should be surrounded by particularly large and prominent landmarks.

b. Beacon Laser - In order to assist the astronaut in acquiring the beacon, equipment should be provided for rapidly changing the divergence angle of the beam. In addition, a mechanism might be included for scanning the beam in a symmetrical pattern around its line of boresight.

c. Recording system - the recording system should have an extremely wide dynamic range. This requirement can be satisfied by either logarithmic recording, or by multichannel recording wherein the dynamic ranges of the various channels are spaced in such a manner as to provide the desired overall system range.

d. Capsule transmitter - the transmitter in the capsule should emit pulses of duration as long as possible, and at a pulse repetition rate of approximately 10 kc. Optical spatial filtering should be incorporated to insure a uniform beam front. The transmitter sighting telescope should employ a variable focal length lens with a wide field of view. Aiming of the transmitter assembly should be accomplished through a set of gimbals which are in turn rigidly attached to the spacecraft.

6.3 Future Ground-Based Laser Propagation Studies

A number of ground-based laser propagation studies should be performed in order to measure the effect of certain optical system parameters on the statistics of the received signal. In addition, an effort should be made to correlate macroscopic atmospheric parameters with the statistics of the received signal. Among the more promising of these studies and experiments are the following:

a. Transmitter aperture diameter - determine the effect of the transmitter aperture diameter over a range extending from 1 millimeter to 1 meter. In particular, measure the effect, if any, of transmitter aperture diameter on beam steering.

b. Transmitter divergence angle - determine the effect of the divergence angle of the transmitted beam over a range extending from 0.01 milliradian to 10 milliradians. In particular, measure the effect of beam divergence on angle of arrival at the receiver. Determine the limiting beam divergence under various atmospheric conditions.

c. Receiver angle of view - determine the effect of the receiver angle of view over a range extending from 0.1 milliradian to 10 milliradians. In particular, measure long-term shifts in the angle of arrival.

d. Receiver aperture area and shape - determine the effect of receiver aperture area and shape. Include areas ranging from 0.01 to 1 square meter, and include shapes that will permit separate determination of horizontal and vertical coherence lengths.

e. Long-term beam bending - measure long-term shifts in beam bending by periodically optimizing transmitter aiming.

f. Range - determine the effect of transmitter-receiver separation by alternately measuring the transmissions from two identical transmitters that are at different distances from the receiver.

g. Atmospheric Conditions - record temperature, pressure, relative humidity, wind velocity, and wind direction at both transmitter and receiver during all experiments. Perform the same experiments with the same system parameters under various atmospheric conditions.

It should be emphasized here that none of the above experiments are absolute measurements of the effect of a certain parameter; rather, these measurements will hopefully yield the relative change in the statistics of the received signal induced by a change in one of the system parameters, in the context of a particular system operating in a particular environment under a particular set of atmospheric conditions. However, it is anticipated that a large number of such measurements would most certainly provide a basis for an evaluation of published theories on optical propagation through the atmosphere. In addition, these investigations would provide the engineering data necessary for designing practical optical communication systems, and for predicting the behavior of these systems under various atmospheric conditions. However, such experiments, while less expensive and more convenient than spaceborne experiments, are not known to be directly applicable to optical communications systems operating through a vertical atmospheric profile.

Melpar is presently engaged in an extensive independent research and development program to perform some of the ground-based experiments listed above. A completely portable, highly versatile, laser transmitting system has been designed and constructed. The source of laser energy in this system is a Spectra-Physics model 125 helium-neon gas laser operated at 6328 Å, which has an output power of about 80 milliwatts. The laser is mounted colinearly with a 2-meter optical bench, so that components for modulating, diverging, spatially filtering, and recollimating the beam can be rapidly installed or interchanged. The entire transmitting system is mounted on a 13-foot aluminum I-beam, which, in turn is mounted between two triangular base pods. Both the elevation and azimuth of the system can be adjusted to within 0.03 milliradian by screw adjustments at the ends of the I-beam. The system is electrically powered by a portable motor-alternator set. When packed and crated, the entire transmitter assembly (including all auxiliary equipment) weighs less than 1000 pounds. Figures 6-1 and 6-2 are photographs of the laser transmitter in operation.
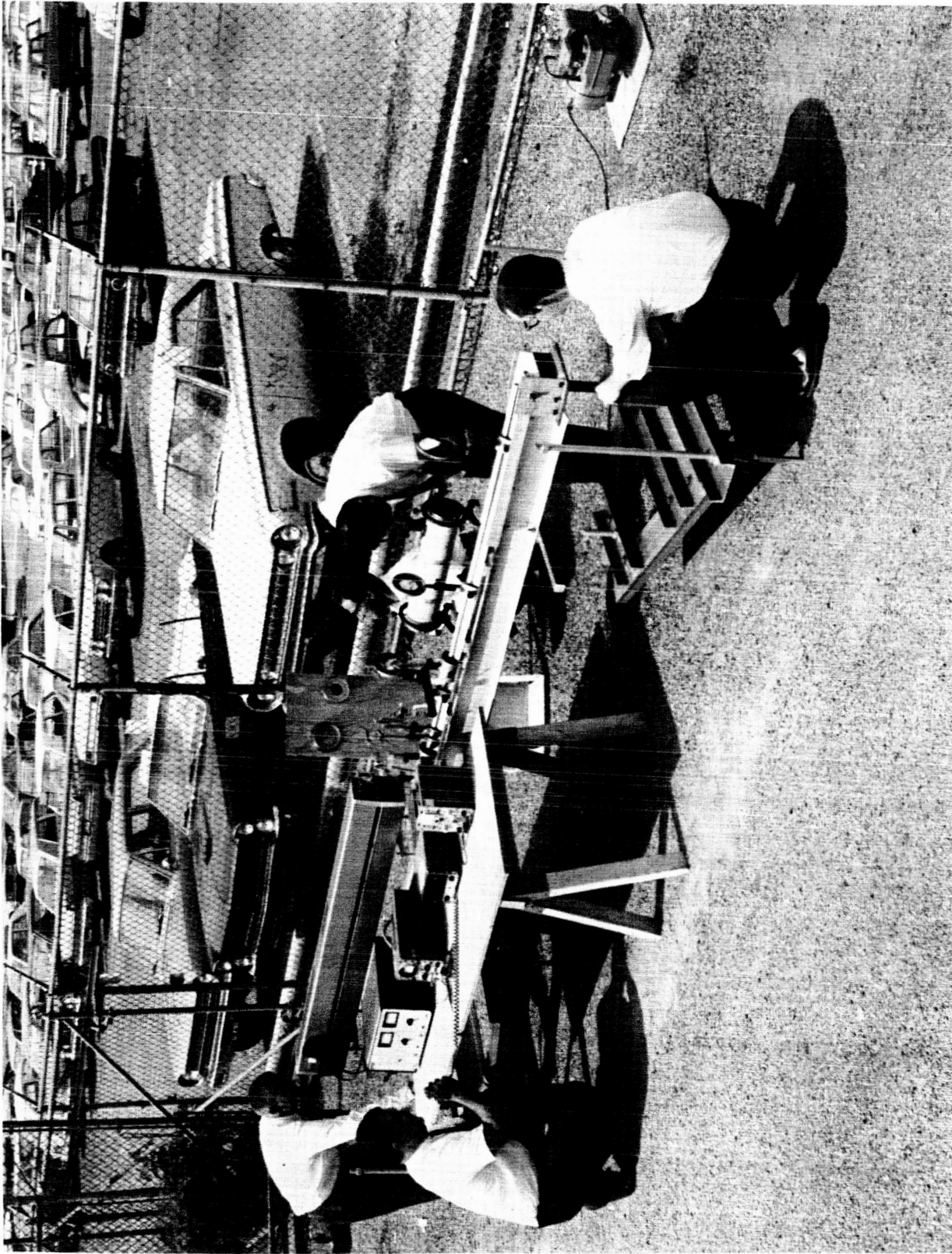
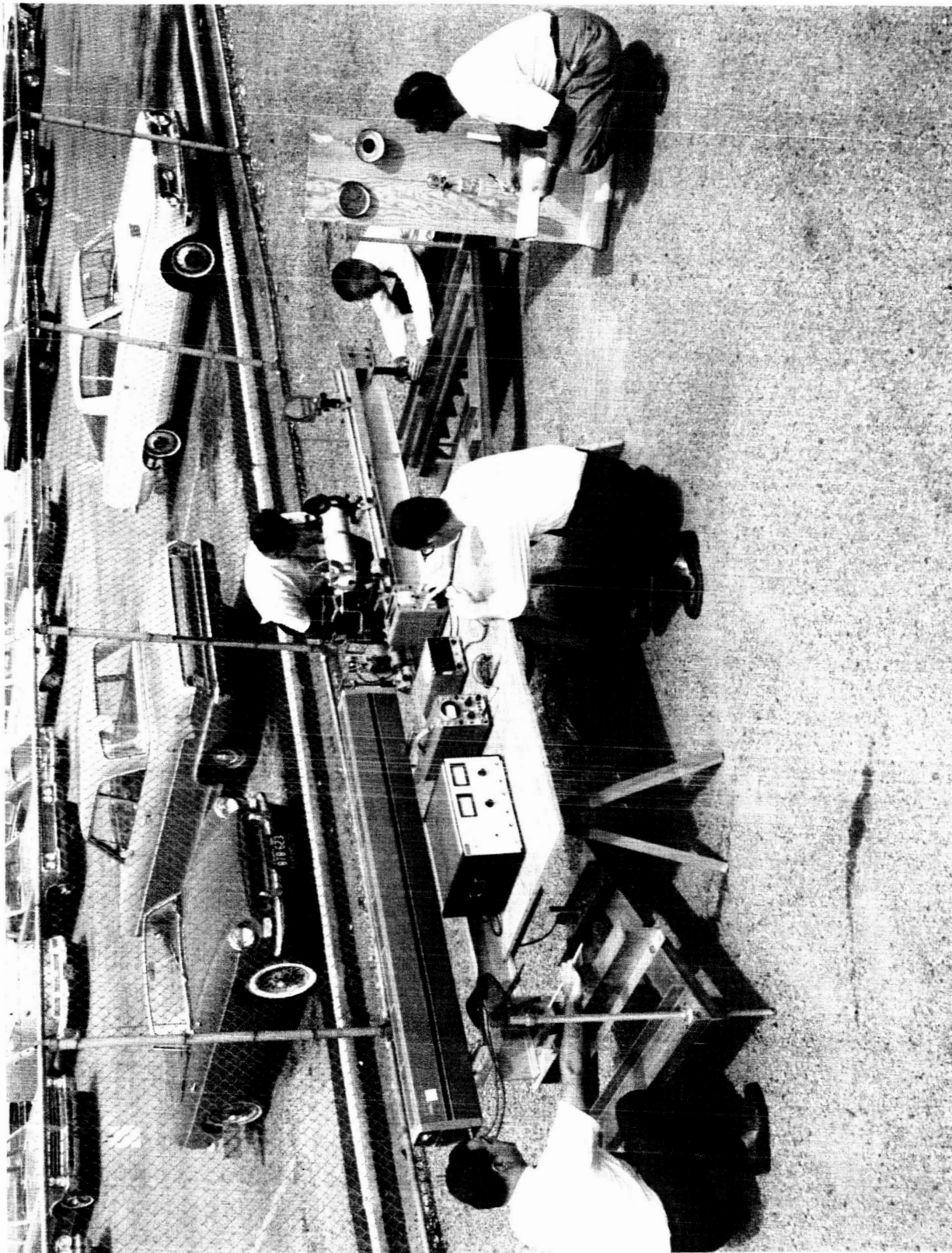Figure 6-1. Front View of Melpar Laser Transmitter in Operation

Figure 6-2. Rear View of Melpar Laser Transmitter in Operation

In addition to the transmitter, Melpar has set up an optical receiving station at its test site located in Centerville, Virginia. The optical receiver at this station is an 8-inch reflecting telescope, mounted on the telescope. The station is equipped for seven-channel FM audio recording, and two-channel AM audio recording. The entire receiving station is housed in a small field laboratory, thereby permitting all-weather operation. Figure 6-3 is a photograph of the exterior of the optical receiving station. Figure 6-4 is an interior view of the station showing the telescope, photomultiplier package, and recording equipment.

The receiving station is at one end of a line-of-sight path to the top of Bull Run Mountain, which is located approximately 13 miles northwest of the Centerville test site. On 29 July 1966, the transmitter assembly was taken to the top of Bull Run Mountain and aimed at the receiving station. Throughout the night of 29 July 1966 and into the morning of 30 July 1966, extensive atmospheric perturbation measurements were performed as a function of transmitter aperture diameter, transmitter beam divergence, and receiver angle of view. Plans are presently being made to perform additional experiments over the Bull Run-Centerville optical link, in order to measure long-term beam bending, ultimate divergence angle, and the effect of receiver aperture shape.
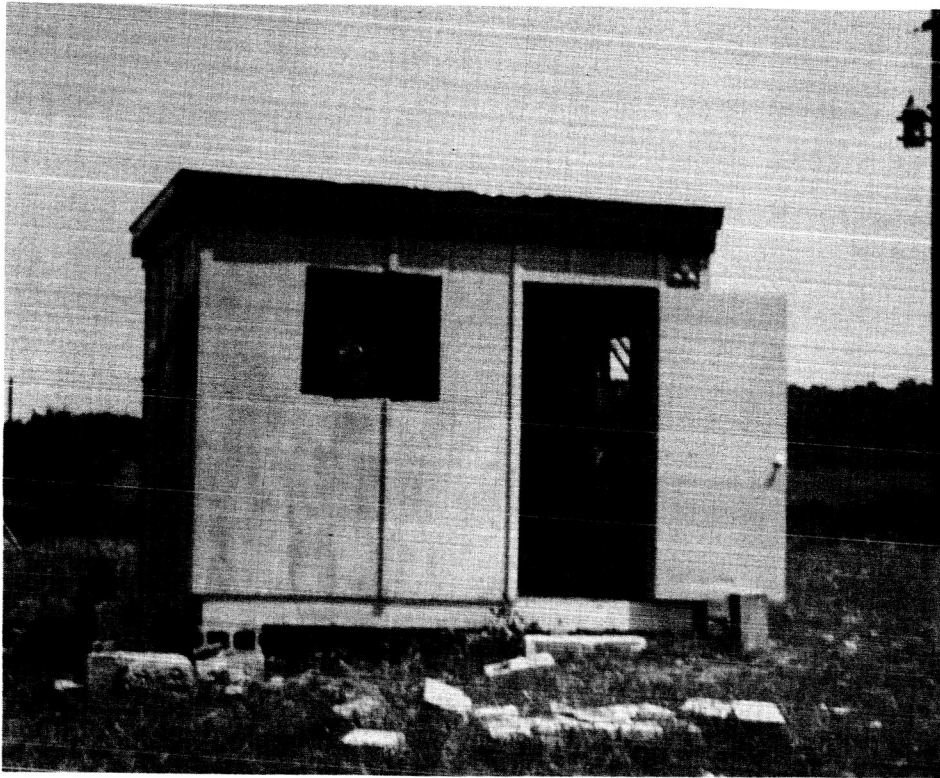
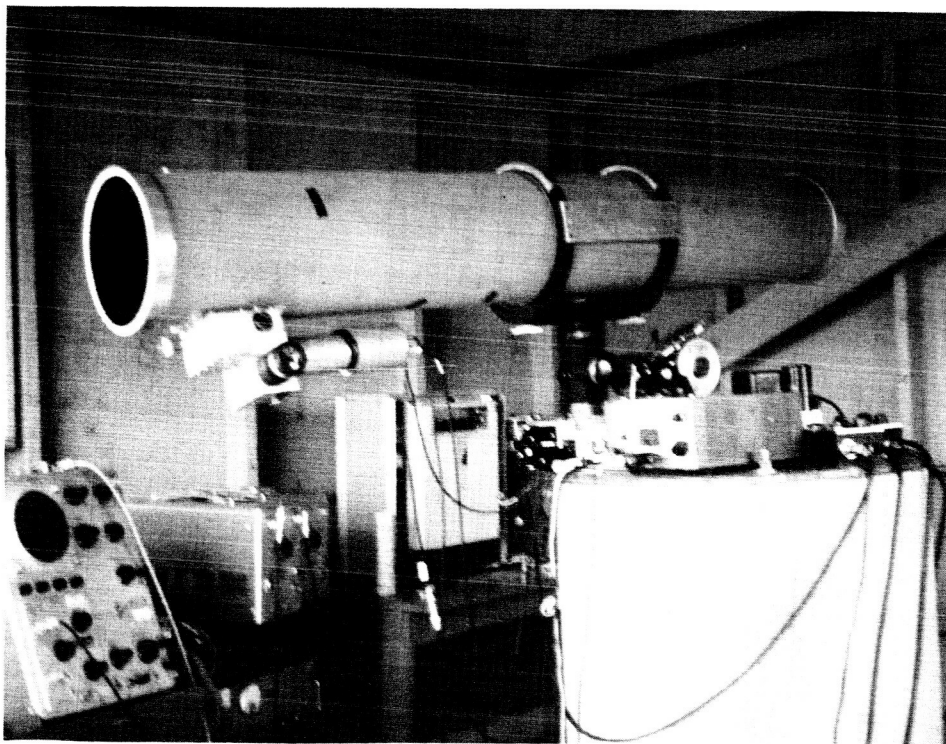Figure 6-3. Exterior View of Melpar Optical Receiving Station

Figure 6-4. Interior View of Melpar Optical Receiving Station

7. REFERENCES

1. Buck, A.L. (1965): "Laser Propagation in the Atmosphere," Proceedings of the Conference on Atmospheric Limitations to Optical Propagation, Central Radio Propagation Laboratory and National Center for Atmospheric Research, Boulder, Colorado, March 1965.

2. Bergman, P.G. (1946): "Propagation of Radiation in a Medium with Random Inhomogeneities," Physical Review, Vol. 5, Nos. 7 and 8, October 1946, p. 486.

3. Campanella, S.J. (1965): "An Investigation of the Time Autocorrelation of Sonic Pulses Propagated in a Medium of Random Temperature Microstructure," D.E.E. Dissertation, School of Engineering and Architecture, Catholic University of America, 1965.

4. Chernov, L.A. (1960): Wave Propagation in a Random Medium, McGraw-Hill Book Co., New York, 1960.

5. Davis, J.I. (1966): "Consideration of Atmospheric Turbulence in Laser System Design," Applied Optics, Vol. 5, No. 1, January, 1966, p. 139.

6. Edwards, B.N. and R.R. Steen (1965): "Effects of Atmospheric Turbulence on the Transmission of Visible and Near Infrared Radiation," Applied Optics, Vol. 4, No. 3, March 1965, p. 311.

7. Hinchman, W.R. and A.L. Buck (1964): "Fluctuations in a Laser Beam Over 9- and 90-Mile Paths," Proceedings of the IEEE, Vol. 52, March 1964, p. 305.

8. Hufnagel, R.E. and N.R. Stanley (1964): "Modulation Transfer Function Associated with Image Transmission Through Turbulent Media," Journal of the Optical Society of America, Vol. 54, No. 1, January 1964, p. 52.

9. Lumley, J.L. and H.A. Panofsky (1964): The Structure of Atmospheric Turbulence, Wiley, New York, 1964.

10. Mintzer, D. (1953A): "Wave Propagation in a Randomly Inhomogeneous Medium. I," Journal of the Acoustical Society of America, Vol. 25, No. 5, September 1953, p. 922.

11. Mintzer, D. (1953B): "Wave Propagation in a Randomly Inhomogeneous Medium. II," Journal of the Acoustical Society of America, Vol. 25, No. 6, November 1953, p. 1107.

12. Subramanian, M. and J.A. Collinson (1965): "Modulation of Laser Beams by Atmospheric Turbulence," Bell System Technical Journal, Vol. 44, March 1965, p. 543.

13. Tartarski, V.I. (1961): Wave Propagation in a Turbulent Medium, McGraw-Hill Book Co., New York, 1961.